BNL-52575
Formal Report
LHC Project Note 199

Proceedings of the

WORKSHOP ON LHC INTERACTION REGION CORRECTION SYSTEMS

Brookhaven National Laboratory
Upton, New York
May 6-7, 1999

Editors
W. FISCHER and J. WEI

Brookhaven National Laboratory
Brookhaven Science Associates
Upton, New York 11973
Under Contract No. DE-AC02-98CH10886
with the United States Department of Energy

CONTENTS

FOREWORD

The Workshop on LHC Interaction Region Correction Systems was held at Brookhaven National Laboratory, Upton, New York, on 6 and 7 May 1999. It was attended by 25 participants from 5 institutions.

The performance of the Large Hadron Collider (LHC) at collision energy is limited by the field quality of the interaction region quadrupoles and dipoles. In three sessions the workshop addressed the field quality of the these magnets, reviewed the principles and efficiency of global and local correction schemes and finalized a corrector layout.

The session on Field Quality Issues, chaired by J. Strait (FNAL), discussed the progress made by KEK and FNAL in achieving the best possible field quality in the interaction region quadrupoles. Results of simulation studies were presented that assess the effects of magnetic field errors with simulation studies. Attention was given to the uncertainties in predicting and measuring field errors.

The session on Global Correction, chaired by J.-P. Koutchouk (CERN), considered methods of reducing the nonlinear detuning or resonance driving terms in the accelerator one-turn map by either sorting or correcting. The session also discussed the crossing angle dependence of the dynamic aperture and operational experience from LEP.

The session on Local Correction, chaired by T. Taylor (CERN), discussed the location, strength and effectiveness of multipole correctors in the interaction regions for both proton and heavy ion operation. Discussions were based on technical feasibility considerations and dynamic aperture requirements. The work on linear corrections in the interaction regions was reviewed.

We thank all participants for their contributions to the success of the workshop. We are grateful to Pam Manning, Rhianna Bianco and Waldo MacKay for their support in organizing the workshop and in preparing the proceedings. We hope that these proceedings are a useful reference for interaction region correction systems in general and the LHC's in particular.

W. Fischer and J. Wei

SUMMARIES

1 WORKSHOP SUMMARY

J. WEI, BNL

During the two-day workshop, representatives from CERN, FNAL, KEK, BNL, and other institutions and universities met and discussed issues relevant to LHC interaction region correction schemes and plans. In this Section, we summarize the proposed IR corrector layout and correction plan. In Sections 2, 3, and 4, summaries of the three individual sessions, Field quality, Global correction, and Local correction, are given by the corresponding session chairmen.

1.1 Proposed IR corrector layout and plan

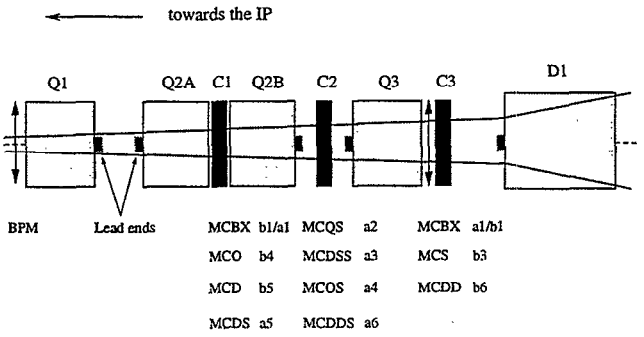

Figure 1: Schematic layout of the proposed LHC inner triplet region correction packages.

The proposed layout and content for the interaction region corrector packages is shown in Fig. 1.

1. The corrector layout for all the 8 inner triplets of the 4 interaction region are identical. This allows constructional and operational standardization as well as sorting.

2. Correctors at IP2 are mainly useful during the heavy ion operation when the β^* at IP2 is low. Correctors at IP2 and IP8 may also be used for global correction. Initially, one may choose not to power IP8 correctors until needed.

3. Each inner triplet contains 3 corrector packages: package C1 located between Q2A and Q2B contains five elements: b_1, a_1, b_4, b_5, and a_5; package C2 located between Q2B and Q3 contains four elements: a_2, a_3, a_4, and a_6; package C3 located between Q3 and D1 contains four elements: b_1, a_1, b_3, and b_6.

4. The strengths designed for each correction element is given in Table 1. Tentatively, the strengths for $n > 2$ multipoles are set here at twice the maximum strength used to locally compensate the lumped multipole errors of IR inner triplet quadrupoles built by FNAL (reference table version 2.0) and KEK (reference table version 3.0), cold D1 built by BNL (reference table version 1.0), and warm D1 (reference table version 1.0). (It was decided that these strength should be moderately chosen to maximize their effectiveness.)

5. The strength for $n = 1, 2$ elements are chosen to be as much as practically achievable.

6. Due to the strong b_6 correction needed, more space is reserved for its coil winding. Therefore, the package C3 that contains the b_6 correction element has only two nonlinear ($n > 2$) layers, while both C1 and C2 have three nonlinear layers.

7. The design strength will be finalized by the end of year 1999 after further measurements are made on the IR magnet prototypes and after further feasibility studies are performed on the corrector spool piece design.

Table 1: Proposed IR corrector package contents and strength. The strength is integrated over the length of the correction element normalized at the reference radius of 17mm. Each inner IR triplet contains one of each type of correction element. The magnetic length of each element is 0.5m.

n	b_n strength	a_n strength	unit
1	3.0	3.0	[T]
2	–	0.51	[T]
3	0.029	0.068	[T]
4	0.027	0.068	[T]
5	0.012	0.012	[T]
6	0.025	0.010	[T]

1.2 Other issues

Consensus is reached on other issues at the workshop pertaining to IR compensation and operation:

1. Updated error tables for IR inner triplet quadrupoles and warm D1 dipoles are needed before the end of September 1999 for the final determination of the IR corrector strength.

2. During the LHC operation, a "threshold" (e.g. 10% of the maximum strength) may be set for the powering of IR correctors below which correctors will not be activated.

3. The orientation of the IR inner triplet quadrupoles and cold D1 is shown in Fig. 1. This arrangement reduces the requirements on the IR corrector power supply strengths.

4. Magnetic tuning shims are not planned to be used for any LHC IR magnets due to mechanical difficulties and uncertainty in magnetic multipole errors.

5. In general, sorting on IR magnets, correctors, and assemblies is encouraged during all stages of the construction to optimize the performance and to minimize the corrector power supply requirements. The decision on the IR corrector layout, however, is made independent of sorting consideration, since sorting is often constraint by real world issues like planning, assembly and installation schedules.

6. Options for global correction will be evaluated in the future to determine the corrector candidates and their locations, preferably in regions where the counter-rotating beams are separated.

7. Impacts from magnetic errors of multipole order higher than $n = 10$ appear to influence the dynamic aperture when the betatron amplitude is larger than 10σ in the presence of the design crossing angle. In practical operation, however, these higher order impacts are likely to be negligible due to their strong amplitude dependence, when the actual dynamic aperture is below 10σ.

8. Alignment of IR magnet cold masses and assemblies is crucial to the collision performance. Reference misalignment tables will be established for the IR magnets and correctors.

2 SUMMARY OF FIELD QUALITY SESSION

J. STRAIT, FNAL

This session reviewed the expected field quality of the Fermilab and KEK IR quadrupoles and calculations of the impact of the field errors on the LHC performance. Data from the existing model magnets were presented and the relation between them and the reference harmonics tables were discussed. A number of recommendations were developed concerning which harmonics are the most dangerous and how the current versions of the reference harmonics tables could be improved.

2.1 Questions for the workshop

A number of questions were posed to the workshop, which are listed below, together with the answers developed during the discussions.

1. What is the optimal choice of corrector layers? This is addressed in Jie Wei's summary presentation.

2. Are corrector positions optimal? The corrector positions will remain as in the original layout: MCBX between Q2a and Q2b, MCQS between Q2b and Q3, and MCBX between Q3 and D1.

3. What should be the lead end orientation for Q3? The lead end should remain facing the IP.

4. Can MCBX.Q3 contain only a horizontal dipole? Both horizontal and vertical layers should be included in this magnet.

5. Should the same correctors be used in IR2 and IR8 as in IR1 and IR5? The same correctors should be installed in all locations and leads for all should be brought through the DFBX, but it is left as an option that some layers might not be powered at the low luminosity IRs.

6. The corrector strength should be set to cover the systematic errors plus how many sigma? This will be discussed in Jie Wei's summary presentation.

7. Do we need a reference misalignment table? This table should be developed in the coming months.

8. Can FNAL eliminate tuning shims? Yes.

2.2 Error contribution in order of importance

Tracking and other beam studies indicate that the errors contributing to machine performance, in order of importance, are

1. b_{10} if it is above about 0.06 units.

2. Random b_6, which is currently 0.6 units in both FNAL and KEK quadrupoles.

3. Multipoles of order 3 and 4 in both lab's magnets.

4. Lead end b_6 in both lab's magnets.

2.3 Reference error tables

Continued discussion is required to ensure that there is a common understanding concerning the use and meaning of the reference harmonics tables. At least two types of meaning are attached to the values in the tables:

1. They are statistical estimates of the errors expected for the magnets to be installed in LHC. This is the usage assumed by those doing tracking studies.

2. They are specifications for magnet manufacturers, with the sum of systematic plus uncertainty plus rms errors taken essentially to be limits. The table entries are treated this way by some magnet builder.

The lack of common understanding results in the tables being perceived as "pessimistic" by the accelerator physicists on the one hand and as justifiably "conservative" by

Table 2: Measured harmonics for FNAL models compared with the reference table.

Field	Measured field harmonics						reference table V2.0	
harmonic	HGQ01	HGQ02	HGQ03	HGQ05	mean	rms	uncertainty	random
b_3	0.36	-0.70	1.04	0.72	0.36	0.76	0.30	0.80
a_3	0.27	0.55	-0.30	0.12	0.16	0.36	0.30	0.80
b_4	0.26	0.18	0.14	–	0.15	0.11	0.20	0.80
a_4	0.73	-0.41	0.32	0.19	0.21	0.47	0.20	0.80
b_5	-0.29	0.09	-0.34	-0.04	-0.15	0.20	0.20	0.30
a_5	0.02	-0.17	0.26	0.05	0.04	0.18	0.20	0.30
b_6	0.33	1.32	0.37	-0.22	0.45	0.64	0.60	0.60
a_6	-0.02	0.03	0.07	-0.03	0.01	0.05	0.05	0.10
b_7	-0.08	-0.01	-0.06	0.01	-0.04	0.04	0.05	0.06
a_7	-0.05	–	-0.03	0.01	-0.02	0.03	0.04	0.06
b_8	0.06	0.01	–	–	0.02	0.03	0.03	0.05
a_8	–	0.02	0.03	–	0.01	0.02	0.03	0.04
b_9	0.04	–	–	–	0.01	0.02	0.02	0.03
a_9	0.01	-0.01	0.01	–	–	0.01	0.02	0.02
b_{10}	0.04	-0.01	–	–	0.01	0.02	0.02	0.03
a_{10}	0.02	–	-0.01	–	–	0.01	0.02	0.03

magnet builders on the other. The definition of the uncertainty $d(b_n)$ does not always appear to be clear. It must be remembered that this is not the same as the mean of the distribution of a finite number of magnets. It is clear that care must be used in treating the statistics of small numbers of magnets.

There was some discussion as to how data from the models and prototypes should be used to revise the tables. How closely should the error table follow from the mean and rms over the models? Should the table be based on all the model data, corrected for known manufacturing deviations, or just on the most recent models? Should the table be revised each time a new model is measured? Should the data be used to set table values directly, or only to adjust the table when the table is inconsistent with the data by a statistically significant amount? Should the data be treated as the best estimate of the field quality of production magnets, or just to set bounds (for example at a 90% confidence level) on the reference table values? No consensus conclusions were drawn.

2.4 *Field quality of FNAL quadrupoles*

The Fermilab reference harmonics table appears conservative relative to the data. Tab. 2 compares the measured harmonics for the first 4 models, corrected for the non-standard pole shims used in the first three models, with the reference table. The comparison reveals:

1. The measured rms $<$ random (b_n/a_n) for all b_n, a_n except b_3 and b_6, for which the measured rms is approximately the random error in the table. Were the reference table a realistic estimate of the expected rms for a production series, perhaps one-third of the measured values would be larger than the entries in the reference table.

2. The measured rms $\ll$ random (b_n/a_n) for a_3, b_4, a_4, by 2-3 times the estimated uncertainty in the measured rms. These are among the most important harmonics noted in Sec. 2.2 above.

3. The measured $\langle b_n \rangle$ and $\langle a_n \rangle$ are all consistent with 0 except $\langle b_4 \rangle = 0.15 \pm 0.05$. This apparently systematic value of b_4 may be small enough to be unimportant, but should be understood by the magnet builders.

It should be noted that this good field quality has been achieved without using the tuning shims.

2.5 *Field quality of KEK quadrupoles*

The draft KEK reference harmonics table V3.0 (Tab. 3) is explicitly conservative at this point. This conservatism is driven by the fact that the body and end designs have been recently changed, but no models of the new design have been built yet. Notable features of the table include:

1. $b_{3,4}/a_{3,4}$ values are larger than in the FNAL table.

2. $d(b_{10})$, $\sigma(b_{10})$ are together larger than the 0.06 "limit."

3. The two-piece stressed yoke can generate a systematic b_4 of approximately 0.7 units according to calculations, but this is not observed in the first two models.

4. Systematic differences exist in the first two models between measurement and calculation for the allowed harmonics: $\Delta b_6 \approx -1.0$ unit and $\Delta b_{10} \approx -0.1$ unit. If the cause of this can be understood, then $d(b_6)$ and $d(b_{10})$ can be reduced.

5. High order entries (except for b_{10}) are essentially the same as in the FNAL table.

Table 3: KEK reference harmonics table V3.0 (draft), body multipoles in units of 10^{-4}, $R_{ref} = 17$ mm).

n	Normal			Skew		
	$\langle b_n \rangle$	$d(b_n)$	$\sigma(b_n)$	$\langle a_n \rangle$	$d(a_n)$	$\sigma(a_n)$
3	–	0.50	1.00	–	0.50	1.00
4	–	0.70	0.80	–	0.30	0.80
5	–	0.20	0.40	–	0.20	0.40
6	0.1	0.50	0.60	–	0.10	0.20
7	–	0.05	0.06	–	0.04	0.06
8	–	0.03	0.05	–	0.02	0.04
9	–	0.02	0.03	–	0.02	0.02
10	–	0.10	0.05	–	0.02	0.03

2.6 *Highest order harmonics in tables*

Currently the error tables include harmonics up to b_{10} and a_{10}, but this may not be a high enough order. If b_{10} is important, why not b_{14}, b_{18}, ...? Calculations done by Norm Gelfand, using the $d(b_{14})$ error from the original FNAL table which included harmonics up to order 14, are said to show a limit on the dynamic aperture of 11-12σ from this harmonic alone. The estimated accuracy of harmonics measurements ranges from $< 1\%$ for $n \leq 3$ to (conservatively) $< 6\%$ for $n \leq 15$, supporting the inclusion of higher order harmonics. Thus both FNAL and KEK need to estimate the higher order harmonics, especially the allowed moments which have the possibility to be more significant, and the effect of these on the beam needs to be evaluated.

2.7 *Reproducibility of harmonic errors*

The limit on the accuracy of the field quality and of the ability to correct the measured field errors may be set by the reproducibility of the field in an individual magnet. FNAL has seen changes in the transfer function and harmonics with thermal cycles (see Sec. 2.4), but has not yet looked for changes with quenching. KEK has observed changes at low field with quenching, but has not presented data on changes with thermal cycles. It remains to be verified that the field errors settle ("train") to constant values after a tolerable number of cycles. The source of the larger variations should be understood in order to try to minimize the changes.

2.8 *Summary, conclusions and recommendations*

1. The new KEK design eliminates the b_{10} problem, but the current values of $d(b_{10})$ and $\sigma(b_{10})$ in the draft V3.0 reference table are conservative at a level that may affect machine performance.

2. Both FNAL and KEK tables appear to have built in margin. That is, it seems likely that the production magnets will have better field quality than that implied by the tables.

3. We need to continue to develop a better common understanding of how to use tables and of the definitions of error types: statistical estimates vs. specifications and limits.

4. Both FNAL and KEK need to review their tables by September. The tables should be the best estimates of the distribution of errors in production series. If margin is included in table, this should be explicitly acknowledged along with the magnitude of the margin. The tables may need to account for changes with thermal cycle or quench. Higher order harmonics, especially the allowed moments, should be examined and included if they are important (10^{-4} at $\approx$20 mm). Both error tables should be entered into the CERN database used by the Field Component & Machine Performance Working Group, chaired by L. Walckiers.

5. The reference harmonics table for the Novosibirsk-built D1 dipoles needs to be updated.

6. The effect on the beam of time dependent field variations at injection should be evaluated.

7. Variation of the transfer function with thermal cycles must be understood, in particular to reduce the effect and to ensure that it "trains" to a stable value after a finite number of cycles.

8. Despite the conservatism, the existing tables seem to be good enough to be correctable with a reasonable set of correction coils. On this basis, FNAL plans not to use tuning shims. KEK has no provision for tuning shims.

9. A reference misalignment table should be developed jointly by the magnet builders and the accelerator physics group.

3 SUMMARY OF GLOBAL CORRECTION SESSION

J.-P. KOUTCHOUK, CERN

This session reviewed the means to minimize or suppress the requirement to locally correct the triplet multipoles. They are based on minimizing a measure of the non-linearity by sorting or correcting. This approach is confronted to the constraints of the real-world, such as those encountered in the RHIC construction. In this session the LEP experience was reviewed and the latest calculations on the beam-beam effect in LHC were presented as well.

3.1 *Sorting*

The sorting of the quadrupoles, including the effect on the two LHC rings, was shown by J. Shi to be definitely effective in terms of dynamic aperture, assuming the official error tables 2.0. J.P. Koutchouk pointed out the large randoms in this tables, which explain the success of sorting,

but do not seem to be observed on the FNAL quadrupole models measured so far. S. Peggs analyzed how the sorting was conducted for RHIC. It appears that for all kinds of magnets, the sorting was used to fix more 'fundamental' quantities than the higher-order multipoles. It was further constrained by real world issues like planning and capability of measuring all magnets cold.

The consensus is that sorting should be kept to fix 'pathologies', i.e. unexpected problems rather than predictable dispersion of characteristics. If this turns out not to be necessary and if the random multipole errors turn out to be as expected in table 2.0, sorting for dynamic aperture remains attractive and should be feasible if planned (magnet storage, ...). Indeed, if sorting can prevent using the multipole correctors, operation will gain in simplicity and efficiency.

3.2 Global correction

These methods require making several hypotheses:

- What are the most important non-linearities?
- What should be the 'measure' for the non-linearity?
- What should be the layout of the correctors?

J. Shi chose to minimize a norm of the one-turn map coefficients order by order. T. Sen rather minimized excitations terms of 3^{rd} order resonances evaluated at the dynamic aperture. The corrector layout obeys no special rule in the first case while the sextupoles in the triplets were used in the second case. The map minimization appears effective and the very first results of the second method show some improvement in spite of an unfavorable sextupole arrangement.

It is not proposed to replace the local correctors by a global correction scheme. The unknowns are still too many: robustness versus optics errors, efficiency in case of an optics change between the non-linear source and the correctors or a tune change, effect of the global minimization of the non-linearity on the beam lifetime.

The advantage of the global scheme is its generality which allows to act even if the exact source is unknown by means of a small number of non-linear 'knobs'. The consensus is to encourage an evaluation of what non-linear knobs could be implemented with the available LHC non-linear correctors and to identify which one would be worth adding.

3.3 Crossing angle

The latest results obtained by T. Sen show that the dynamic aperture due to the beam-beam only is limited at 8.5σ for the nominal crossing angle. The latter appears to be the very minimum for a decent dynamic aperture. Increasing it to $\pm 175\ \mu$rad gives a very significant decrease of amplitude growth in 4D tracking, especially in the range from 8 to 11σ.

The field quality requirements on the quadrupoles should not be relaxed, since the crossing angle cannot be decreased, and in fact may likely to be increased in the future.

3.4 LEP experience

Although the electron beam dynamics in LEP is very different, the review of the LEP experience shows the importance of a good and versatile instrumentation, and the requirement to take into account the complexity of operation and machine studies (13000 vertical orbit corrections in one year!). The beam based alignment using K-modulation turned out to be very useful and allowed the detection of PU misalignments far above expectations (up to 2 mm).

4 SUMMARY OF LOCAL CORRECTION SESSION

T. TAYLOR, CERN

The desired correction strengths of the local correction windings appear to be well within the range which can be obtained using the CERN techniques for making spool pieces. The distribution of the seven windings, with two windings in the dipoles and three in the skew quadrupole, is also acceptable. Using the baseline values, a check of the true engineering feasibility of the windings will be made at CERN.

The baseline strengths include a safety factor of at least two. If the multipoles come out to be much weaker than presently estimated, this could lead to having windings running at a very small fraction of their maximum value, which is operationally undesirable. It was suggested that the level below which a multipole would be considered to be acceptable without correction should be determined, and that this information should also be taken into account in the final determination of spool corrector strengths.

The final design of the spool pieces will be made after the next update of the expected multipole errors in the magnets, which is targeted for next September.

Overview of LHC Low-β Triplets and Correction Scheme Issues

R. Ostojic

CERN, Division LHC, Geneva, Switzerland

1. Introduction

The LHC experimental insertions consist of a low-β triplet, a pair of separation dipoles, and a matching section of four quadrupoles. The superconducting low-β quadrupoles must accommodate separated beams at injection, provide high field gradients and low multipole errors for colliding beams, and sustain considerable heat load from secondary particles generated in the high luminosity ATLAS and CMS experiments. In the other two experiments, ALICE and LHC-b, the separation dipoles and matching sections share the available space with the injection equipment, which implies less flexibility for beam separation. In this report we give an overview of the layout and required performance of the LHC experimental insertions, and discuss issues related to the triplet correction scheme that should be discussed during this Workshop.

2. LHC Experimental Insertions

The layout of the Large Hadron Collider comprises eight straight sections available for experiments and major machine systems [1]. The two high luminosity p-p experiments, ATLAS and CMS, are located on the symmetry axis of the machine, at interaction points 1 and 5. The other two experiments, ALICE and LHC-b, are at points 2 and 8, where the counter rotating beams are injected in Ring 1 and Ring 2, respectively. In these four insertions, a pair of recombination-separation dipoles guides the two beams onto crossing orbits. In points 1 and 5, the first separation dipole D1 is a conventional resistive magnet, while D2 is a superconducting magnet. In points 2 and 8, where space is tight and luminosity lower, both separation dipoles are superconducting magnets.

Table 1. Nominal collision parameters for LHC experimental insertions

Insertion	p-p				Heavy-ion			
	β^* (m)	ξ (μrad)	Δ (mm)	L ($cm^{-2}s^{-1}$)	β^* (m)	ξ (μrad)	Δ (mm)	L ($cm^{-2}s^{-1}$)
IR1	0.5	±150 (V)	0	10^{34}				
IR2	10	±100 (V)	±0.5	10^{30}	0.5 50	±75 (V)	0	10^{28}
IR5	0.5	±150 (H)	0	10^{34}	0.5	±75 (H)	0	10^{28}
IR8	1 50	±150 (V) ±50 (V)	0	10^{32}				

The nominal collision parameters of the LHC experimental insertions are summarised in Table 1. For p-p runs, the high luminosity insertions will operate at the highest luminosity of

10^{34} $cm^{-2}s^{-1}$, which correspond to a β^* of 0.5 m. In order to minimise the effects of long range beam-beam interactions the beams will collide with a crossing angle of ±150 μrad, in the vertical plane in IR1 and horizontal in IR5. The other two insertions will also observe p-p collisions. They will, however, operate in a detuned mode, corresponding to the injection optics with a β^* of 10 m. Furthermore, in order to reduce the luminosity in IR2 to the level of acceptable for the ALICE experiment (10^{30} $cm^{-2}s^{-1}$), halo-type collisions with parallel beam separation Δ of ±0.5 mm are envisaged. For heavy-ion runs, it is presently foreseen that two experiments will collect physics data: the dedicated heavy-ion experiment ALICE in IR2, and the CMS experiment in IR5. Luminosity of 10^{28} $cm^{-2}s^{-1}$ is expected for a β^* of 0.5 m. Due to the heavy-ion bunch spacing of 125 ns, the crossing angle can be reduced in this mode to ±75 μrad with a still satisfactory beam lifetime.

3. Baseline Layout and Performance of the Low-β Triplet

The low-β triplets, Fig.1, consist of four wide aperture superconducting quadrupoles [2]. The outer two quadrupoles, Q1 and Q3, are 6.3 m long, while the central one is divided for engineering reasons into two identical units, Q2a and Q2b, 5.5 m each. The triplets are identical in all insertions, and are at 23 m from the interaction points. In the high luminosity insertions, a 1.8 m copper absorber (TAS), located within the front shielding of the experiments, ensures the protection of the triplets. The main parameters of the low-β quadrupoles are given in Table 2.

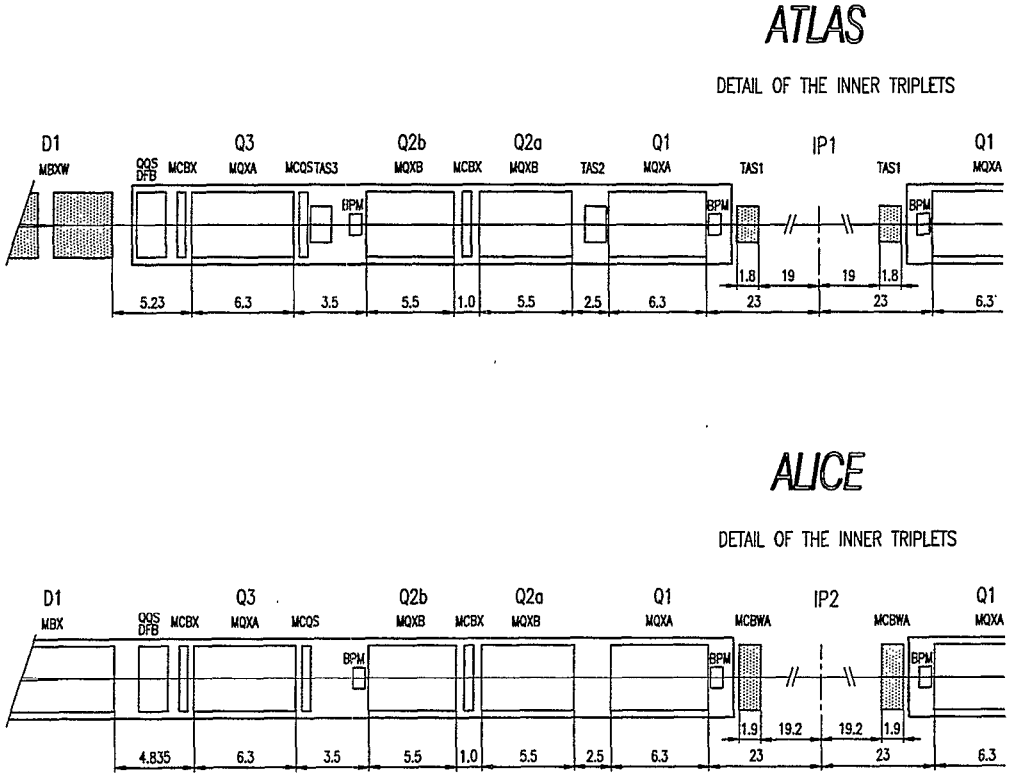

Fig.1. Baseline layout of the LHC low-β triplets in IR1 and IR2

One of the most important issues in the design of the low-β triplets is the protection of the superconducting quadrupoles against the high flux of secondary particles emanating from the p-p collisions. This issue has been thoroughly studied [3] and it has been found that the Q2a quadrupole, where the power density due to the secondaries is the highest, can be better protected by optimising its distance from Q1. Based on these studies, the separation between Q1-Q2a has

been set to 2.5 m. This is sufficient place for a supplementary absorber (TAS2). The protection of the triplets is further improved by increasing the wall thickness of the cold bore by reducing its inner diameter to 60 mm, Table 2, and by including an absorber TAS3 in between Q2 and Q3. In IR2 and IR8, these absorbers are not needed, and the inner diameter of the cold bore is set to its nominal value of 63 mm for the purpose of increasing the geometrical acceptance of the triplets.

Table 2. Nominal parameters of the LHC low-β quadrupoles

Aperture		
Coil aperture		70 mm
Cold bore ID	IR2/8	63 mm
	IR1/5	60 mm
Operating Gradient		205 T/m
Alignment		
Initial radial		0.3 mm rms
Initial tilt		0.3 mrad rms
Twist		0.3 mrad/m
Longitudinal		1 mm rms

The space of 1 m between Q2a and Q2b is reserved for the combined horizontal-vertical orbit corrector (MCBX). In this location the β-function is maximum in one plane (x or y, depending on the polarity of Q2), while the maximum in the orthogonal plane occurs upstream of Q3, where an additional orbit corrector is envisaged. These correctors are capable of compensating individual misalignment of the quadrupoles by an initial amount given in Table 2. Experience in operating the machine and the development of beam-based techniques should result in considerable improvement of quadrupole alignment. The triplet is also equipped with a skew quadrupole corrector in between Q2b and Q3 (MCQS), and two directional beam position monitors, one in front of Q1 and the other between Q2b and Q3.

Decision has been recently taken in the sense that the Q1 and Q3 quadrupoles (MQXA) will be supplied by KEK as part of the Japanese contribution to the LHC, while Q2a and Q2b (MQXB), as well as the superconducting D1 in IR2 and IR8, will be part of the US contribution. The corrector packages and BPMs will be supplied by CERN. The cold-mass integration and cryostating will be done by Fermilab as part of the US-LHC project.

The operational parameters of the LHC, in particular the crossing angle and β* in collision, imply that the two beams are offset by as much as 8 mm from the quadrupole axis. As a result, the low-β quadrupoles must satisfy stringent field quality requirements. Several recent discussions on field quality issues [4] have resulted in reference error tables for the two quadrupole types. The latest version of the tables contains important systematic and random errors, as well as uncertainties expected in production magnets.

The performance for the LHC low-β triplets is defined in terms of the target dynamic aperture, calculated on the basis of tracking over 10^5 turns. Having in mind the collision parameters given in Table 1, the target performance of the LHC for p-p collisions is 12 σ for the average and 10 σ for the minimum dynamic aperture, Table 3. With the rms beam size of 1.5 mm, this corresponds to a good field region of the quadrupoles of 26 mm. A similar target dynamic aperture is required for heavy-ion collisions.

Table 3. Nominal tunes and target dynamic aperture of the LHC

Betatron tunes (H/V)	63.31/59.32
Synchrotron tune	0.00212
Chromaticity (H/V)	2/2
Target performance	
p-p high luminosity	
Average DA	12 σ
Min DA	10 σ
Heavy-ions	
Average DA	< 12 σ

On the basis of the present version of the MQXA and MQXB error tables, it is clear that the target performance will be difficult to achieve without higher-order multipole correctors [5]. The layout of the triplet provides three locations for these correctors, nested within the dipole and skew quadrupole correctors. The basic assumptions for defining these correctors are:

- Magnetic length of 500 mm, as for MCBX and MCQS
- Operating margin of about 50% which takes into account the background field of the main linear correctors (3 T, H/V for the MCBX, and 30 T/m for the MCQS)
- Normal field correctors located preferentially within MCBX, skew within MCQS
- Number of nested multipole layers limited to 2 for normal correctors, and 3 for skew correctors.

The expected strength of the multipole correctors, Table 4, based on using the LHC sextupole corrector wire (rated at 600 A) and satisfying the above guidelines [6], gives an indication of the expected correction range.

Table 4. Expected strength of multipole correctors

Multipole Corrector	Field (T) @ 17 mm	
b3, a3	0.100	0.150
b4, a4	0.066	0.086
b5, a5	0.037	0.044
b6, a6	0.020	0.020
b10	0.003	

4. Correction Scheme Issues

The present Workshop is an outstanding opportunity to review a number of issues related to the low-β triplet layout and correction scheme, in particular the definition of the multipolar

corrector location, strength and technology. Below is a list, necessarily incomplete, of questions we should discuss during the Workshop:

Inner triplet layout

- The present orientation of the quadrupole lead ends was determined on the basis of compensation of lead end b6 errors. With better knowledge of the field errors, can we consider that the orientation of the quadrupoles is still optimal?
- The positions of corrector packages were determined in the early stages of the triplet design. Is there reason to consider alternative layouts, in particular could we envisage that the first MCBX dipole is moved to the Q3 end of Q2?
- In order to minimise the number of corrector leads, could we envisage only a vertical dipole corrector at Q3 (MCBX.Q3)?
- Should the corrector packages in IR2 and IR8 triplets be identical to, or could they be a subset of those installed in high luminosity insertions IR1 and IR5?

Corrector strength and technology

- Is the strength of linear correctors MCBX and MCQS adequate?
- What is the minimal set of multipole correctors and what are the positions that minimise their strength? In particular is there a need for more than two correctors in any package?
- What are the criteria for setting the multipole corrector strengths? In particular:
    a) What version of the quadrupole error table should be used (presently available, or updated with the latest results of R&D models)?
    b) What accuracy of field measurements should be assumed?
    c) Should the strength be determined as the maximum value over the set of N random machines, or rather as Avg + n SD? What are the choices of N and n which give statistically relevant results?
    d) Should sorting strategies be included when selecting N random machines?
- What is the interplay between corrector alignment and their strength and position? Is the corrector alignment of 0.5 mm rms appropriate?
- The nominal corrector current should match one of the standard LHC bi-polar power supplies (±60, ±120, or ±600 A). Is there a clear preference for one of these ranges?

I hope the lively discussions we all expect and look forward to during the Workshop will result in clear statements as to these and other issues related to the layout and compensation scheme of the LHC low-β triplets.

References

[1] The LHC Study Group, *The Large Hadron Collider*, Conceptual Design, CERN/AC/95-05.

[2] R. Ostojic, T.M. Taylor and S. Weisz, "Systems Layout of the Low-β Insertions for the LHC Experiments", PAC'97, Vancouver, LHC Project Report 129

[3] J. Strait and N. M. Mokhov, "Optimisation of the LHC Interaction Region With Respect to Beam-Induced Energy Deposition", EPAC'96, Barcelona, LHC Project Report 43.

[4] LHC Accelerator Physics Workshop, Fermilab, Oct. 19-20, 1998

[5] J. Wei et al, "Insertion Region Local Correction for the LHC", PAC'99

[6] M. Karppinen, private communication

THE FIELD QUALITY OF THE 1-METER MODEL KEK-LHC LOW-β QUADRUPOLE MAGNETS

Y. Ajima, T. Nakamoto, T. Ogitsu, N. Ohuchi , M. Qiu, T. Shintomi,
K. Tsuchiya, and A. Yamamoto, KEK, Tsukuba, Japan

Abstract

Two 1-m model magnets of the KEK-LHC low-β quadrupole magnet were constructed and tested. The two magnets reached a field gradient of more than 240T/m. Magnetic field measurements were performed with two kinds of harmonic coils. In this paper, the field qualities of the straight section and the end regions are reported and compared with the calculations.

1 INTRODUCTION

KEK has made two 1-m model magnets for the R&D of the LHC low-β quadrupole magnets [1, 2]. The first magnet (No.1-a) had additional shims at the pole surfaces of the coils to keep the pre-stress in the coil at 55MPa in the azimuthal direction. The thickness of the shims was 0.2mm for the inner two layers and 0.1mm for the outer two layers, respectively. Iron yokes almost covered the straight section, and the length was 599mm. Due to the additional shims, the magnet had a b_6 of 1.25units in calculations. The multipole components of the magnet are summarized in Tab. 1.

Table 1: Calculated multipole components of No.1-a, No.1-b and No. 2 in the straight section (units).

Multipole	No.1-a	No.1-b & 2
b_6	+1.25	-0.20
b_{10}	-0.89	-0.84

The second magnet (No.2) was fabricated as designed. There were no additional shims. Therefore, the calculated multipole components are different from those of the No.1-a magnet. Especially the b_6 shows a large difference of 1.45units. The straight section and the ramp area of the magnet were covered with iron yokes.

The first magnet was re-assembled to remove the additional shims (No.1-b). Therefore, the calculated field characteristics in the straight section are the same as the No.2 magnet. The whole magnet is covered with iron yokes.

The calculation of the magnet return end for the No.1-b has been completed using ROXIE, and the results are summarized in Tab. 2. The definition of each section for the KEK magnet is shown in Fig. 1.

2 FIELD MEASUREMENT SYSTEM

The field measurements were performed by two harmonic coils. One is 200mm long, and it is used for measuring the field profile along the magnet length [3]. The other is 25mm long. It was designed to see the fine structure of the field profile in the end regions. The radii of the both harmonic coils are 22mm. The harmonic coils consist of seven windings: a tangential winding, three dipole windings and three quadrupole windings. The inductive voltages of the windings are measured by integrators (Metrolab PDI 5025). The harmonic coils are supported in the warm tube in the magnet bore, and their temperatures are kept at room temperature by dry nitrogen gas.

In the 200mm harmonic coil, a radial coil is installed. It is used for measuring the field gradient. It is one turn coil, and the length and the radius are 200mm and 22mm, respectively.

The measurements are performed in a vertical cryostat. The harmonic coils are moved vertically, and the position of the harmonic coil is measured by a magnetic scale. The revolution speed of the harmonic coils is 0.208Hz. The azimuthal position is measured by an angular encoder.

Table 2: Calculated multipole components along the return end (units·meter).

Multipole	
b_2	+1658.6
b_6	+1.329
b_{10}	-0.128

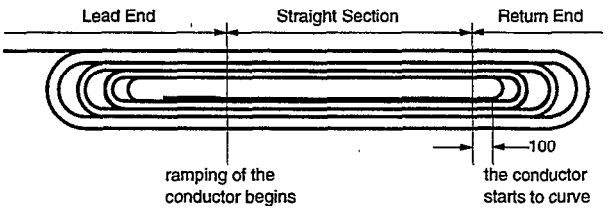

Figure 1: Definition of the lead end, straight section and return end of the 1-m model magnet.

3 FIELD MEASUREMENT RESULTS

3.1 *Multipole components as a function of position*

The harmonic coils were moved longitudinally be a constant amount d_z, and at each position, the measurements of ten rotations were performed with a constant current (Z-scan measurement). The summary of the measurements is shown in Tab. 3. The No.1-a magnet was only measured by the 200mm long harmonic coil. The No.2 and No.1-b magnets were measured by the both harmonic coils. The field

Table 3: Summary of Z-scan measurement.

Magnet	No.1-a	No.2	No.1-b
Harmonic coil	200	200	200
Current (A)	7000	7000/6400	7200
d_z (mm)	100	100	200
Harmonic coil	NA	25	25
Current (A)	NA	20	20
Harmonic coil	NA	NA	410
d_z (mm)	NA	NA	200

profiles along the No.1-b magnet, which were obtained by the 25mm long harmonic coil, are shown in Figs. 2 - 5.

In Fig. 3, the b_4 mainly comes from the lead end, it is negligible in the return end. In the both ends, the b_6 shows a large peaks of over 30units. The peaks are induced by the geometry of the ends and this is explained by the 3-D calculation. In Fig. 5, the b_{10} comes almost entirely from the straight section.

The multipole components along the straight section are summarized in Tab. 4. The data of the No.1-a magnet were obtained by the measurements of the 200mm long harmonic coil, and the No.2 and the No.1-b magnets were obtained by the 25mm long harmonic coil. The multipole coefficients were re-calculated at the radius of 17mm. The data in the table are plotted in Figs.6 and 7. In Fig. 7, the allowed multipoles, which are the design, are shown by arrows with he measurements. The b_6 and b_{10} of the magnets have offsets to the calculations, which are -0.6 to -1.5units for the b_6 and -0.1 to -0.15units for the b_{10}.

The multipole components along the magnet ends are summarized in tables 5 and 6. The coefficients are normalized by the quadrupole components at the straight section.

The lead end was measured for the No.1-a and the No.1-b magnets, and the return end was measured for the No.2 and the No.1-b magnets. In the lead end, large multipole components are b_4, b_5 and b_6. The values will be compared to the calculations. In the return end, the multipole components are calculated as shown in Tab. 2. Both the No.2 and No.1-b magnets show a good agreement to the calculation for b_6 and b_{10}. The No.2 magnet has a b_5 of -1.05 units·m while it is -0.03 for the No.1-b magnet.

Table 4: Multipole components along the straight section.

Magnet	No.1-a	No.2	No.1-b
Multipole	a_n/b_n (units)	a_n/b_n (units)	a_n/b_n (units)
3	-0.32/-1.60	1.55/-1.70	-0.55/-1.52
4	0.85/-1.12	-0.71/-1.34	0.49/-0.80
5	-0.27/-0.02	-0.56/-0.08	-0.37/-0.01
6	0.06/-0.04	-0.38/-1.67	0.53/-0.82
7	-0.02/0.02	0.13/0.05	-0.07/0.01
8	0.00/-0.05	-0.05/-0.30	0.02/-0.02
9	0.22/0.00	0.09/0.26	0.00/-0.01
10	-0.08/-1.01	0.01/-0.90	0.04/-0.93

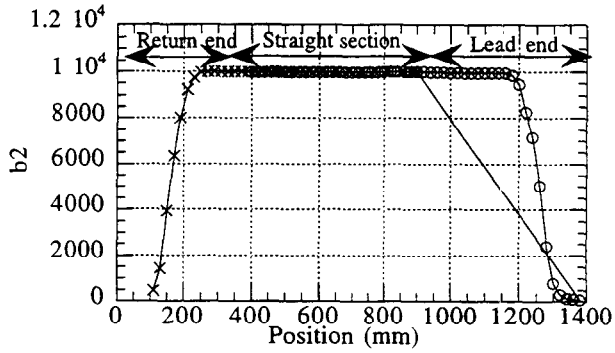

Figure 2: b_2 profile along the No.1-b magnet.

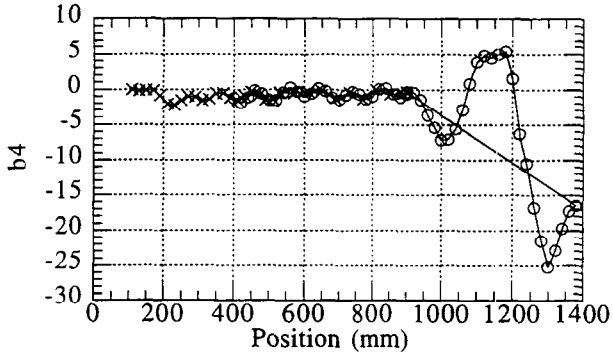

Figure 3: b_4 profile along the No.1-b magnet.

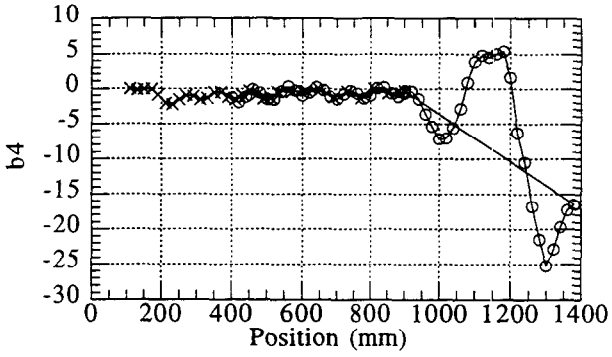

Figure 4: b_6 profile along the No.1-b magnet.

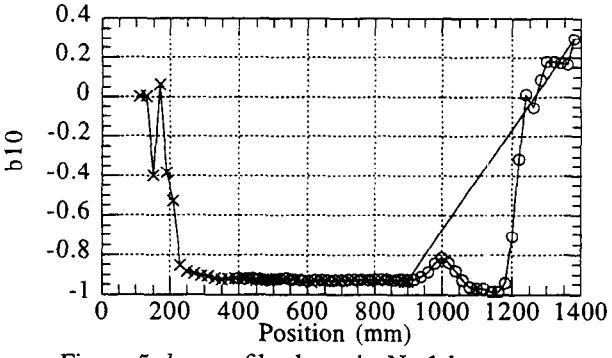

Figure 5: b_{10} profile along the No.1-b magnet.

The No.1-b magnet was measured at the injection stage by the 200mm long harmonic coil. The field quality at the magnet center is summarized in Tab. 7. The b_6 shows a difference of -1.9units from that at 7200A. This is due to the magnetization of the superconductor. The effect on b_{10} is small, and the difference is -0.05units.

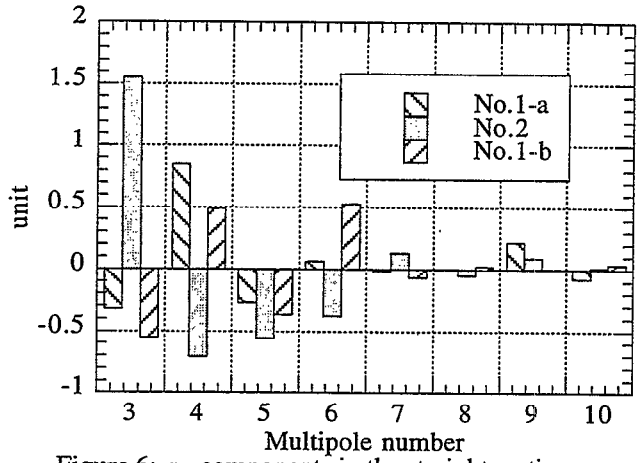

Figure 6: a_n components in the straight section.

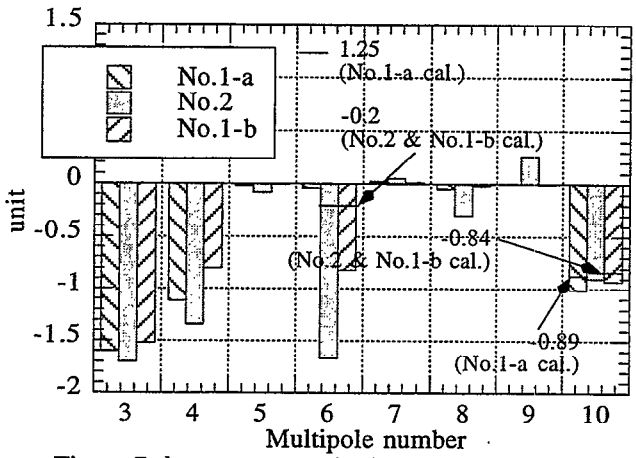

Figure 7: b_n components in the straight section.

3.2 *Current dependence of a multipole field*

The current dependence of the multipole components was measured at the magnet center with the 200mm long harmonic coil while stopping the current ramp. Before the measurements the magnet current was cycled from 50A to 7200A four times due to Z-scan measurements. The measurement scheme is shown in Fig. 8. In the scheme, we quenched the magnet at 7603A in order to measure the effect of the quench on the multipole components. After the quench, the measurements were performed at magnet currents of 410A and 7200A during up- and down-ramping.

In Figs. 9 to 12, the measured values of b_3 through b_6 are shown. The open circle symbols correspond to the measurements of the first cycle, and the cross symbols correspond to the measurements after the quench. As seen in Fig. 12, the b_6 has a hysteresis of 6units at the injection stage. The b_3 shows a change with magnet current, and the value of the change is -0.4units from 2000A to 7200A.

In the first cycle after the quench, large differences between pre- and post-quench multipole values were measured at 410A. The differences of b_4 and b_6 are -1.1 and -0.6units respectively. The differences became smaller with cycling the magnet current, and the multipole coefficients became close to the values before the quench. At 7200A, the quench effects on the multipoles were negligible.

Table 5: Multipole components along the lead end.

Magnet	No.1-a	No.1-b
Multipole	a_n/b_n	a_n/b_n
	(units·meter)	(units·meter)
2	0.00/2975	0.00/3077
3	0.14/0.31	-0.01/-0.07
4	0.15/-1.92	-0.02/-3.10
5	-0.39/-1.24	0.20/-0.06
6	0.05/2.10	0.04/2.47
7	-0.02/-0.04	-0.02/0.01
8	-0.04/0.02	0.02/0.04
9	0.08/0.21	0.02/0.00
10	-0.02/-0.27	0.01/-0.22

Table 6: Multipole components along the return end.

Magnet	No.1-a	No.1-b
Multipole	a_n/b_n	a_n/b_n
	(units·meter)	(units·meter)
2	0.00/1690	0.00/1693
3	0.22/0.19	-0.14/0.07
4	-0.03/0.18	-0.18/-0.24
5	0.02/-1.05	0.01/-0.03
6	-0.07/1.00	-0.05/1.03
7	0.02/-0.04	-0.01/-0.01
8	0.01/-0.11	-0.01/-0.01
9	0.04/-0.18	0.00/-0.00
10	0.00/-0.13	0.01/-0.12

Table 7: Multipole components at the injection stage.

Magnet	No.1-b
Multipole	a_n/b_n
	(units)
3	-0.25/-0.24
4	-0.74/0.18
5	-0.27/0.15
6	-0.07/-2.74
7	-0.12/0.17
8	0.18/0.01
9	-0.04/-0.03
10	-0.07/-0.98

4 SUMMARY

The field quality of the two 1-m model magnets can be summarized as follows:

Straight section

- The sextupole and octupole components are -1.6 to 1.7units.
- The b_6 has an offset of -0.6 to -1.5units to the design.
- The b_{10} has an offset of -0.1 to -0.15 units. In the No.3 magnet, b_{10} is designed to be 0.001units while the previous magnets have the b_{10} of -0.84units. The b_{10} is expected to be within 0.1units.

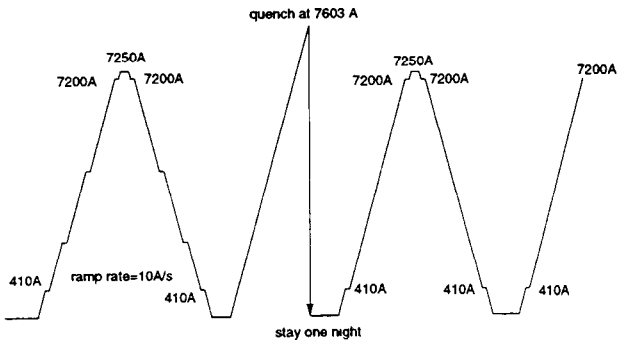

Figure 8: The measurement scheme of the current dependence.

Return end

- The allowed multipoles are almost consistent with the design.
- In the new design, the b_6 and b_{10} are 0.003 and -0.037units m, respectively.

Lead end

- Compared to the return end, the b_4 and b_6 are relatively large. This is due to the wiring of the conductor out of the coil. The wiring position of the conductor will be re-designed.

Current dependence

- The b_6 has a hysteresis of 6units at the injection stage.
- In the first ramp after the quench, the sextupole to the dodecupole components show differences of 1unit to the values before quench at the injection stage.

5 REFERENCES

[1] A. Yamamoto, K. Tsuchiya, et al. "Design study of a Superconducting Insertion Quadrupole Magnet for the Large Hadron Collider", IEEE Trans. Applied Superconductivity, Vol. 7, No. 2, pp. 747-750 (1997).

[2] T. Nakamoto, et al, "Quench and Mechanical Behavior of an Insertion Quadrupole Model for LHC", presented in ASC-98, Palm Desert, (1998).

[3] N. Ohuchi, et al, "Magnetic Field Measurements of a 1-m Long Model Quadrupole Magnet for the LHC Interaction Region", presented in ASC-98, Palm Desert, (1998).

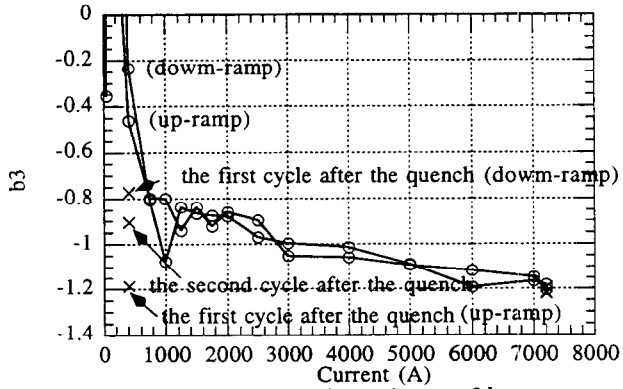

Figure 9: Current dependence of b_3.

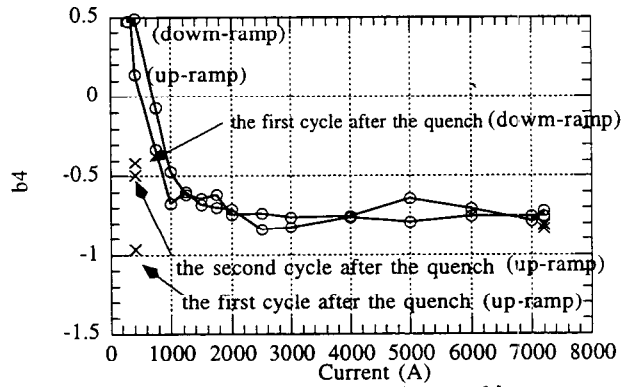

Figure 10: Current dependence of b_4.

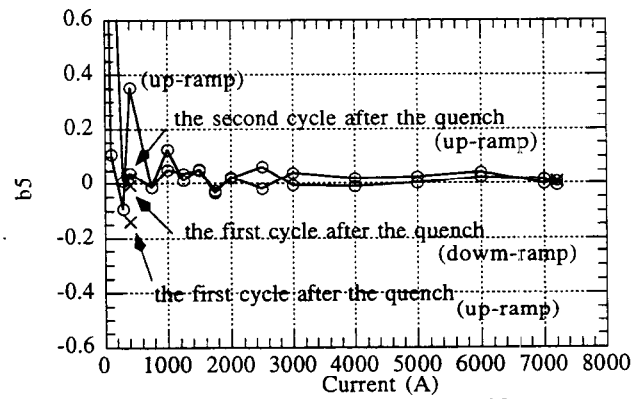

Figure 11: Current dependence of b_5.

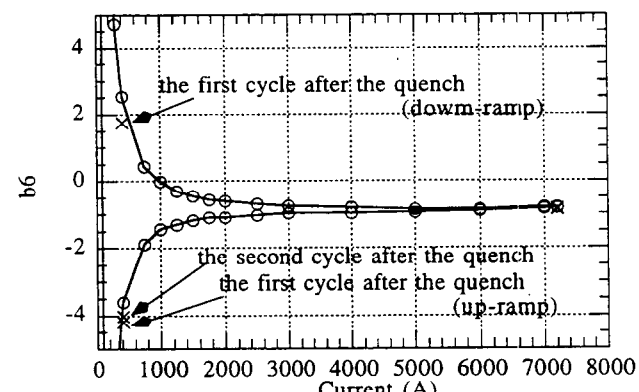

Figure 12: Current dependence of b_6.

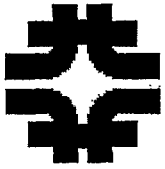

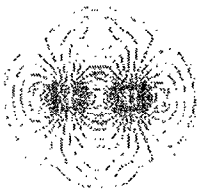

Workshop on LHC IR Correction Systems

Field Quality in FNAL Model Magnets

P. Schlabach

6 May 1999

Outline

- **Field quality**
  - **apparatus and analysis**
  - **transfer function and field angle**
  - **evolution of the body harmonics**
  - **end field**
- **Studies of the ability to modify the design field with tuning shims**

Apparatus and Analysis

- measurements made in vertical dewar using rotating coil
  - probes
    - 0.25 m length, 2.5 cm OD (HGQ01)
    - 0.82 m length, 4.1 cm OD
    - 2 dipole, 2 quad bucking coils, tangential main coil
- probe signals, current read by 6 HP3458 DVMs simultaneously triggered by angular encoder
- probe centered using feed down of quadrupole to dipole
- 17 mm R_{ref}

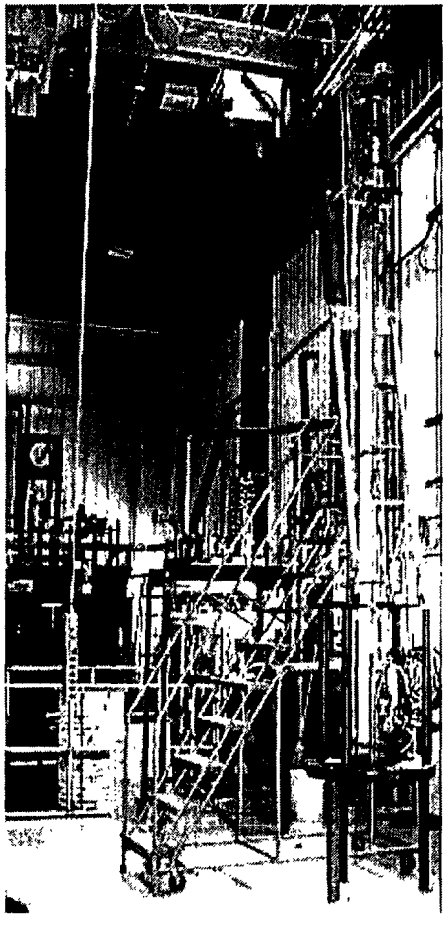

Apparatus and Analysis

- Improvements in apparatus have been made
  - –longer, larger radius probe improves signal-noise
  - –better centering bearings
  - –larger radius, multi-sectioned driveshaft separated by flexible couplings
- Improved measurements

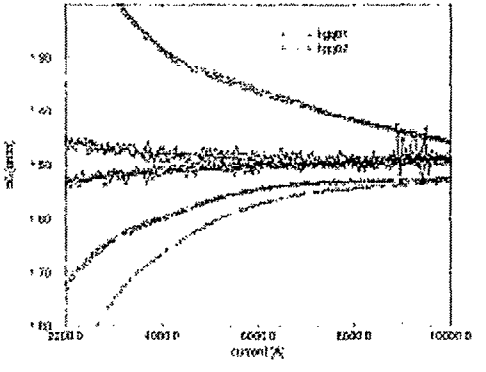

Transfer Function and Field Angle

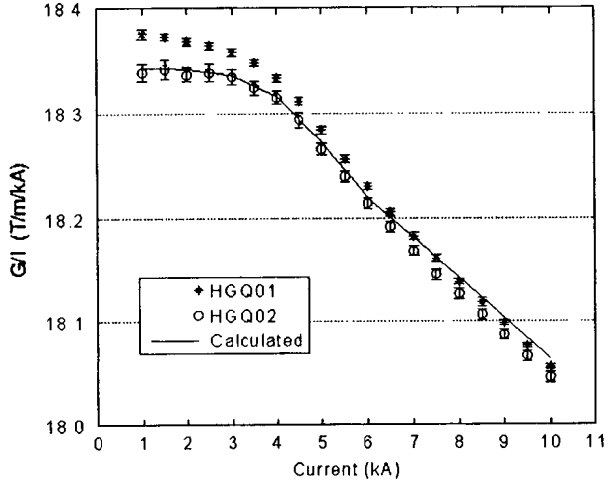

- Transfer function
  - G/I=18.35 T/m/kA at low currents
  - Iron saturation effect reduces transfer function by 2% at nominal current

Transfer Function and Field Angle

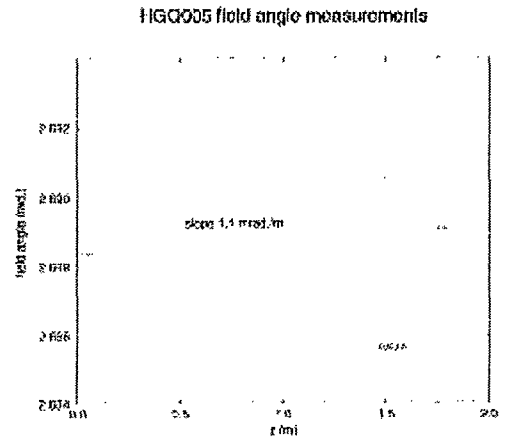

Field angle

Magnet twist (mrad/m):

	mech.meas.	magn.meas.
HGQ01	6	7
HGQ02	0.6	<1
HGQ03	1.0	1
HGQ05	0.9	1.1

Next steps:

- twist reduction below 0.3 mrad/m → tooling optimization, yoke/skin welding procedure

Field Harmonics

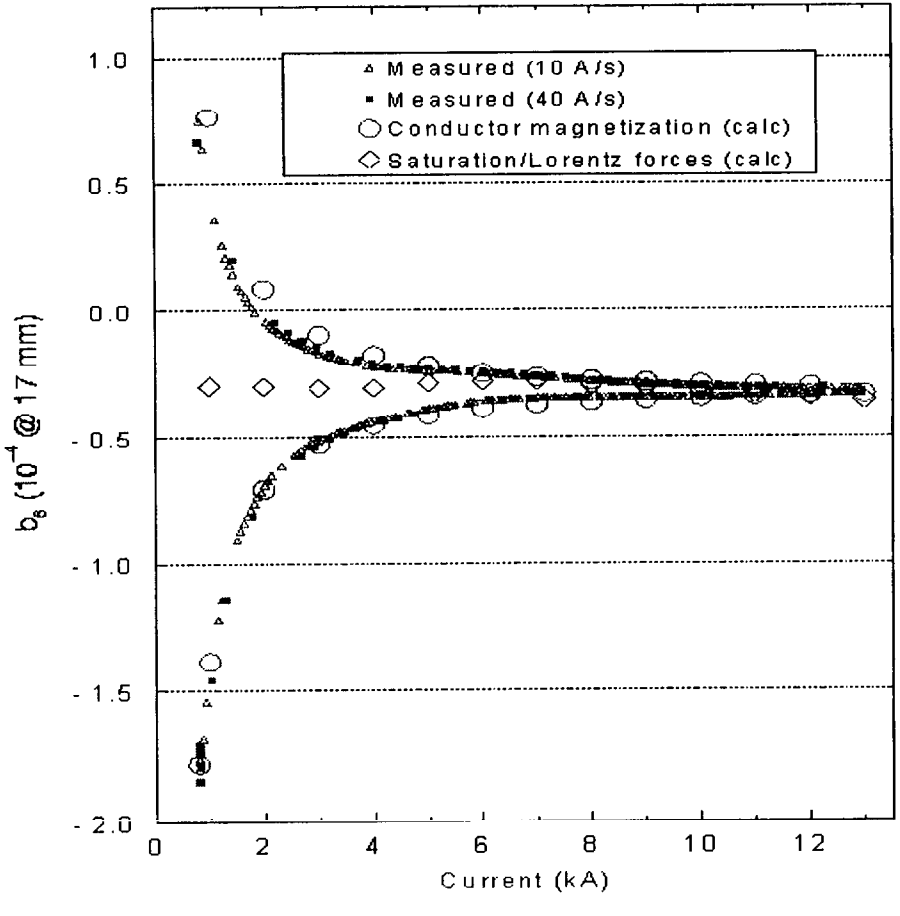

- Iron saturation and Lorentz force effects on b_6 at high currents are small

  Coil magnetization effect on b_6 at low currents is in a good agreement with calculations

- There is no noticeable effect of coil magnetization, iron saturation and Lorentz force on b_{10}

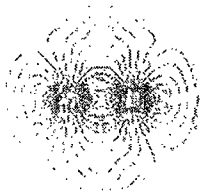

Measured Field Harmonics Summary

Field	Measured Field Harmonics (6kA)				Ref. Table v2.0	
Harm.	HGQ01	HGQ02	HGQ03	HGQ05	Uncert.	Random
b3	0.36	-0.70	1.04	0.72	0.3	0.8
a3	0.27	0.55	-0.30	0.12	0.3	0.8
b4	0.26	0.18	0.14	0.00	0.2	0.8
a4	2.00	0.53	0.32	0.19	0.2	0.8
b5	-0.29	0.09	-0.34	-0.04	0.2	0.3
a5	0.02	-0.17	0.26	0.05	0.2	0.3
b6	-3.91	-1.54	-1.02	-0.30	0.6	0.6
a6	-0.02	0.03	0.07	-0.03	0.05	0.1
b7	-0.08	-0.01	-0.06	0.01	0.05	0.06
a7	-0.05	0.00	-0.03	0.01	0.04	0.06
b8	0.06	0.01	0.00	0.00	0.03	0.05
a8	0.02	0.02	0.03	0.00	0.03	0.04
b9	0.04	0.00	0.00	0.00	0.02	0.03
a9	0.01	-0.01	0.01	0.00	0.02	0.02
b10	0.04	-0.01	0.00	0.00	0.02	0.03
a10	-0.12	-0.09	-0.05	0.01	0.02	0.03

- Harmonics measured at magnet center
- Steady improvement in field quality
  - improvements in coil fabrication procedure have produced coils closer to design values
- HGQ05 field harmonics smaller than reference table except for b_3

Predicted Field Based on As-Built Cross-Section

	HGQ01	HGQ02	HGQ03	HGQ05
a4	1.27	0.94		
b6	-4.24	-2.86	-1.39	-0.08
a8	0.02	0		
b10	-0.14	-0.09	-0.04	0.01

- adjustments made to
  - curing cavity size
  - curing pressure
  - cable insulation scheme
  - bare cable size
- coil shim thickness reduced by a factor of 2 from each magnet to the next
- more uniform coil size and modulus

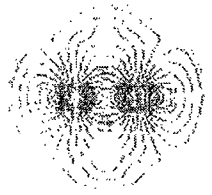

Summary of Body Field Harmonics of the 4 Models

field	Measured – Calculated Field Harmonics						Ref. Table v2.0	
harm.	HGQ01	HGQ02	HGQ03	HGQ05	Mean	RMS	Uncert.	Random
b3	0.36	-0.70	1.04	0.72	0.36	0.76	0.3	0.8
a3	0.27	0.55	-0.30	0.12	0.16	0.36	0.3	0.8
b4	0.26	0.18	0.14	0.00	0.15	0.11	0.2	0.8
a4	0.73	-0.41	0.32	0.19	0.21	0.47	0.2	0.8
b5	-0.29	0.09	-0.34	-0.04	-0.15	0.20	0.2	0.3
a5	0.02	-0.17	0.26	0.05	0.04	0.18	0.2	0.3
b6	0.33	1.32	0.37	-0.22	0.45	0.64	0.6	0.6
a6	-0.02	0.03	0.07	-0.03	0.01	0.05	0.05	0.1
b7	-0.08	-0.01	-0.06	0.01	-0.04	0.04	0.05	0.06
a7	-0.05	0.00	-0.03	0.01	-0.02	0.03	0.04	0.06
b8	0.06	0.01	0.00	0.00	0.02	0.03	0.03	0.05
a8	0.00	0.02	0.03	0.00	0.01	0.02	0.03	0.04
b9	0.04	0.00	0.00	0.00	0.01	0.02	0.02	0.03
a9	0.01	-0.01	0.01	0.00	0.00	0.01	0.02	0.02
b10	0.04	-0.01	0.00	0.00	0.01	0.02	0.02	0.03
a10	0.02	0.00	-0.01	0.00	0.00	0.01	0.02	0.03

- Correct the measured field by the as-built calculations so we can use the ensemble of magnets to predict the behavior of the ensemble of production magnets
  - assumes coil size varations are controlled during production
- mean and RMS for 4 magnets are mostly at or below the values in the reference table

Summary of Body Field Harmonics of the 4 Models

- AP studies show reference harmonics yield required dynamic aperture
- HGQ05 as-built field corrections are very small
- HGQ05 field compares favorably with reference table
- After correction for production effects, the mean and RMS of the harmonics for the 4 models compares favorably with the reference table

the Magnet Test Facility

fermilab

End Field Measurement

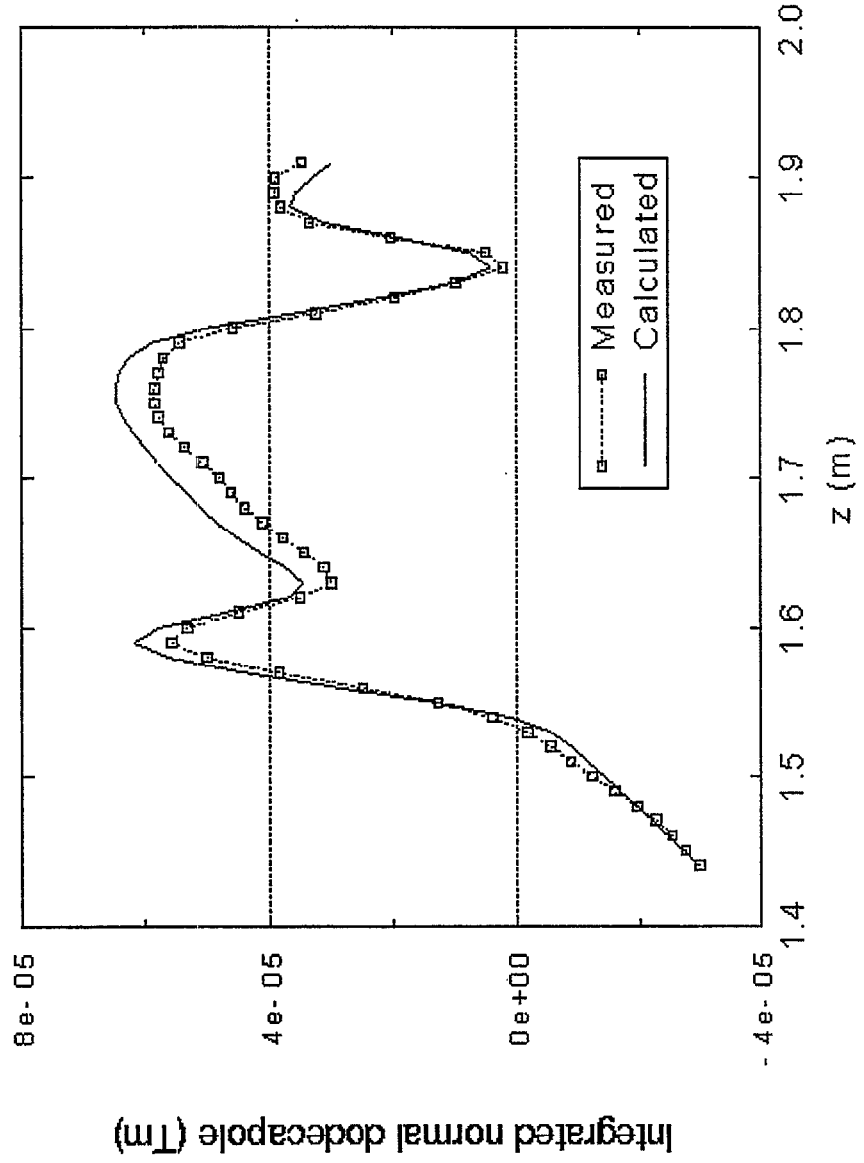

End Harmonics Optimization

	End Design Field				Ref. Table v2.0					
Field	Lead end		Return end		Lead end			Return end		
harm	v1.1	v2.0	v1.1	v2.0	mean	uncert	sigma	mean	uncert	sigma
b_6	6.6	4.6	1.2	0.1	2.0	2.0	0.75	0.0	1.0	0.75
b_{10}	-0.3	-0.1	-0.2	-0.1	-0.2	0.2	0.1	-0.2	0.2	0.1
a_6	-0.5	-0.1			0.0	0.5	0.15	-	-	-
a_{10}	-0.1	0.0			0.0	0.1	0.1	-	-	-
	[1.31, 2.03]		[-0.57, 0.25]		reference integration interval					
v1.1	*HGQ02, HGQ03*									
v2.0	*optimized end design*									

- end field quite sensitive to shimming of magnet end regions during production
- optimized end design in HGQ06

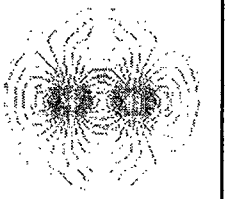

800 kA n	up/down ramp average	up-down ramp
b 3	0.804	0.047
b 4	0.056	0.031
b 5	-0.054	-0.033
b 6	-0.488	-2.825
b 7	0.007	0.005
b 8	-0.009	0.000
b 9	0.000	-0.004
b10	0.012	0.047
b11	0.001	0.000
b12	0.000	0.000
b13	-0.002	-0.001
a 3	0.129	-0.001
a 4	0.251	0.209
a 5	0.079	-0.008
a 6	0.000	0.084
a 7	0.017	-0.007
a 8	-0.005	0.008
a 9	0.001	-0.001
a10	-0.005	0.004
a11	0.000	0.002
a12	0.000	0.000
a13	-0.004	-0.002

Injection Field

- conventional wisdom is that the IR quads "don't matter" at injection
- should they matter these are the harmonics
- there are also changes ("drift") in various harmonic components while sitting at injection

the Magnet Test Facility

fermilab

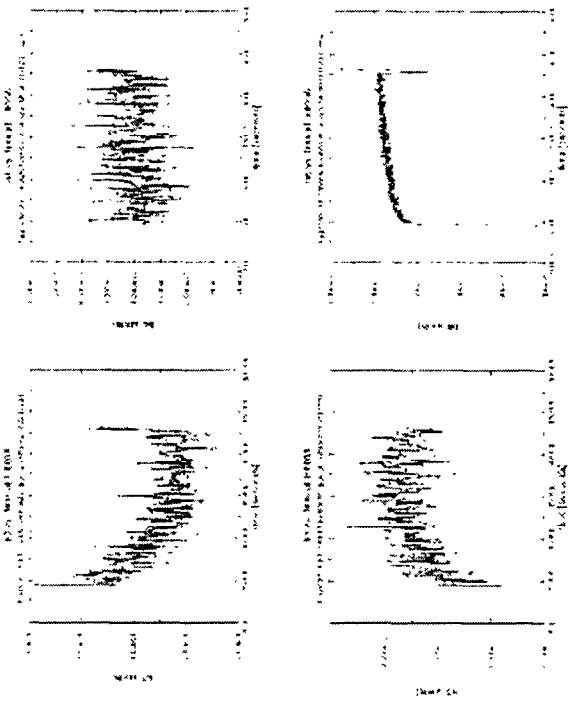

the Magnet Test Facility

fermilab

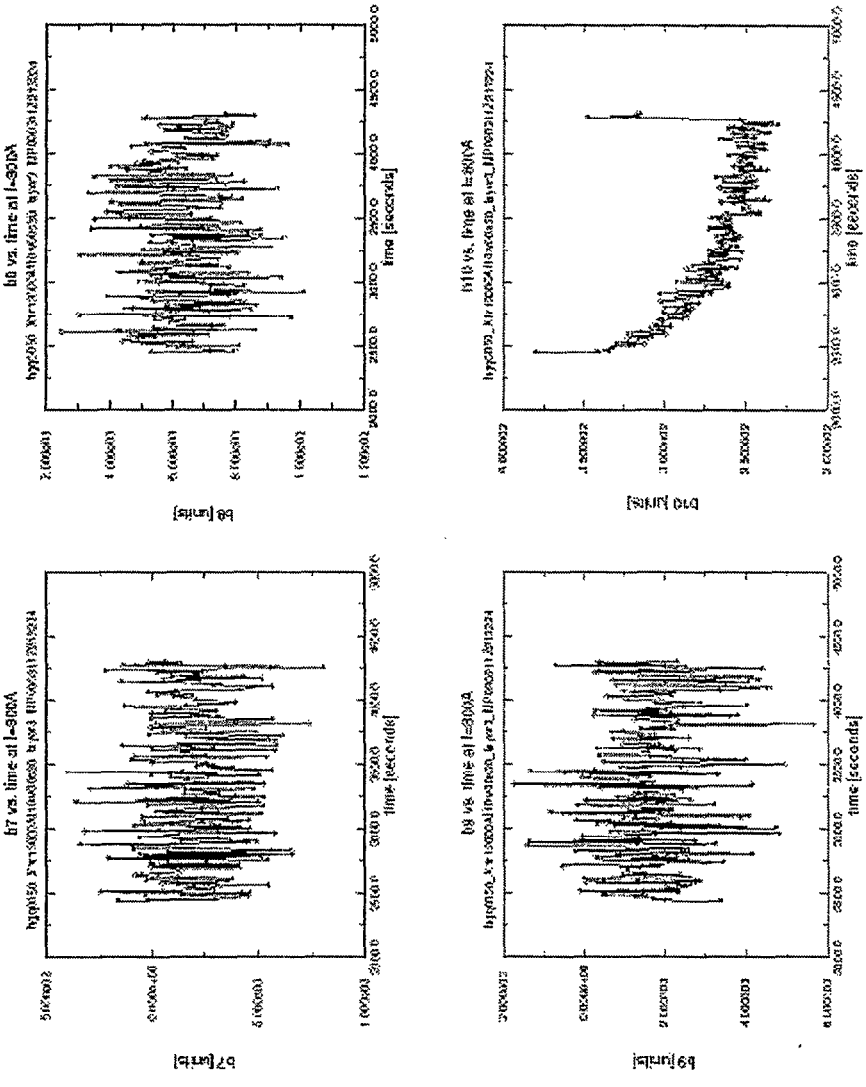

the Magnet Test Facility

fermilab

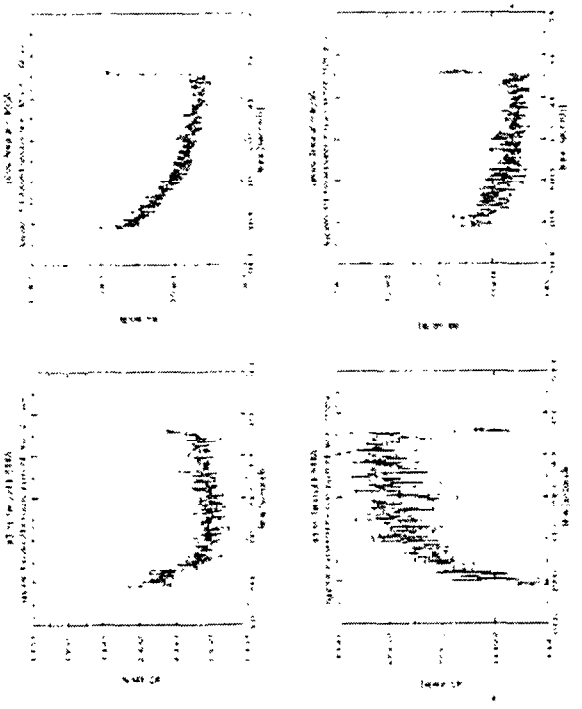

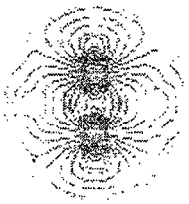

the Magnet Test Facility

fermilab

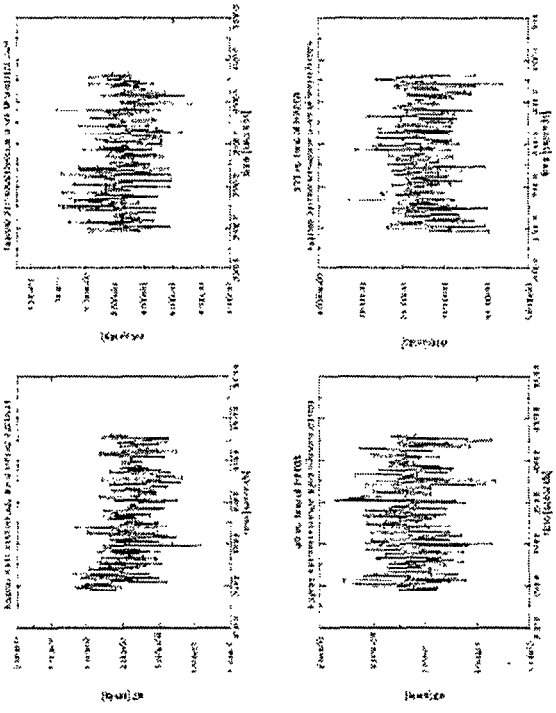

Field Tuning Using Shims

- magnet cross section contains 20 mm holes for insertion of field tuning shims
- nominal design has each half filled by iron half by non-magnetic material
- changing the thickness of magnetic relative to non-magnetic material "tunes" the field
- the various shim positions tune different harmonic components

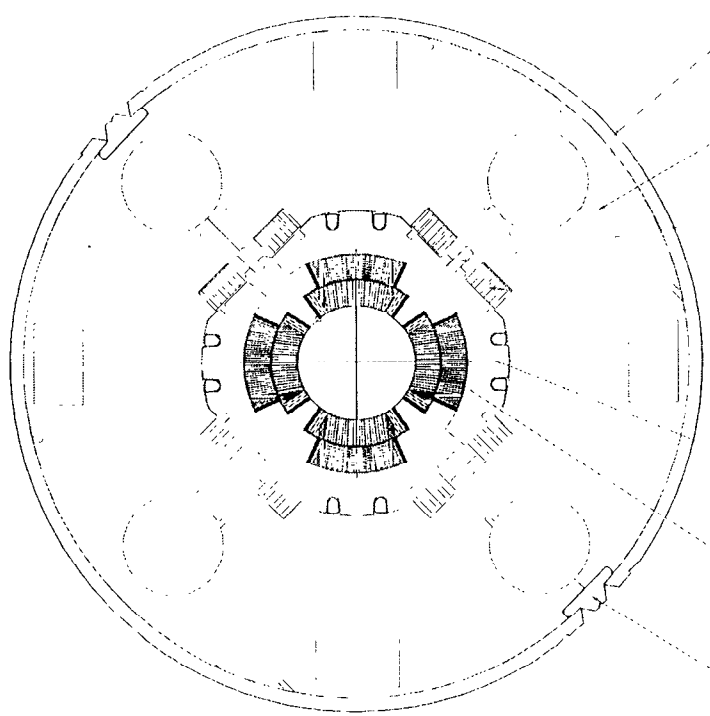

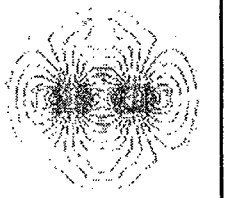

Tuning Shims: measured, predicted field changes

- after completion of cold testing, HGQ03 was used to test our ability to tune the field
- a shim pattern was selected which would tune skew octupole (a_4) leaving other harmonics unchanged
- required shims of 4.1, 15.9 mm nominal thickness
- expected changes:
  - $-a_4$ -2.9 units
  - –other harmonics "unchanged"
- measured changes:
  - $-a_4$ -3.1 units
  - –small changes in sextupole

n	normal	skew
3	0.34±0.01	-0.19±0.01
4	0.05±0.01	-3.13±0.01
5	0.01±0.01	0.01±0.01
6	0.04±0.02	0.02±0.02

Tuning Shims: axial variation

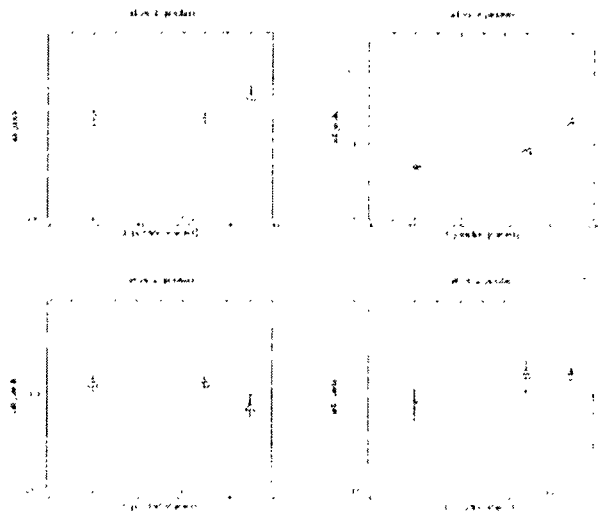

- skew octupole varies by 0.25±0.01 units from one end of the magnet to the other
- measured variation in other harmonics consistent with no variation at the 1-2 σ level

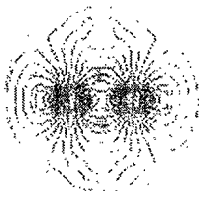

Change in Field with Shim Thickness

- two sets of shims allow us to calculate Δb_n (Δa_n)/ Δf
  - f is the thickness of the magnetic part of the shim

	calculated		measured	
n	$\Delta b_n/\Delta f$	$\Delta a_n/\Delta f$	$\Delta b_n/\Delta f$	$\Delta a_n/\Delta f$
3	0.51	0.00	0.48	0.00
4	0.14	-0.08	0.10	-0.07
5	0.01	-0.03	0.01	-0.02

Summary of Studies of Tuning Shims

- We have targeted a tuned field and achieved it with 0.2-0.3 units accuracy based on calculations of the field change as a function of shim thickness
  - In practice, better accuracy would be achieved as we would use the measured field change as a function of shim thickness and use these functions to choose shim sizes
  - Accuracy set by the accuracy of magnetic measurements which in turn is a function of how much current we can safely put through the magnet
- The variation in the tuned field along the length of the magnet is consistent with zero except for the skew octupole which varies by 0.25 units
- No variation in the field due to variations in shim manufacturing is measured
- We have what we need (including the measured change in field as a function of shim thickness) to use tuning shims except for the correlation between field of collared coil measured warm and field of cold cryostated magnet

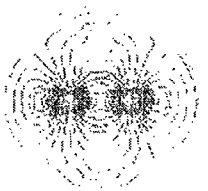

Summary of Field Harmonics of the 4 Models

- Field quality in HGQ05 adequate for a production magnet
- Model magnet ensemble field quality adequate, after correcting for production defects which we can control (and have in HGQ05)

* MQX field quality adequate without resorting to tuning shims

- End field quality will improve with new end design of HGQ06

ASPECTS OF THE PERTURBATION BY b_{10}

J.-P. Koutchouk,
CERN, Geneva, Switzerland

Abstract

Following the proposal to mix the US and KEK magnets to overcome the consequences a too large in error table v2.0, a crash study was initiated at CERN. Its results show that the of table v2.0 is potentially dangerous and that it must be reduced below 0.1 units.

1 INTRODUCTION

The effect of = 0.2 units was considered from different point of views: feed-down on lower-order multipoles, dynamic aperture at 10 turns and frequency map analysis.

2 FEED-DOWNS OF b_{10}

As noted by J. Shi'in his study of global correction [1] and by S. Fartoukh [2], most likely acts by feed-down to lower orders. It is in fact easy to calculate by hand the feed-down due to the off-axis orbit caused by the crossing angle. In Table 1, we assume a beam displacement of 6 mm in the quadrupole (while the real displacement ranges from 4.5 mm to 7 mm at the entrance and exit of the triplet). It is

	n	n	n	a_n	a_n	a_n
3	0+**.01**	.51	1.00	0-**.01**	.51	1.00
4	0+**.04**	.29	.57	0	.29	.57
5	0+**.17**	.19	.38	0+**.17**	.19	.38
6	0+**.49**	.50	.19	0	.10	.19
7	0+**.92**	.05	.06	0-**.92**	.05	.06
8	0+**1.12**	.02	.03	0	.02	.03
9	0+**.79**	.01	.01	0+**.79**	.01	.01
10	.25	.03	.01	0	.01	.01

Table 1: KEK Table v2.0 with the feed-downs of added to the systematics, for an horizontal displacement of +6 mm; the fields are expressed in units at 17 mm

clear that a systematic = .2 produces lower-order perturbations often significantly larger than those due to the design and uncertainties. Just from inspection and knowing that is the second limit after [3], it is easy to conclude that shall not exceed 0.1 or even less.

3 INFLUENCE OF b_{10} ON THE DYNAMIC APERTURE

Mixed or unmixed layouts of the triplet quadrupoles were tested for dynamic aperture. This work, carried out by F. Schmidt [4] was done in the following way: the uncertainty is added to the systematic imperfection in such a way as to maximize it; all quadrupoles are then allocated the same multipole errors calculated in the above mentioned way. Tracking is carried out over 10 turns, 6D. The random part of the errors is not included to disentangle the pure effect of systematic . Furthermore it is known [3] that random is the next limit after and that the US and KEK tables show very different values for random while they would be expected to be the same; they have indeed be equalized in the latest version of the tables. It is very clear on figure 1

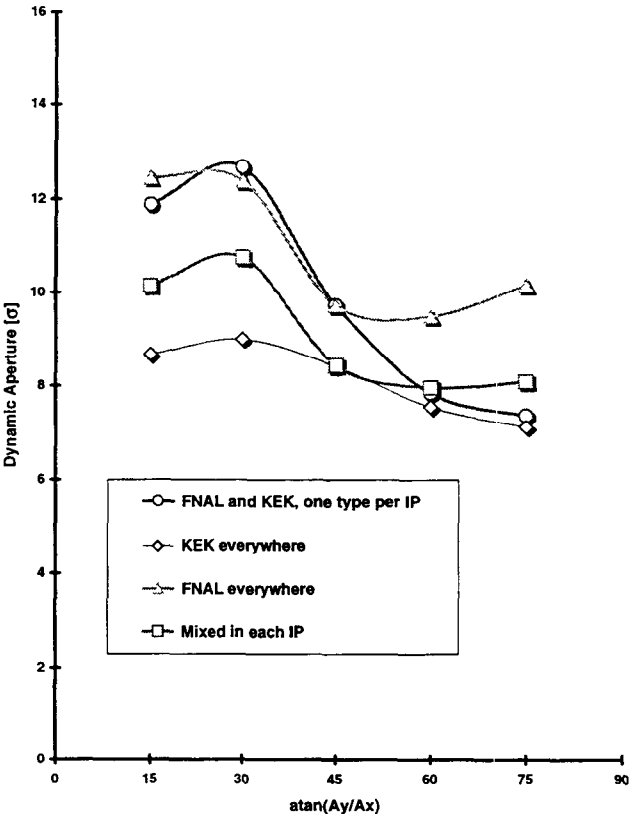

Figure 1: Dynamic aperture versus initial amplitude ratio for various triplet scenarios

that = .2 causes a loss of dynamic aperture of 2 , i.e. 20%, **whatever the scenario, mixed or not mixed.**

4 SIGNATURE OF b_{10} ON FREQUENCY MAPS

Another approach to the question is the qualitative inspection of the frequency maps calculated for the various scenarios. This work was carried out by I. Papaphilippou [5]. A very large number of initial conditions, characterized by the radius of the circle in the , plane are tracked for 1000 turns, 4D. The tunes are calculated over the last 100 turns

and displayed as a function of amplitude. The range of amplitudes extends to 15 , to take into account both the short tracking time and the missing 3rd degree of freedom. Here again, only the systematic and uncertain imperfections are considered. In the scenario where KEK magnets are installed in all IR's, the perturbation of the frequency space is very pronounced. 10 particles are trapped by the (1,-1) sub-resonance. From experience, these particles are expected to be unstable. If KEK magnets are installed in half of the IR, the footprint is smaller though unstable 10 particles are still expected. In the mixed scenario, the footprint shrinks drastically for medium amplitude particles. However large amplitude particles are still attracted by the (1,-1) resonance much more than in the case where systematic vanishes (FNAL only).

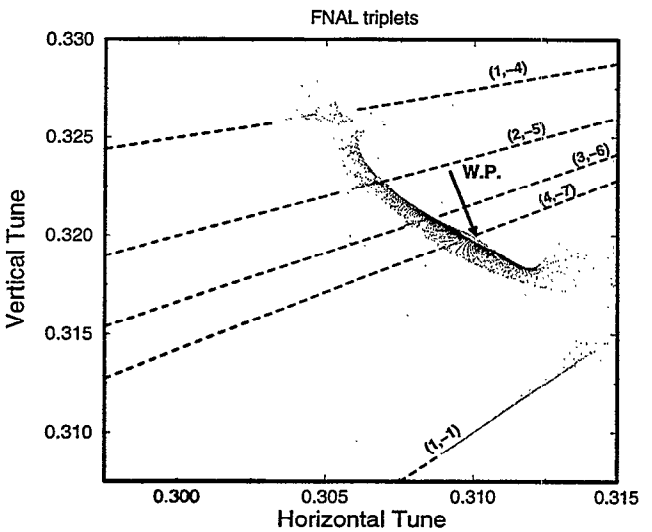

Figure 2: Frequency map for FNAL triplets only

Given two important missing ingredients in the tracking: the modulation of the parameters and the beam-beam interaction, it would be risky, at this stage, to accept such a distortion of the dynamics. Furthermore, the effect are systematic and therefore the phase advance between the IR's matter. We do not know whether the present situation is a best or a worst case. It will not be maintained anyway as the tune split is changing to maximize the dynamic aperture at injection.

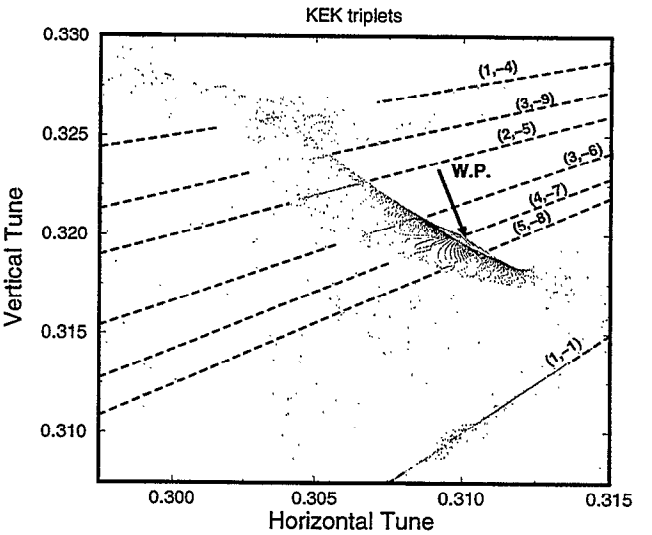

Figure 3: Frequency map for KEK triplets only

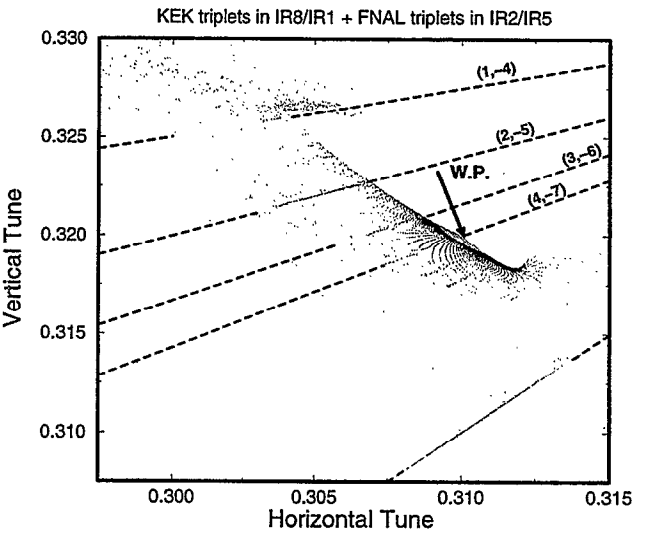

Figure 4: Frequency map for FNAL and KEK triplets not mixed

5 CONCLUSION: TARGET b_{10}

If we assume that the dynamic aperture is only related to , it is possible to scale exactly to recover the 2 loss. Because of the crossing angle, we further have to assume that either acts as such or that it acts through a feed-down, say . The scaling is such that, if $_n$ is multiplied by , the dynamic aperture is divided by $^{/(n-2)}$. To recover the 20% loss, the scaling shows that = .2 should be decreased by a factor of 4, i.e. the target = .0 . This value seems reasonable if compared to the measured harmonics of all FNAL models which are all weaker [6]. This estimate is of course rough and tracking would be required if the target would be difficult or expensive to reach. It is however consistent with the requirement stemming from the calculation of feed-downs.

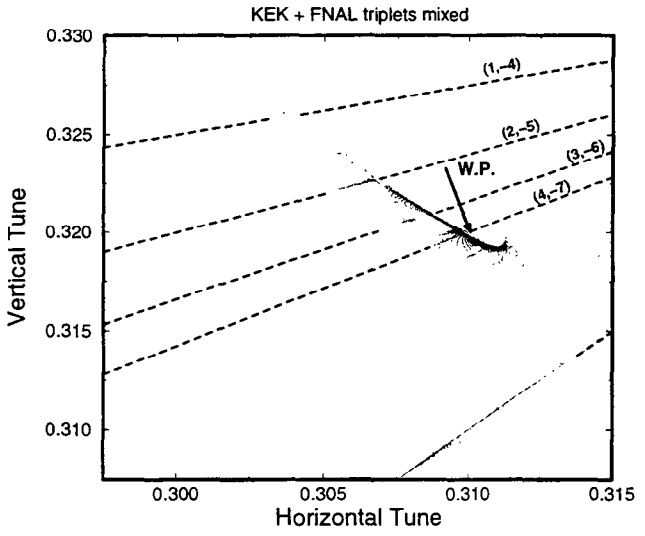

Figure 5: Frequency map for the mixed case

6 REFERENCES

[1] J, Shi, PAC99 and this workshop.
[2] S. Fartoukh, private communication, Cern, April 1999.
[3] J. Wei *et al.*, PAC99 and W. Fischer, this workshop.
[4] H. Grote and F. Schmidt, 'LHC dynamic aperture studies at collision energy including beam-beam and triplet errors', Cern 1999, to be published.
[5] I. Papaphilippou, Contribution to the crash study on b_{10}, unpublished, Cern, April 1999.
[6] G.L. Sabbi *et al.*, PAC99.

UNCERTAINTIES IN PREDICTING AND MEASURING FIELD ERRORS*

A. Jain# and P. Wanderer
Brookhaven National Laboratory, Upton, NY 11973-5000, USA

Abstract

Sources of random and systematic field errors in superconducting magnets are described briefly. Predicting such errors in a series production has to rely upon data in prototypes, data in similar magnets, or calculations. The case of D1 insertion dipoles for the LHC perhaps represents the most favorable situation, as these magnets will be almost identical to the RHIC arc dipoles. Uncertainties in predicting field errors for this "best case" are illustrated using data in RHIC dipoles. Once the magnets are built and measured, field quality uncertainties could result from measurement errors and changes in the magnets with quenches and thermal cycles. Such uncertainties are also discussed for the case of RHIC arc dipoles.

1 TYPES OF FIELD ERRORS

The field errors in magnets are generally expressed in terms of the normal (b_n) and skew (a_n) harmonics in a series expansion of the field given by

$$B_y + iB_x = B_0 \times 10^{-4} \sum_{n=1}^{\infty} (b_n + ia_n) \left(\frac{x+iy}{R_{ref}} \right)^{n-1} \qquad (1)$$

where B_0 is a normalizing field and R_{ref} is a reference radius, chosen to be 17 mm in the case of LHC. In this paper, a value of 25 mm will be used frequently for data from RHIC arc dipole magnets. Ideally, for a $2m$-pole magnet, all coefficients other than $n = m$ should vanish. In practice, several of these coefficients may be non-zero due to design or construction limitations.

For a given production series, the average value of each harmonic will be referred to as the *mean* or *systematic* value of that harmonic. Similarly, the standard deviation of each harmonic over the entire production gives an indication of the extent of variation from one magnet to another and will be referred to as the *random* value of the harmonic. After the magnet production is completed and all the magnets are measured, it is no longer necessary to describe the ensemble of magnets with these statistical parameters for tracking, since the individual data are available, although it may still be a convenient and useful description.

At the pre-production stage, the systematic and the random values of the harmonics are not known. In order to evaluate the impact of field quality that is likely to be achieved in the magnets, one has to make a reasonable estimate of these parameters. Purely based on a good design, the *systematic* values of all the terms unallowed by symmetry, as well as most of the harmonics allowed by symmetry, are *expected* to be zero. There can be some exceptions to this. For example, it may not be possible to make some higher order allowed terms zero with the available number of adjustable parameters in the coil design. Similarly, in the RHIC arc dipoles, a systematic non-zero value of unallowed skew quadrupole is expected at high fields due to an asymmetric placement of the cold mass in the cryostat [1]. Another example of an anticipated non-zero systematic value of an unallowed harmonic is shown in Fig. 1 for the normal 16-pole term in the 13 cm aperture QRK quadrupoles in RHIC, before the magnetic tuning shims [2] are inserted (R_{ref} = 40 mm).

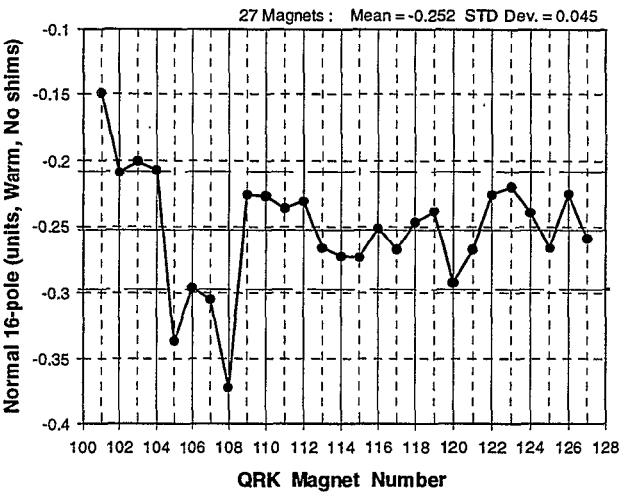

Fig. 1: Example of a non-zero systematic unallowed term.

Although one would like to see the systematic errors in the actual production match the expectations based on design, very often this is not the case due to various reasons. In order to cover such a situation, another parameter, called *uncertainty in the mean*, was used at RHIC. This is an estimate of how much the true systematic value in a given production could deviate from the expected value. This uncertainty is a complex function of tolerances in parts, quality control, production techniques employed, etc.

2 SOURCES OF FIELD ERRORS

2.1 Sources of Random Errors

Random field errors result from random variations in the dimensions of various parts and in other assembly parameters. Other sources of random errors are variations in superconductor parameters, such as magnetization. Such errors can generally be kept to very small values by good quality control at all stages of magnet production. Some lowest order harmonics (both allowed and

* Work supported by the US Department of Energy under contract no. DE-AC02-98CH10886.

jain@bnl.gov

unallowed) may be quite sensitive to construction errors, and may be hard to control. If deemed unacceptable, such errors can be reduced by some type of post construction correction, such as tuning shims [2]. For example, the standard deviation of normal sextupole in as-built QRK quadrupoles for RHIC was 2 units (R_{ref} = 40 mm), but was reduced to 0.4 unit with tuning shims. Changes in the magnet field quality due to thermal cycles and quenches (see Sec. 5.1.4) can also contribute to random errors.

2.2 Sources of Systematic Errors

Systematic errors could be anticipated, or unanticipated. Sources of such errors include:

2.2.1 Design limitations

These are the systematic errors that are anticipated from the design. For example, some high order allowed harmonics may not be made zero with the available number of wedges. Similarly, some unallowed integral harmonics may be non-zero due to inherent asymmetries in the ends. Another example mentioned earlier is the skew quadrupole at high fields in the RHIC arc dipoles.

2.2.2 Calculation limitations

These are generally the low order allowed terms which may result, for example, due to inaccurate modeling of how various turns of the conductor stack up in the coil winding process. Also, there may be some errors in predicting harmonics at high fields due to iron saturation, Lorentz forces, etc.

2.2.3 Tolerances in parts

There may be systematic differences between the "design" and "as-built" parts, within the specified tolerances. These would result in systematic field errors.

2.2.4 Distortions during assembly process

The assembly process could introduce distortions that produce both allowed and unallowed harmonics [3]. For example, the RHIC arc quadrupole yokes were assembled the same way as dipoles, which introduced a large systematic normal octupole harmonic. This was corrected by using asymmetric midplane shims [4].

The systematic errors can be reduced by a careful design, design iterations based on prototypes, small low-cost mid-production corrections if necessary, and post-production corrections such as tuning shims.

3 PREDICTING FIELD ERRORS

Before the magnets are actually built, predicting field errors is of considerable importance from the point of view of tracking studies. Magnet design, production strategies, as well as the correction schemes that may be necessary in the accelerator depend on the outcome of such studies. Obviously, the goal is to arrive at a set of field harmonics, each characterized by a *mean*, *standard deviation* and an *uncertainty in the mean*, which is as close to reality as possible. Too optimistic expectations may not be met in the actual production and could lead to unforeseen loss of performance. On the other hand, expectations of larger harmonic errors may be easily met in production, but could lead to inclusion of correctors that may not really be required. A balancing act in this process involves using as much design and construction experience as possible in making a list of expected harmonics. Also, it will be prudent to reevaluate any large expected field errors if initial tracking studies suggest undesirable effects on the beam. In such cases, every effort should be made to improve the expectations. This could be done by cutting into any unduly comfortable safety margins, and/or by chalking out a contingency plan (small adjustments to shims to fix systematic errors, use of tuning shims to fix both systematic and random errors, etc.) to deal with any large harmonics encountered during production. Such a contingency plan essentially amounts to reducing the "uncertainty in the mean" in the table of expected harmonics. If individual magnets are shimmed, then the random errors are also expected to be reduced.

3.1 Uncertainties in Predicting Field Errors

A key factor in making good predictions of field errors is the availability of good data. Measurements in several prototypes are the most valuable in this process. However, it may not always be feasible to build many prototypes, especially when a production run of only a few magnets is involved. In such cases, estimates have to be based on data in other similar magnets, numerical simulations with random variations in dimensions of various parts, experience with effectiveness of mid course correction strategies, etc. Obviously, the uncertainties in predicting field errors depend on the type of data used, and must be evaluated on a case by case basis.

4 D1 DIPOLES FOR LHC

The superconducting D1 dipoles of 8 cm aperture for the LHC insertion regions perhaps represent the most favorable condition for predicting the field errors. These dipoles are to be built by BNL using the RHIC arc dipole

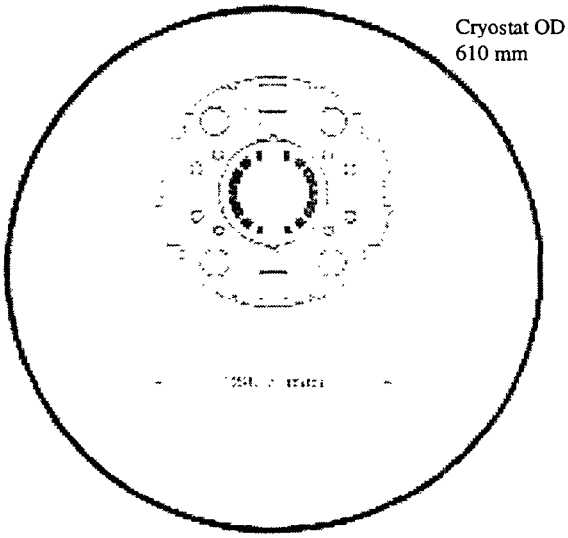

Fig. 2: RHIC arc dipole cold mass inside a cryostat

design, shown schematically in Fig. 2, except that the cold mass will not have a sagitta. Thus, the nearly 300 full length (9.45 m) dipoles in RHIC may be treated as "prototypes" for a production run of only five D1 magnets. In this section, the process of estimating field errors in D1 magnets will be discussed in detail.

4.1 Field Errors (Warm)

All the RHIC dipoles were measured warm, whereas about 20% of the magnets were also measured cold. An example of warm measurement data is shown in Fig. 3, which is a trend plot of the average skew octupole harmonic in the straight section of the 9.45 m long RHIC DRG/DR8 dipoles. As expected for an unallowed term, the mean value is practically zero, and the standard deviation is 0.5 unit. These numbers represent the expected values of systematic and random skew octupole in the D1 magnets (warm). Similar estimates can be obtained for other harmonics.

It is also seen from Fig. 3 that there is a considerable magnet to magnet variation (±1.5 unit) in the skew octupole harmonic. In a new production run with different tooling and with only a few magnets, the mean may not be as close to zero as it is for the RHIC dipoles. This introduces an uncertainty in the mean value. Strictly speaking, it is not possible to deduce this uncertainty from Fig. 3. Nevertheless, the largest deviation from mean seen in any single magnet represents an upper bound for this uncertainty.

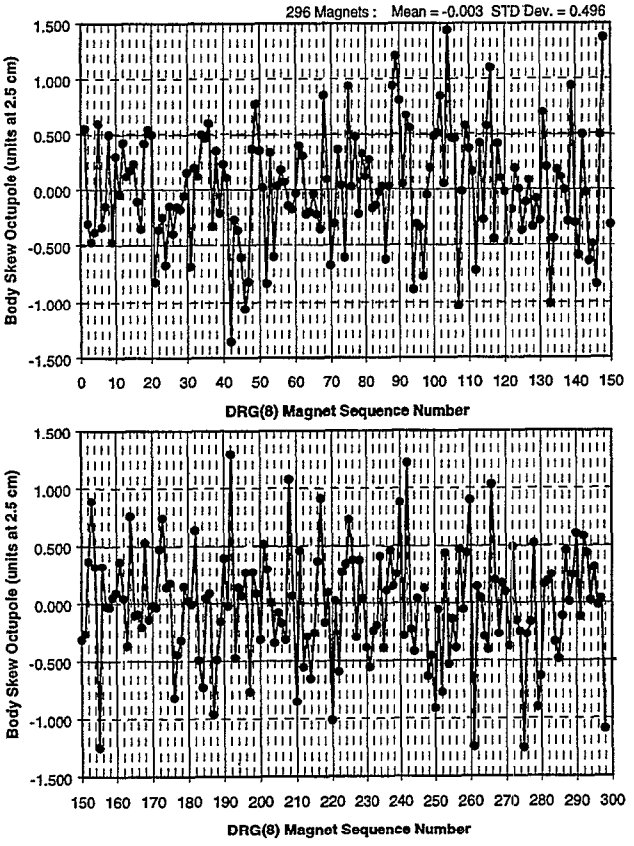

Fig. 3: Trend plot showing skew octupole in the straight sections of 9.45 m long RHIC dipoles.

4.2 Field Errors (Cold)

One is really interested in the field quality under actual operating conditions, rather than the warm harmonics. The harmonics at any magnet excitation can be obtained from the warm values by adding contributions due to warm-cold offsets (if any), contributions due to the superconductor magnetization, and contributions from changes at high fields due to saturation of iron yoke and Lorentz forces. Each of these contributions can be estimated for the D1 magnets from data in RHIC dipoles.

4.2.1 Warm-cold offsets

These are the changes resulting entirely from a change in geometry due to cool down. While most harmonics should not change, some low order allowed terms may be affected. This effect can be estimated by comparing the geometric values (obtained by averaging the values measured during up and down ramps) at intermediate field levels with the warm measurements. Such a comparison is made in Fig. 4 for the normal and skew sextupole terms measured warm and at 1800 A (1.28 T), well above the injection currents of 570 A for RHIC and ~300 A for LHC, but well below onset of saturation. The solid line represents the case of no change between the two measurements. There is no change in the skew sextpole component upon cool down, but the normal sextupole undergoes a systematic change of −0.9 unit. Similar plots can be used to obtain offsets for other harmonics. Table 1 summarizes the systematic changes observed in various harmonics upon cool down. In the table, $\sigma(\Delta b_n)$ and $\sigma(\Delta a_n)$ are the standard deviations representing magnet to magnet variations. These variations introduce an uncertainty in predicting the cold harmonics from the warm harmonics.

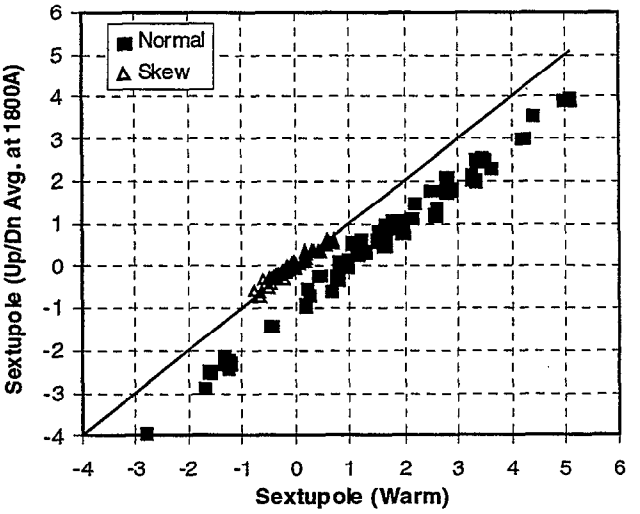

Fig. 4: Geometric values of sextupole harmonics measured cold and warm at the same 1 m long section in RHIC arc dipoles. R_{ref} = 25 mm.

Table 1
Changes in harmonics on cool down in RHIC arc dipoles (in "units" at 25 mm reference radius)

n*	Δb_n	$\sigma(\Delta b_n)$	Δa_n	$\sigma(\Delta a_n)$
2	–0.22	0.24	0.53	0.59
3	–0.94	0.20	0.03	0.10
4	–0.01	0.08	0.02	0.11
5	0.04	0.08	0.01	0.05
6	0.00	0.04	0.00	0.04
7	–0.05	0.03	0.01	0.02
8	–0.01	0.02	–0.01	0.02
9	–0.01	0.02	–0.01	0.02
10	0.04	0.04	0.03	0.02
11	–0.02	0.01	–0.01	0.01

[* $n = 2$ denotes the quadrupole term]

4.2.2 Superconductor magnetization

The effect of superconductor magnetization is significant for low order allowed harmonics, particularly at smaller currents. These effects can be estimated from the measured harmonics during the upward and downward ramps of the magnet current. Fig. 5 shows the correlation between sextupole harmonics measured on the up and the down ramps at a current of 300 A (0.21 T field). The solid

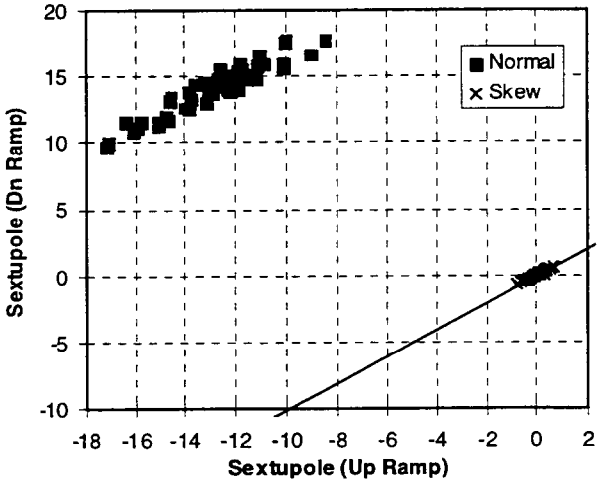

Fig. 5: Correlation between the sextupole terms measured at 300 A (0.21 T) during the "up" and the "down" ramps of a DC loop in RHIC arc dipoles. $R_{ref} = 25$ mm.

line corresponds to no change in harmonics. While there is no hysteresis effect on the unallowed skew sextupole, the normal sextupole is higher in the down ramp by 26.9 units. The contribution from superconductor magnetization is half of this amount. Similar plots can be used to obtain contributions for all the harmonics. The results are summarized in Table 2 for several fields of interest for D1 dipoles in LHC.

4.2.3 Current dependence of harmonics

As the dipole field is increased, the iron in the yoke begins to saturate. Since the field strength is not uniform

Table 2 Differences between "Down Ramp" and "Up Ramp" harmonics in RHIC arc dipoles. $R_{ref} = 25$ mm, $n = 2$ is quadrupole.

n	b_n(Dn) – b_n(Up)			a_n(Dn) – a_n(Up)		
	300A (0.21 T)	5200A (3.52 T)	5800A (3.85 T)	300A (0.21 T)	5200A (3.52 T)	5800A (3.85 T)
2	–0.51	–0.01	–0.01	–0.51	–0.08	–0.01
3	26.90 (σ=0.66)	1.04 (σ=0.13)	0.58 (σ=0.14)	0.04	0.01	0.00
4	–0.02	0.00	0.00	0.15	–0.05	–0.01
5	0.61	0.01	0.04	0.00	0.00	0.00
6	–0.05	0.00	0.00	–0.07	0.00	0.00
7	0.96	0.03	0.03	0.00	0.00	0.00
8	0.02	0.00	0.00	0.02	0.00	0.00
9	–0.19	0.00	0.00	0.00	0.00	0.00
10	–0.02	0.00	0.00	–0.03	0.00	0.00
11	0.25	0.01	0.00	0.00	0.00	0.00

in the yoke, the permeability also no longer remains uniform. Another effect at high fields is a possible deformation of the magnet coil due to high Lorentz forces. These effects introduce additional field errors at high fields. The current dependence of various harmonics is a function of the details of the yoke design and other mechanical factors. The high field behavior of the normal sextupole in RHIC arc dipoles is illustrated in Fig. 6 where values at 1800 A are compared to those at 5200 A and 5800 A in all the magnets that were cold tested. The solid line corresponds to the case of no change in harmonics with current. There is some magnet to magnet variation in the saturation behavior. The results for all harmonics at 5800 A (3.85 T) are summarized in Table 3. The standard deviations, $\sigma(\Delta b_n)$ and $\sigma(\Delta a_n)$, indicate the degree of uncertainty in predicting the saturation behavior for the same magnet design. The uncertainty could be more if a new yoke design, or changes in production parameters are involved. As an example, it is planned to use

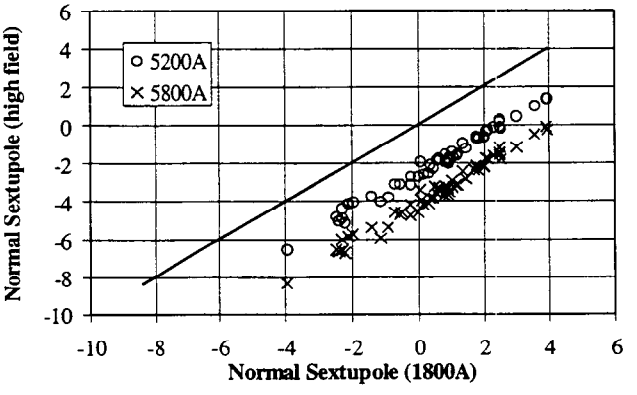

Fig. 6: Correlation between the geometric sextupole terms measured at 1800 A (1.27 T), 5200 A (3.52 T) and 5800 A (3.85 T) in RHIC arc dipoles. $R_{ref} = 25$ mm.

Table 3 Changes in harmonics at high fields in RHIC arc dipoles. Δb_n and Δa_n are the differences between Up/Dn average values at 5800 A (3.85 T) and 1800 A (1.27 T). $R_{ref} = 25$ mm

n*	Δb_n	$\sigma(\Delta b_n)$	Δa_n	$\sigma(\Delta a_n)$
2	0.32	0.11	–2.97	1.28
3	–4.12	0.26	–0.11	0.08
4	0.11	0.02	–0.64	0.16
5	–0.19	0.07	–0.02	0.01
6	–0.04	0.05	–0.07	0.03
7	1.14	0.01	0.00	0.00
8	0.00	0.00	0.01	0.01
9	0.02	0.01	0.00	0.00
10	0.01	0.00	0.00	0.00
11	–0.04	0.00	0.00	0.00

steel yoke keys in D1 magnets instead of stainless steel keys used in the RHIC arc dipoles. This would change the high field behavior of the sextupole and the decapole harmonics, thus introducing uncertainties beyond the standard deviations listed in Table 3.

5 UNCERTAINTIES IN MEASURING FIELD ERRORS

Once all magnets in a production series are built and measured, the predictions of field quality, and uncertainties in those predictions, are of limited interest, although for magnet series where less than 100% are cold tested, the uncertainties in predicting cold harmonics from warm harmonics are still of interest. If the measurements were perfect, then the impact of field errors in the as-built magnets can be studied. However, measurement errors contribute to uncertainties in the field errors, which may have to be accounted for in such studies. Thus, an understanding of the uncertainties in the measured harmonics becomes more important at this stage. The measurement errors can be classified as systematic and random.

The systematic and random measurement errors obviously depend on the type of measurement system used, data analysis details, etc. A system of rotating coils, with precision voltmeters or integrators, is the most widely used method to measure field harmonics. In this section, possible sources of systematic errors with such systems will be described briefly.

5.1 Systematic Errors in Measurements

Systematic measurement error in any given harmonic is defined as a deviation of the measured value from the true value. It is difficult to experimentally determine systematic errors, unless a reference magnet with well known harmonics is available. In a recent study, a 18 cm aperture DX magnet for RHIC was used as a reference magnet to "measure" systematic measurement errors in the 10 cm aperture D0 dipoles [5]. In most cases, such a reference magnet is not available and the systematic errors must be estimated based on possible contributions from various sources [6].

5.1.1 Coil construction and calibration errors

A measuring coil of finite length will have random variations of various mechanical parameters, such as radius, angular position, etc. along the length due to construction errors. Such variations will cause a systematic error in harmonic measurements. For two dimensional fields, relatively simple estimates of such measurement errors can be obtained for a variety of coil construction errors. A detailed discussion of this subject can be found in reference [6].

Once a measuring coil is constructed, the accuracy of measurements depends also on the calibration of various geometric parameters. With good calibration techniques, the effect of calibration errors on harmonics can be reduced to negligible levels. Particular care has to be exercised in using long integral coils to measure short magnets. Since the coil parameters can vary along the length due to construction errors, it is important to obtain a calibration for the section of the coil that is actually used.

An analysis of systematic measurement errors for the RHIC arc dipoles can be found in reference [7]. Table 4 summarizes the total systematic error (for typical measuring coil construction errors), as a percentage of the harmonic being measured. The maximum systematic errors in magnets with field quality similar to RHIC arc dipoles can be obtained by applying these percentages to the maximum value of each harmonic observed in these dipoles. These maximum errors, in units at a reference radius of 25 mm, are also listed in Table 4. As can be seen

Table 4 Maximum systematic measurement errors estimated due to coil calibration and construction errors. $R_{ref} = 25$ mm. Based on reference [7].

n	Systematic error possible	Maximum value of harmonic in RHIC arc dipoles (units)		Max. systematic error due to coil calib./constr. (units)	
		Normal	Skew	Normal	Skew
2	0.78%	1.380	5.881	0.011	0.046
3	1.08%	7.866	1.729	0.085	0.019
4	1.38%	0.293	1.399	0.004	0.019
5	1.68%	1.334	0.335	0.022	0.006
6	1.98%	0.107	0.516	0.002	0.010
7	2.28%	0.527	0.191	0.012	0.004
8	2.59%	0.042	0.143	0.001	0.004
9	2.89%	0.316	0.045	0.009	0.001
10	3.19%	0.019	0.032	0.001	0.001
11	3.49%	0.580	0.015	0.020	0.001
12	3.78%	0.008	0.020	0.000	0.001
13	4.25%	0.214	0.028	0.009	0.001
14	4.74%	0.062	0.046	0.003	0.002
15	5.27%	0.777	0.080	0.041	0.004

from this table, the estimated errors due to coil construction and calibration errors are below 0.1 unit for all harmonics.

5.1.2 Rotational imperfections of measuring coil

The signal from a rotating coil is a function of the coil position and velocity. This can be affected by imperfections such as vibration and wobble of the rotation axis, or angular jitter in data taking. These imperfections give rise to spurious harmonics, or systematic errors. It can be shown [6] that such spurious harmonics can be suppressed by the use of "bucking". Modern measurement systems invariably incorporate bucking coils for dipole and quadrupole fields, thus eliminating systematic errors due to rotational imperfections in these magnets. However, when such systems are used to measure magnets of a higher multipolarity, the advantages of bucking may not be available. As an example, a systematic decapole harmonic of several units was introduced in the measurements of octupole correctors for RHIC due to lack of octupole bucking.

5.1.3 Offset, tilt, sag, etc. of the measuring coil

Even if the rotational axis of the measuring coil has no vibration or wobble, it may not be aligned with the magnetic axis of the magnet. The rotation axis may be displaced uniformly from the magnet axis, or it could be at an angle (tilt), or its position could vary along the length due to sag of the measuring coil. The measured harmonics in such cases differ from the true harmonics due to feed down effects. In most cases, these effects can be minimized by proper "centering" of data. For quadrupoles and higher multipolarity magnets, the magnetic center can be unambiguously defined by feed down from the main harmonic. The centering is not so uniquely defined for dipole magnets. A novel centering technique employing a temporary quadrupole field was used for all RHIC dipoles [8]. This technique provides an unambiguous and precise determination of dipole center. With good centering in a dipole magnet, potential uncertainty in the determination of the quadrupole harmonic due to feed down from large sextupole terms is considerably reduced.

5.1.4 Changes in the magnet itself

During the testing of RHIC magnets, it was found that several harmonics change after the magnet is subjected to quenches and/or thermal cycles [9]. These changes were observed, and studied extensively, in 10 cm aperture D0 dipoles and 13 cm aperture quadrupoles for RHIC. These changes introduce uncertainties in the field errors, even though good measurement data may be available.

Harmonic changes with thermal cycle are available for one RHIC arc dipole, DRG101. Fig. 7 shows the normal and skew sextupole harmonics measured at eight straight section locations in DRG101 at 5kA during two different cool downs. A systematic change of ~0.2 unit is seen in the normal sextupole component after a thermal cycle (Fig. 7a). This change is observed at all axial positions. On the other hand, there is no change in the skew

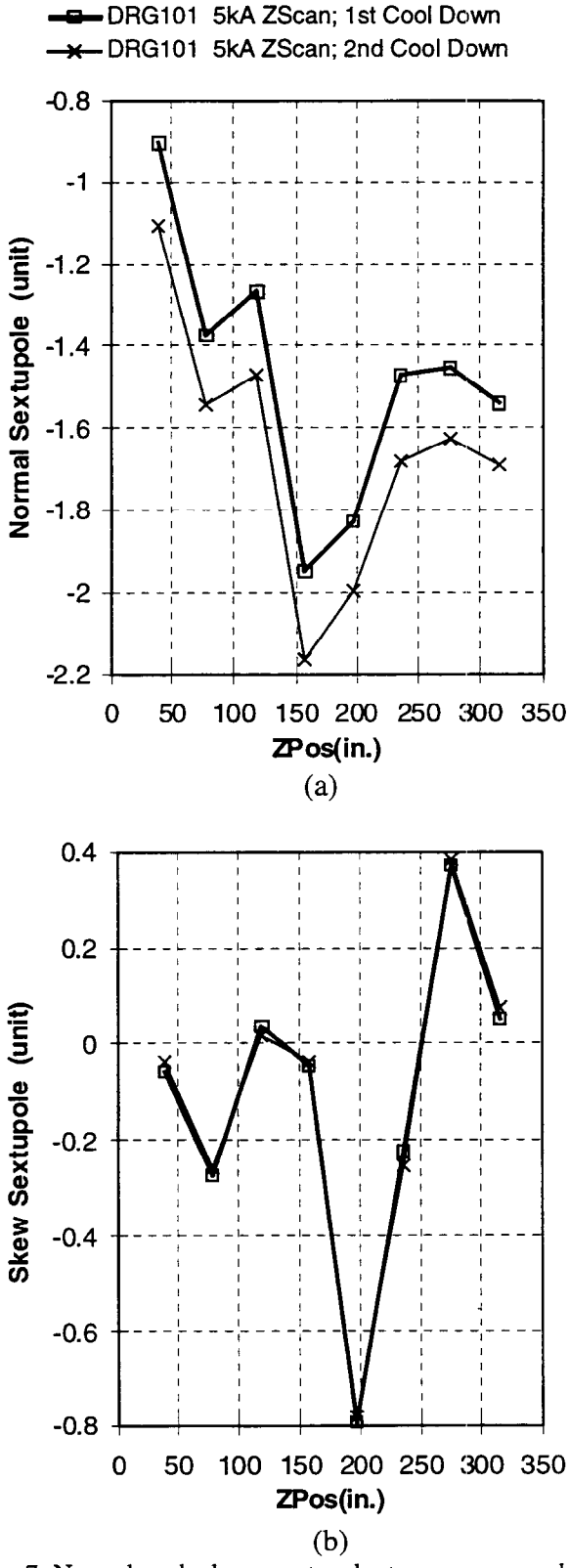

Fig. 7: Normal and skew sextupole terms measured at 5kA in DRG101 during the first and the second cool downs.

sextupole term (Fig. 7b). This shows that there is an additional measurement uncertainty for the normal sextupole term. The changes in all the harmonics at all the eight positions are shown graphically in Fig. 8. The

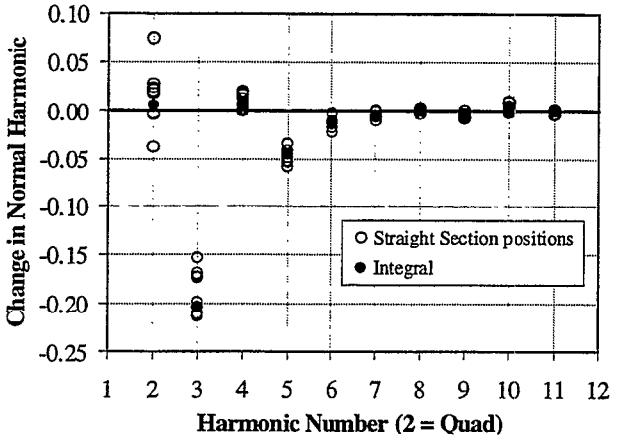

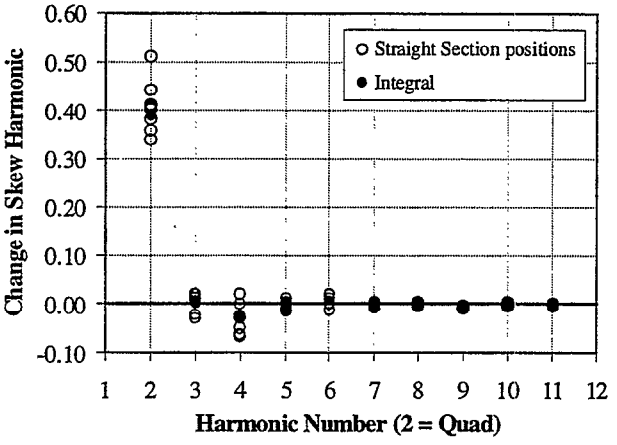

Fig. 8: Changes in the normal and skew harmonics measured at 5kA in DRG101 during the first and the second cool downs. The open circles denote changes at the eight straight section positions and the filled circles denote changes in the integral values.

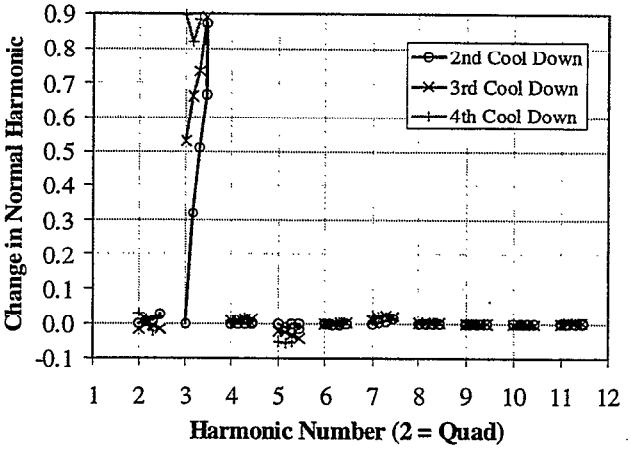

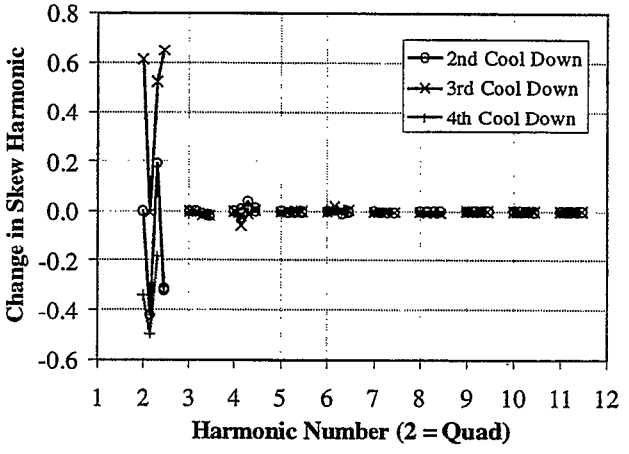

Fig. 9: Changes in the normal and skew harmonics in 10 cm aperture dipole DRZ106 with thermal cycles and quenches. The different points on a curve denote harmonics measured after quenches during the same cool down. $R_{ref} = 31$ mm.

changes are below 0.1 unit for all harmonics, except the normal sextupole and the skew quadrupole terms.

No data on harmonic changes with quench are available in RHIC arc dipoles. The effect was studied extensively in the 10 cm aperture D0 dipoles for RHIC. Fig. 9 shows the changes in the normal and skew harmonics (at a reference radius of 31 mm) with quenches during three different cool downs. All harmonic changes are calculated with respect to the measurements in the second cool down, before any quenches. The three curves for each harmonic are for the three cool downs. Different points on each curve correspond to measurements after successive quenches. The normal sextupole changes by 0.9 unit as a result of quenches during the second cool down. On a subsequent cool down, there is some recovery, but the new value before quench differs from the very first measurement by 0.5 unit. This trend continues for the fourth cool down, although dependence on quenches now becomes weak. The changes in other harmonics are well below 0.1 unit, except for the skew quadrupole term, which shows variations of up to 0.6 unit. The changes in the arc dipoles with quenches (for which no data exist) are likely to be similar to the D0 dipoles. Clearly, such changes are much larger than the systematic errors of measurement discussed earlier, and represent the largest source of measurement uncertainty. Fortunately, only a couple of terms seem to be affected in the case of dipoles. Several lowest order harmonics could be affected in the case of quadrupoles.

It is believed that the use of plastic spacers in the RHIC magnets may be contributing to changes in conductor positions after thermal cycle and quench. If the magnet coil is well constrained using metal collars, it is likely that the harmonics would not change as much. Limited data in the 18 cm aperture DX dipoles for RHIC, where a stainless steel collar is used, show that the harmonic changes are indeed smaller. Thus, it may be possible to reduce the uncertainty associated with changes in the magnet itself by choosing an appropriate mechanical design for the magnet.

5.2 Random Errors in Measurements

Random errors in measurements result from inherent system noise and occasional system malfunction. Some harmonics may be affected by stray fields due to magnet

leads in the vicinity of the measuring coil. The leads may not always be configured the same way during measurements on different days, thus giving different results.

While one has to generally guess the systematic measurement errors, the random errors can be readily measured by performing multiple measurements on the

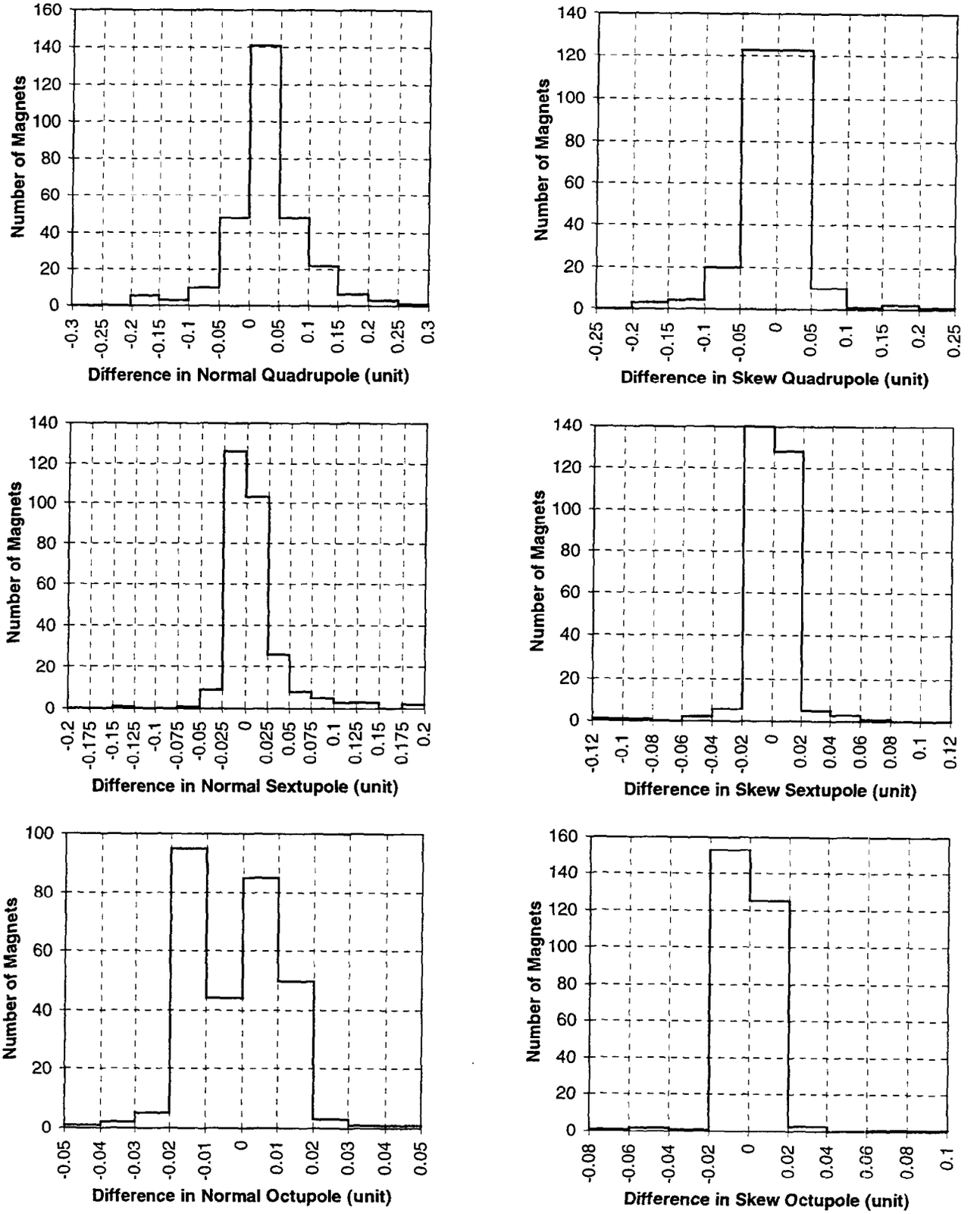

Fig. 10: Distributions of differences between two measurements of warm integral harmonics in 287 arc dipoles. The measurements were carried out using BNL supplied mole equipment at Northrop-Grumman. R_{ref} = 25 mm

same magnet. Such multiple measurements can also help in monitoring the system performance. As an example, two Z-scans were done on all RHIC dipoles at the vendor's location as a means of monitoring reliability of the measurements.

A comparison of the two Z-scans using the same measuring equipment in nearly 300 dipoles gives a good estimate of random errors. Fig. 10 shows the distribution of differences between low order integral harmonics measured in the two Z-scans. For almost all harmonics, the distributions have a strong peak at zero, which means there is practically no systematic difference between the two Z-scans. The standard deviation is the largest (~0.05 unit) for the quadrupole terms, and reduces rapidly for higher order harmonics. The standard deviations for all the harmonics are listed in Table 5. As can be seen from the table, the random errors are practically negligible for all harmonics.

Table 5 Std. Deviations of differences between two integral measurements of harmonics in RHIC arc dipoles.

Harmonic	Std. Dev. of difference in harmonics (units at 25 mm)	
	Normal	Skew
Quadrupole	0.061	0.043
Sextupole	0.033	0.015
Octupole	0.012	0.010
Decapole	0.004	0.005
Dodecapole	0.003	0.004
14-pole	0.002	0.002
16-pole	0.001	0.002
18-pole	0.001	0.001
20-pole	0.001	0.001
22-pole	0.001	0.001
24-pole	0.001	0.001
26-pole	0.001	0.001
28-pole	0.002	0.002
30-pole	0.002	0.002

6 SUMMARY

Various sources of systematic and random field errors in superconducting magnets were discussed briefly. Extensive data in RHIC arc dipoles can be used effectively to estimate harmonics in the D1 magnets for LHC, which have a similar design. Uncertainties in predicted harmonics arise mainly from changes in tooling and other magnet parts from one production to another. Additional uncertainties arise due to small uncertainties in the estimation of various contributions to harmonics at any given operating point. Once all the magnets are built and measured, uncertainties in field quality are governed by measurement errors and changes in the magnet itself after thermal cycles and quenches. The true measurement errors, both systematic and random, have been shown to be negligible in the case of RHIC. Thus, uncertainties in our knowledge of the field quality of the magnets installed in the accelerator arise primarily from the changes in the magnets themselves.

7 ACKNOWLEGEMENTS

The data presented in this paper were taken with the collective effort of a large number of physicists, engineers and technicians of the RHIC magnetic measurements group. Thanks are due to all of them for their diligent work and persistent efforts to improve the quality of the data.

8 REFERENCES

[1] A. Jain, R. Gupta, P. Thompson and P. Wanderer, "Skew Quadrupole in RHIC Dipole Magnets at High Fields", Proc. MT-14, Tampere, Finland, June 11-16, 1995, in *IEEE Trans. Magnetics*, Vol. 32, No. 4, July 1996, p.2065-8.
(accessible from http://magnets.rhic.bnl.gov/publications.htm)

[2] R. Gupta, M. Anerella, J. Cozzolino, B. Erickson, A. Greene, A. Jain, S. Kahn, E. Kelly, G. Morgan, P. Thompson, P. Wanderer and E. Willen, "Tuning Shims for High Field Quality in Superconducting Magnets", Proc. MT-14, Tampere, Finland, June 11-16, 1995, in *IEEE Trans. Magnetics*, Vol. 32, No. 4, July 1996, p.2069-73.

[3] P. Ferracin, W. Scandale, E. Todesco and P. Tropea, "A Method to Evaluate the Field-shape Multipoles Induced by Coil Deformations", Proc. PAC99, New York, paper THP107
http://ftp.pac99.bnl.gov/Papers/Wpac/THP107.pdf

[4] R. Gupta, A. Jain, S. Kahn, G. Morgan, P. Thompson, P. Wanderer and E. Willen, "Field Quality Improvements in Superconducting Magnets for RHIC", Proc. Fourth European Particle Accelerator Conference, London, UK, June 27-July 1, 1994.

[5] A. Jain and P. Wanderer, "Random and Systematic Errors in Harmonic Measurements with the D0 Mole", Magnet Group Note 580-11 (RHIC-MD-281), January 25, 1999.
(accessible from http://magnets.rhic.bnl.gov/publications.htm)

[6] A. Jain, "Harmonic Coils", CERN Accelerator School on Measurement and Alignment of Accelerator and Detector Magnets, Anacapri, Italy, April 11-17, 1997. CERN Report 98-05, p. 175-217.
(accessible from http://magnets.rhic.bnl.gov/publications.htm)

[7] A. Jain, "Estimation of Errors in the Measurement of Harmonics in RHIC Arc Dipoles", Magnet Group Note 570-11 (RHIC-MD-271), November 18, 1997.
(accessible from http://magnets.rhic.bnl.gov/publications.htm)

[8] C.R. Gibson, D.W. Bliss, R.E. Simon, A.K. Jain and P. Wanderer, "Locating the Magnetic Center of the SSC CDM Using a Temporary Quadrupole Field", Proc. *1992 Applied Superconductivity Conf.*, Chicago, Aug.23-28, 1992 in IEEE Trans. on Applied Superconductivity, **3**, No.1, p.646-9 (March, 1993).

[9] R. Gupta, A. Jain, J. Muratore, P. Wanderer, E. Willen, and C. Wyss, "Change in Field Harmonics after Quench and Thermal Cycles in Superconducting Magnets", Proc. PAC97, Vancouver, B.C., Canada, 12-16 May, 1997, p.3347-3349.
http://www.triumf.ca/pac97/papers/pdf/3P005.PDF

LHC INTERACTION REGION QUADRUPOLE ERROR IMPACT STUDIES*

W. Fischer, V. Ptitsin and J. Wei, BNL, USA; R. Ostojic, CERN, Switzerland; J. Strait, FNAL, USA

Abstract

The performance of the Large Hadron Collider (LHC) at collision energy is limited by the field quality of the interaction region (IR) quadrupoles and dipoles. In this paper we study the impact of the expected field errors of these magnets on the dynamic aperture. We investigate different magnet arrangements and error strength. Based on the results we will propose and evaluate a corrector layout to meet the required dynamic aperture performance in a companion paper.

1 INTRODUCTION

The LHC interaction region consists of a low-β quadrupole triplet (Q1-Q3) and a separation dipole (D1) on either side of the interaction point (IP), as shown in Fig. 1. The superconducting triplet quadrupoles are built by FNAL and KEK, and assembled in cryostats at FNAL. The separation dipoles in the high luminosity interactions points IP1 (ATLAS) and IP5 (CMS) are room-temperature magnets supplied by IPN-Novosibirsk. In IP2 (ALICE) and IP8 (LHC-B), where the beams are injected into the two rings, the D1 magnets are superconducting, built by BNL.

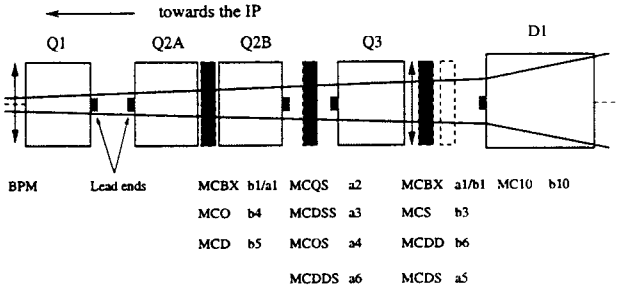

Figure 1: Schematic layout of the LHC inner triplet region.

The target dynamic aperture for the magnet field quality is set at 12 times the transverse rms beam size ($12\sigma_{xy}$) after 100,000 turns, for both injection and collision. During injection and ramping, the impact of IR magnets is small compared with that of the arc magnets. On the other hand, during p-p collisions the reduction of beam size at IP1 and IP5 results in a large beam size ($\sigma_{xy} = 1.5$mm) at the corresponding triplets (Tab. 1). Furthermore, beam-beam interactions require a crossing angle of $\pm 150\mu$r corresponding to a closed orbit of up to ± 7.3mm. The target $12\sigma_{xy}$ thus corresponds to about 71% of the magnet coil radius. Similarly, during ion collision [1] when the beam size is squeezed at IP2, the impact from the cold D1 is also noticeable. Compensation of field errors of the cold IR magnets is of primary importance in improving the performance of the LHC at collision [2].

Table 1: LHC parameters for protons at collision (7 TeV).

tunes H/V/L	63.31/59.32/0.00212
β^* IP1,5,2,8 H/V [m]	0.5/0.5, 0.5/0.5, 15/10, 13/15
$\Phi/2$ IP1,5,2,8 H/V [μrad]	0/150, 150/0, 0/-150, 0/-150
max rms beam size [mm]	1.5
max orbit offset H/V [mm]	$\pm 7.3/\pm 7.3$

The impact of IR magnetic field errors has been analysed previously [3, 4]. Since the first field quality analysis of the US-LHC magnets [3], there have been several iterations of design and test of the magnets that lead to improvements of the field quality. For the FNAL-built quadrupoles, the systematic b_6 in the lead end and the systematic b_{10} in the body have both been reduced; the random b_3 and b_4 in the body are small compared with the first prediction even without employing magnetic tuning shims; the higher order ($n > 6$) multipole errors have also been small. For the KEK-built quadrupoles, the main focus has been on a re-design of the cross section to reduce the systematic b_{10} in the body. This paper summarizes the studies that used the latest expected field errors before this workshop.

2 EXPECTED FIELD ERRORS

The leading sources of dynamic aperture reductions are the field errors of the FNAL and KEK triplet quadrupoles. The expected errors of the FNAL quadrupoles (version 2.0) are given in Tab. 2. With the experience of model construction and measurements, and design iterations that occurred through close interaction between the magnet and accelerator physics groups, knowledge and confidence in the expected body and end-field errors has substantially improved. The KEK quadrupole errors used in the simulations reported in this article are shown in Tab. 3. However, the coil cross-section of the KEK quadrupole has been recently redesigned in order to substantially reduce the geometric b_{10} error. The new KEK error table (version 3.0) is shown in Tab. 4. These errors have not been used for simulations reported here and only serve for reference purposes.

The errors for the IPN-Novosibirsk built warm D1 are shown in Tab. 5. These errors are expected to be satis-

* Work performed under the auspices of the US Department of Energy.

Table 2: Expected field errors of FNAL low-β quadrupole at collision (version 2.0, $R_{ref} = 17$ mm). $\langle . \rangle$, $d(.)$ and $\sigma(.)$ denote the mean, mean uncertainty and rms of the harmonics, respectively.

n	Normal			Skew		
	$\langle b_n \rangle$	$d(b_n)$	$\sigma(b_n)$	$\langle a_n \rangle$	$d(a_n)$	$\sigma(a_n)$
body	[unit]					
3	–	0.3	0.8	–	0.3	0.8
4	–	0.2	0.8	–	0.2	0.8
5	–	0.2	0.3	–	0.2	0.3
6	–	0.6	0.6	–	0.05	0.1
7	–	0.05	0.06	–	0.04	0.06
8	–	0.03	0.05	–	0.03	0.04
9	–	0.02	0.03	–	0.02	0.02
10	–	0.02	0.03	–	0.02	0.03
LE	[unit·m]		(length=0.41 m)			
2	–	–	–	16.4	–	–
6	0.82	0.82	0.31	–	0.21	0.06
10	-0.08	0.08	0.04	–	0.04	0.04
RE	[unit·m]		(length=0.33 m)			
6	–	0.41	0.31	–	–	–
10	-0.08	0.08	0.04	–	–	–

Table 3: Expected field errors of KEK low-β quadrupole at collision (version 2.0, $R_{ref} = 17$ mm).

n	Normal			Skew		
	$\langle b_n \rangle$	$d(b_n)$	$\sigma(b_n)$	$\langle a_n \rangle$	$d(a_n)$	$\sigma(a_n)$
body	[unit]					
3	–	0.51	1.0	–	0.51	1.0
4	–	0.29	0.57	–	0.29	0.57
5	–	0.19	0.38	–	0.19	0.38
6	–	0.5	0.19	–	0.10	0.19
7	–	0.05	0.06	–	0.05	0.06
8	–	0.02	0.03	–	0.02	0.03
9	–	0.01	0.01	–	0.01	0.01
10	0.25	0.03	0.01	–	0.01	0.01
LE	[unit·m]		(length=0.45 m)			
2	–	–	–	13.4	–	–
6	2.28	–	–	0.07	–	–
10	-0.17	–	–	-0.02	–	–

factory. The BNL built cold D1 magnets have the same coil design as the RHIC arc dipoles and their field quality is well established. These errors are shown in Tab. 6. In the next section we evaluate the dynamic aperture under nominal collision conditions and explore the optimum quadrupole arrangement to minimize the error impact.

3 DYNAMIC APERTURE TRACKING ANALYSIS

The leading errors of the IR quadrupoles are the systematic b_6 and b_{10}, which are allowed by the quadrupole symmetry. We assess the effect of magnetic errors by the tune spread of particles with amplitudes of up to 6 times the transverse

Table 4: Expected field errors of KEK low-β quadrupole at collision (version 3.0, $R_{ref} = 17$ mm).

n	Normal			Skew		
	$\langle b_n \rangle$	$d(b_n)$	$\sigma(b_n)$	$\langle a_n \rangle$	$d(a_n)$	$\sigma(a_n)$
body	[unit]					
3	–	0.50	1.00	–	0.50	1.00
4	–	0.70	0.80	–	0.30	0.80
5	–	0.20	0.40	–	0.20	0.40
6	0.1	0.50	0.60	–	0.10	0.20
7	–	0.05	0.06	–	0.04	0.06
8	–	0.03	0.05	–	0.02	0.04
9	–	0.02	0.03	–	0.02	0.02
10	–	0.10	0.05	–	0.02	0.03
LE	[unit·m]		(length=0.45 m)			
2	–	–	–	13.4	–	–
6	2.28	–	–	0.07	–	–
10	-0.17	–	–	-0.02	–	–

Table 5: Expected field errors of Novosibirsk-built warm dipoles (D1) at collision (version 1.0, $R_{ref} = 17$ mm).

n	Normal			Skew		
	$\langle b_n \rangle$	$d(b_n)$	$\sigma(b_n)$	$\langle a_n \rangle$	$d(a_n)$	$\sigma(a_n)$
body	[unit]					
3	0.3	0.1	0.06	–	–	–
5	0.1	0.05	0.03	–	–	–
7	-0.02	0.005	0.003	–	–	–
9	-0.02	0.005	0.003	–	–	–
11	-0.04	0.005	0.003	–	–	–
13	0.04	0.005	0.003	–	–	–

rms beam size ($6\sigma_{xy}$), and by the dynamic aperture determined by 6D TEAPOT [5] tracking after either 10^3 or 10^5 turns, averaged over 10 random sets of magnetic errors at 5 emittance ratios ϵ_x/ϵ_y. Tracked particles have 2.5 times the rms momentum deviation ($2.5\sigma_p$) [3, 4]. Uncertainties in the mean are set at their full amount with either plus or minus sign. Due to computing power limitations, we track particles in most cases for only 1,000 turns. In Sec. 3.2 we show the difference in the dynamic aperture when particles are tracked up to 100,000 turns.

3.1 *Tracking results*

The tune spread due to multipole errors scales as $(x_c + \sqrt{\beta_{xy}\epsilon_{xy}})^{n/2}/\epsilon_{xy}^{n/2}$, where x_c is the closed orbit, β_{xy} the lattice β-function and ϵ_{xy} the emittance. The b_{10} error of the KEK magnets alone produces a tune spread of 0.61×10^{-3} at $6\sigma_{xy}$ thereby reducing the dynamic aperture by $2\sigma_{xy}$ (Tab. 7).

A possibility for reducing the impact of the KEK geometric b_{10} could be to adopt a "mixed" triplet scheme where Q1 and Q3 are KEK quadrupoles and Q2 FNAL quadrupoles. This arrangement would lead to a 30% reduction of the tune spread, and an 18% increase of the dynamic

Table 6: Expected field errors of BNL-built cold dipoles (D1) at collision (version 1.0, $R_{ref} = 25$ mm).

n	Normal			Skew		
	$\langle b_n \rangle$	$d(b_n)$	$\sigma(b_n)$	$\langle a_n \rangle$	$d(a_n)$	$\sigma(a_n)$
body	[unit]					
2	0.10	0.80	0.28	0.63	3.47	1.55
3	-3.30	3.43	1.82	-0.26	0.58	0.21
4	0.01	0.25	0.09	0.04	1.08	0.42
5	0.53	0.81	0.41	-0.07	0.19	0.06
6	-0.14	0.12	0.04	-0.05	0.56	0.17
7	1.14	0.20	0.11	-0.01	0.07	0.03
8	-0.01	0.04	0.01	-0.01	0.15	0.05
9	0.01	0.12	0.05	-0.01	0.03	0.01
10	0.05	0.06	0.02	0.04	0.04	0.02
11	-0.57	0.04	0.02	-0.01	0.02	0.01
LE	[unit·m]					
2	-0.47	2.26	0.99	-1.42	4.27	1.77
3	22.35	2.93	1.10	-9.85	1.01	0.39
4	0.04	0.73	0.23	0.09	0.75	0.29
5	-0.43	0.69	0.22	2.23	0.30	0.13
6	0.02	0.29	0.12	0.01	0.29	0.10
7	0.92	0.11	0.05	-0.86	0.13	0.06
8	–	0.06	0.03	-0.02	0.08	0.03
9	-0.04	0.08	0.03	0.25	0.05	0.02
10	-0.01	0.08	0.03	-0.01	0.04	0.02
11	-0.06	0.03	0.01	-0.04	0.02	0.01
RE	[unit·m]					
2	0.22	1.81	0.66	0.91	4.50	1.91
3	6.08	2.67	1.16	0.29	1.03	0.34
4	–	0.36	0.16	0.24	0.73	0.31
5	0.03	0.66	0.23	–	0.31	0.11
6	0.03	0.17	0.06	-0.01	0.24	0.10
7	-0.04	0.13	0.06	-0.03	0.12	0.05
8	-0.03	0.07	0.03	-0.02	0.11	0.04
9	-0.17	0.08	0.03	–	0.05	0.02
10	-0.07	0.08	0.04	-0.02	0.10	0.05
11	-0.12	0.04	0.01	0.01	0.02	0.01

aperture, as shown in Tab. 7.

The mixed arrangement increases the possibility for magnet sorting [6, 7] and helps randomizing the uncertainty. It may also reduce the number of needed spare magnets and simplifies the engineering process. However, combining quadrupoles of different transfer functions implies a more complicated powering scheme. While a common bus is still possible, issues that need to be investigated are the natural compensation of ripple in a triplet and the dynamic behavior at injection related to snap back and eddy-current effects [8].

In order to estimate the b_6 impact, we assume that FNAL magnets are placed at IP1 and 5 and gradually decrease the total b_6 to 30% of its original value assuming a positive $d(b_6)$. Tab. 7 shows a steady increase of the dynamic aperture from $9.3\sigma_{xy}$ to $12.1\sigma_{xy}$.

The orientation of the quadrupoles was chosen to minimize the lead end b_6 impact [3, 4]. With the mixed quadrupole scheme, the minimization is less effective however. In order to reduce the number of electric buses through Q3, it was further suggested to reverse the orientation of Q3. This leads to a reduction of the average dynamic aperture of 0.4 σ, and to an increase of the b_6 corrector strength. As the random b_6 is large, this effect could be alleviated by sorting [6, 7].

Table 7: Comparison of dynamic aperture (DA) for various triplet arrangements (10^3-turn DA in units of σ_{xy} with $1\sigma_{xy}$ step size).

Case	DA mean	DA rms	DA min
FNAL IP5, 8; KEK IP1, 2:			
	8.5	1.4	7
without b_{10}	10.3	1.5	7
FNAL as Q2; KEK as Q1, Q3 (mixed):			
	10.0	1.5	8
reversed Q3 LE	9.6	2.0	6
FNAL IP1, 5; KEK IP2, 8:			
	9.3	2.1	6
80% b_6	9.9	2.0	6
50% b_6	11.0	1.8	8
30% b_6	12.1	1.7	9

3.2 *Short versus long term tracking*

We re-confirmed [3] the difference between the dynamic aperture determined after 10^3 and 10^5 turns for two selected cases, an uncorrected machine with a small dynamic aperture and a machine that has a large dynamic aperture due to a costly correction scheme, named "scheme 4" in Ref. [9]. The difference (Tab. 8) is $0.7\sigma_{xy}$ or 7% for the uncorrected case, and $0.9\sigma_{xy}$ or 5% for the corrected case.

Table 8: Comparison of 1,000-turn and 100,000-turn dynamic aperture (DA).

Case	DA mean	DA rms	DA min
no correction (10^3)	10.0	1.5	8
no correction (10^5)	9.3	1.4	7
scheme 4 (10^3)	17.6	1.6	14
scheme 4 (10^5)	16.7	1.5	13
target (10^5)	12	–	10

4 SUMMARY

With the error tables used in this study we find that the systematic b_{10} error is the leading source of a dynamic aperture reduction followed by the random b_6 error. Mixing magnets of different origin can help reach the target dynamic aperture as it gives an improvement of about $1.5\sigma_{xy}$. This would be equivalent to a reduction of the systematic

b_{10} and uncertainty of b_6 errors by about 50%. Further benefits of mixing could be expected through the randomization of the uncertainties and a broader selection of magnets. We expect that the new KEK error table (version 3.0) with an eliminated systematic b_{10} gives a substantially better dynamic aperture.

We thank J. Gareyte, J.-P. Koutchouk, O. Brüning and J. Miles for lattice assistance and discussions, and many others, including M. Harrison, A. Ijspeert, J. Kerby, M.J. Lamm, S. Peggs, T. Sen, R. Talman, T. Taylor and A.V. Zlobin.

5 REFERENCES

[1] V. Ptitsin, W. Fischer, J. Wei, "LHC interaction region region correction in heavy ion operation", these proceedings.

[2] J. Wei, "Principle of interaction region local correction", these proceedings.

[3] J. Wei et al., "US-LHC IR magnet error analysis and compensation", EPAC 1998 proceedings (1998) p. 380.

[4] J. Wei et al., "Interaction region local correction for the Large Hadron Collider", PAC 1999 proceedings (1999) p. 2921.

[5] L. Schachinger, R. Talman, Part. Accel. **22**, 35 (1987).

[6] J. Wei, R. Gupta, M. Harrison, A. Jain, et al, PAC99 (1999).

[7] J. Shi, Nuclear Instruments and Methods A (1999).

[8] J-P. Koutchouk, private communications.

[9] W. Fischer et al., "LHC interaction region correction scheme studies", these proceedings.

Sorting of High-Gradient Quadrupoles in LHC Interaction Regions

J. Shi*
Department of Physics & Astronomy, University of Kansas, Lawrence, KS 66045, USA

Abstract

Sorting of superconducting high-gradient quadrupoles in the LHC interaction regions with the vector sorting scheme is found to be quite effective in enlargement of the dynamic aperture and improvement of the linearity of the phase-space region occupied by beams. Since the sorting is based on the local compensation of multipole field errors, the effectiveness of the sorting is robust.

1 INTRODUCTION

The beam dynamic of the LHC during collisions is dominated by the magnetic field errors in superconducting high-gradient quadrupoles (MQX) in the triplets of the LHC interaction regions (IRs). Sorting of magnets, in which the magnets are installed according to measured field errors so that the errors on different magnets are partially compensated with each other, has been the easiest way in many cases to reduce the detrimental effects of the random errors without introducing complications. The difficulty to achieve such an effective self compensation of the random errors is to find an optimized magnet configuration which can significantly increase the stability domain of beams, since even for a small number of magnets, the total number of possible magnet arrangements is exceedingly large. During the last decade, several sorting strategies have been proposed and studied extensively [1-8]. Most of them are, however, effective when only one multipole component in the error field is dominant. Recently, a vector sorting scheme has been developed for a systematical control of many multipole components [7,8]. Applications of the vector sorting scheme to arc dipoles as well as insertion quadrupoles of large storage rings have been found to be quite effective in increasing the dynamic aperture and improving the linearity of the phase-space region occupied by beams even when more than one multipole components are responsible for the aperture limitation [7,8]. In the low-β insertion triplets of the LHC IRs, excursion of many beam particles from the magnetic axis is very large because of large β-functions and beam separations during collisions. This makes many high-order multipoles of the field errors in MQX important. On the other hand, large β-functions in the triplets result in a very small phase advance within each triplet and the self compensation of the field errors among the quadrupoles can be relatively easy even though a limited number of interchangeable quadrupoles are available for the sorting. In this report, the effectiveness of the sorting of MQX has been studied with the latest FNL and KEK reference harmonics (version 2.0) [9].

* This work is supported by the National Science Foundation under Grant No. PHY-9722513 and the University of Kansas General Research Fund.

2 SORTING STRATEGY

The LHC has four interaction points (IPs): IP1 and IP5 are high luminosity points ($\beta^* = 0.5$ m) and IP2 and IP8 low luminosity points. The layout of the inner triplets of the four IPs is almost identical. Each inner triplet comprises four MQX of which two outer quadrupoles, Q1 and Q3, are 6.3 m long (long MQX) and the inner two, Q2A and Q2B, are 5.5 m long (short MQX). Due to the large β_{max} ($\sim$ 4700 m) in the inner triplets of IP1 and IP5, the field quality of MQX of IP1 and IP5 is far more important than that of IP2 and IP8. Therefore, the sorting primarily focuses on the selection of MQX for IP1 and IP5. Since the phase advances are close to zero within each inner triplet of IP1 and IP5, the vector sorting with 2π-cancellation [7,8] can be used for the four MQX in each triplet. The sorting of MQX must, however, observe several constraints. First, of a total of 16 long and 16 short MQX in four IRs, 8 long and 8 short MQX will be built in Fermilab and the others will be built in KEK. Due to hardware constraints such as differences in cryostats, the FNL-made and KEK-made MQX may not be interchangeable. Moreover, after cold measurements, Q2A and Q2B will be welded together so that they are not be separable afterward. Due to a large systematic b_{10} in KEK-made MQX, two different configuration, mixed and unmixed configuration, for installation of MQX are currently under consideration. Sorting of MQX are therefore studied with both of these configurations. In the unmixed configuration, the FNL-make MQX are assumed to be installed in the triplets of IP1 and IP2, and the KEK-made MQX in the triplets of IP5 and IP8. In the mixed configuration, four MQX in each triplet are mixed with two quadrupoles from Fermilab and another two from KEK. In this case, the FNL-made MQX are installed at Q2A and Q2B and KEK-made MQX at Q1 and Q3. For the unmixed configuration, the sorting has to be done with 8 long MQX and 4 pairs of short MQX for each pair of high and low luminosity IPs. For the mixed configuration, on the other hand, there are 16 FNL-made long MQX and 8 pairs of KEK-make short MQX for sorting. It should be noted that even with this small number of magnets, the number of possible magnet configurations is still very large.

To have a better understanding of the sorting scheme for MQX, let's examine the section map of each inner triplet. Let $(\vec{\xi}_0, \vec{\eta}_0)$ and $(\vec{\xi}_4, \vec{\eta}_4)$ be the normalized phase-space variables just before Q1 and immediately after Q3, respectively. Since the phase advances in each triplet are almost

zero, the transfer map from $(\vec{\xi}_0, \vec{\eta}_0)$ to $(\vec{\xi}_4, \vec{\eta}_4)$ is

$$\left(\vec{\xi}_4, \vec{\eta}_4\right) = \left(\vec{\xi}_0, \vec{\eta}_0 + \Delta\vec{\eta}\right) \quad (1)$$

where $\Delta\vec{\eta}$ is the nonlinear perturbation due to the multipole field errors in the four MQX. In the thin-lens approximation, the field errors are simply expressed as nonlinear kicks. Due to large variations of β-functions across the MQX, each MQX has to be sliced into a number of pieces in order to use the thin-lens approximation. For the jth piece of the ith MQX, the kick can then be written as

$$\Delta\vec{\eta}_{ij} = \sum_{n=2}^{N} \left[b_n^{(i)} \vec{F}_n^{(ij)}\left(\vec{r}_{ij}\right) + a_n^{(i)} \vec{G}_n^{(ij)}\left(\vec{r}_{ij}\right) \right] \quad (2)$$

where N is the maximal order of multipoles considered. $b_n^{(i)}$ and $a_n^{(i)}$ are coefficients of the nth-order normal and skew multipoles of the ith MQX, respectively. $\vec{F}_n^{(ij)}(\vec{r}_{ij})$ and $\vec{G}_n^{(ij)}(\vec{r}_{ij})$ are vectorial polynomials of $\vec{r}_{ij}$ in degree n, which can be obtained from the multipole expansion of the errors, and

$$\vec{r}_{ij} = \left(\beta_x^{\frac{1}{2}} \xi_{0x} + \delta x_{ij},\ \beta_y^{\frac{1}{2}} \xi_{0y} + \delta y_{ij}\right) \quad (3)$$

where (β_x, β_y) are the β-functions at the jth piece of the ith MQX and $(\delta x_{ij}, \delta y_{ij})$ is the closed-orbit offset in horizontal and vertical direction due to a crossing angle. The first-order perturbation of $\Delta\vec{\eta}$ in the transfer map (5) is then

$$\begin{aligned}(\Delta\vec{\eta})_1 &= \sum_{i=1}^{4} \sum_{j} \Delta\vec{\eta}_{ij} \quad (4)\\ &= \sum_{n=2}^{m} \sum_{i=1}^{4} \left[b_n^{(i)} \sum_{j} \left(\vec{F}_n^{(ij)}\right) + a_n^{(i)} \sum_{j} \left(\vec{G}_n^{(ij)}\right) \right]\end{aligned}$$

where the summation over j is to sum up all the kicks of a MQX. If $(\Delta\vec{\eta})_1$ can be minimized by sorting the quadrupoles, the multipole field errors in four MQX of each triplet will be partially compensated. In order to examine the magnitude of nonlinear perturbations, a $4N$-dimensional vector $\vec{S}^{(i)} = \left(S_1^{(i)}, ..., S_{4N}^{(i)}\right)$ is used to represent the nonlinear error field on each quadrupole, which is defined by

$$\begin{aligned} S_n^{(i)}(\vec{\xi}_0) &= b_n^{(i)} \sum_j F_{nx}^{(ij)}\left(\vec{r}_{ij}\right), \\ S_{N+n}^{(i)}(\vec{\xi}_0) &= b_n^{(i)} \sum_j F_{ny}^{(ij)}\left(\vec{r}_{ij}\right), \\ S_{2N+n}^{(i)}(\vec{\xi}_0) &= a_n^{(i)} \sum_j G_{nx}^{(ij)}\left(\vec{r}_{ij}\right), \\ S_{3N+n}^{(i)}(\vec{\xi}_0) &= a_n^{(i)} \sum_j G_{ny}^{(ij)}\left(\vec{r}_{ij}\right), \end{aligned}$$

for $n = 1, ..., N$. The magnitude of the first-order perturbation due to the field errors of the ith MQX at phase space locations of $\vec{\xi} = \vec{\xi}_0$ is defined by the normal of $\vec{S}^{(i)}$,

$$|\Delta\vec{\eta}_i| = \left|\vec{S}^{(i)}(\vec{\xi}_0)\right| = \sqrt{\sum_{n=1}^{4N} \left[S_n^{(i)}(\vec{\xi}_0)\right]^2}, \quad (5)$$

and the magnitude of the first-order perturbation in the sectional map of a triplet is then

$$\begin{aligned}|(\Delta\vec{\eta})_1| &= \left|\sum_{i=1}^{4} \vec{S}^{(i)}\right| \quad (6)\\ &= \sqrt{\sum_{n=2}^{N} \left[\left(\sum_{i=1}^{4} b_n^{(i)} \vec{F}_n^{(i)}\right)^2 + \left(\sum_{i=1}^{4} a_n^{(i)} \vec{G}_n^{(i)}\right)^2 \right]}.\end{aligned}$$

The sorting of MQX is thus based on the minimization of $|(\Delta\vec{\eta})_1|$, where $\xi_{0x} = \xi_{0y} = \xi_0$ is a parameter to optimize the sorting. ξ_0 can be chosen initially in such a way that it corresponds to the dynamic aperture of the lattice without sorting. The sorting can then be optimized by tuning ξ_0. It should be noted that the minimization of the normal of the vector sum of all error fields in each triplet in Eq. (6) effectively excludes unintended cancellation of the error fields between different orders of multipoles. Any sorting scheme relying on such cancellation (e.g., cancelling sextupole field with decapole field) is harmful as the effect of sorting will then strongly depend on phase-space locations. Since the feed-down effect of high-order multipoles due to an angle crossing of beams at IPs are different for two counter-rotating beams, the sorting has to be done simultaneously with two counter-rotating beams.

3 EFFECT OF THE SORTING ON THE BEAM DYNAMICS

The LHC collision lattice V5.0 is used in this study. Only the field errors of MQX are included. The random multipole components of MQX are chosen with Gaussian distributions centered at zero and truncated at $\pm 3\sigma_{b_{n+1}}$ or $\pm 3\sigma_{a_{n+1}}$ where $\sigma_{b_{n+1}}$ and $\sigma_{a_{n+1}}$ are the rms value of the nth-order normal and skew multipole coefficient, respectively. Fermilab and KEK reference harmonics of version 2.0 is used in this study. The uncertainty of a systematic error is simply added to the systematic error in such a way that it maximizes the systematic error. The crossing angle of two counter-rotating beams is taken to be 300 μrad and the fractional parts of horizontal and vertical tunes are $\nu_x = 0.31$ and $\nu_y = 0.32$, respectively. Tracking of particle motion has been done without synchrotron oscillations and momentum deviations. The dynamic aperture (DA) has been calculated with 10^5-turn tracking. To improve the statistical significance of the simulations, we used 100 different samples of random multiple components generated with different seed numbers in a random number generator routine. All the multipoles up to 9th order in the field errors of MQX are included.

Table 1: Dynamic aperture of 5 worst cases in 100 random samples of LHC collision lattice with the mixed configuration. $\nu_x = 0.31$, $\nu_y = 0.32$, and the crossing angle is 300μrad. The unit of dynamic aperture is σ.

	Case 9	Case 39	Case 50	Case 26	Case 46	$\langle DA \rangle_{50}$	$(DA)_{min}$
Original DA	6.5	6.7	6.7	6.8	7.0	8.0	6.5
2nd-order Global Correction	8.1	7.7	8.8	9.1	8.6	9.0	7.7
3rd-order Global Correction	10.1	10.0	9.9	10.7	9.8	10.2	9.2
4th-order Global Correction	10.7	10.7	10.6	10.8	10.6	11.7	9.6
5th-order Global Correction	11.3	11.0	10.6	11.0	10.9	11.3	10.1
6th-order Global Correction	11.4	11.9	10.6	11.0	10.9	11.6	10.3
Sorting (beam1)	12.0	10.0	12.8	10.8	10.0	11.0	9.0
Sorting (beam2)	10.0	11.0	9.2	9.6	10.5	10.3	9.0

Table 2: The same as Table 1 but with the unmixed configuration

	Case 44	Case 47	Case 12	Case 5	Case 20	$\langle DA \rangle_{50}$	$(DA)_{min}$
Original DA	5.5	5.6	6.1	6.9	6.8	8.0	5.5
2nd-order Global Correction	8.1	8.8	10.0	8.8	8.6	9.0	7.7
3rd-order Global Correction	9.6	9.4	10.0	10.3	9.9	10.2	9.1
4th-order Global Correction	10.5	10.2	10.8	10.9	10.6	11.0	10.0
5th-order Global Correction	12.2	11.0	11.3	11.6	11.1	11.5	10.3
6th-order Global Correction	12.3	11.2	11.7	12.1	11.9	12.0	10.4
Sorting (beam1)	12.4	10.6	13.3	10.4	9.5		
Sorting (beam2)	11.3	10.0	13.2	11.4	9.0		

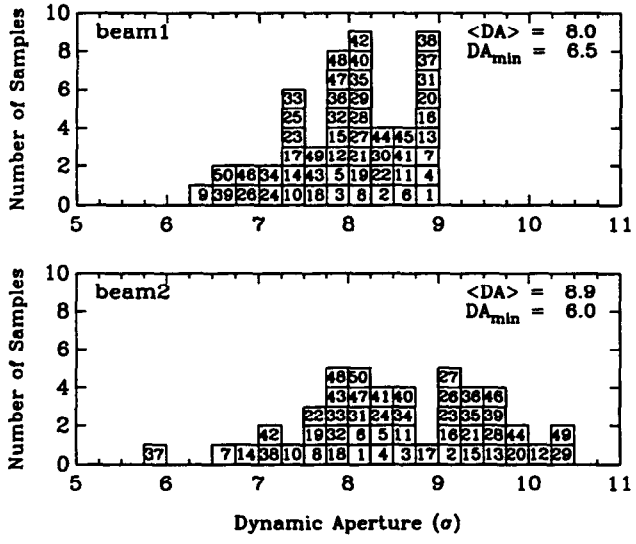

Figure 1: Dynamic aperture of two counter-rotating beams of fifty samples of the mixed configuration without the sorting and nonlinear correctors for MQX. The number in each block identifies each sample.

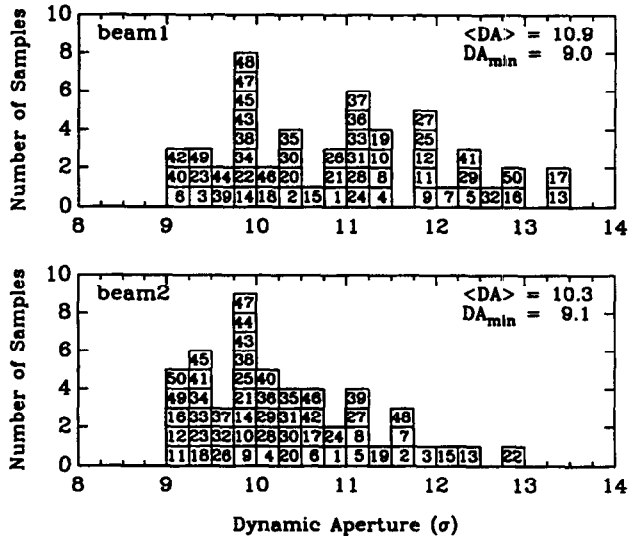

Figure 2: The same as Fig. 1 but with the sorting of MQX.

Figs. 1 and 2 plot the DA of two counter-rotating beams of fifty samples with or without the sorting of MQX for the mixed configuration. No any nonlinear corrector were used in these cases. These fifty samples were the fifty worst cases of the hundred random samples without the sorting in regarding of the DA of beam 1. Without the sorting, the smallest and the average DA of the fifty samples is 6.5σ and 8.0σ for beam 1, and 6.0σ and 8.9σ for beam 2, where σ is the transverse beam size. After the sorting, the smallest and the average DA for both beams are increased to more than 9.0σ and 10.0σ, respectively. In Figs. 3 and 4, the percentage increase of the DA after the sorting is plotted *vs.* the DA without sorting for the fifty samples of the mixed and

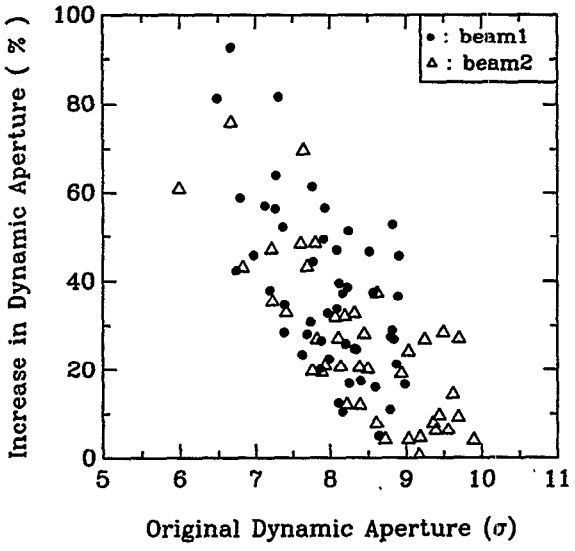

Figure 3: The increase of the DA after the sorting vs. the DA without the sorting for two counter-rotating beams of the fifty samples of the mixed configuration.

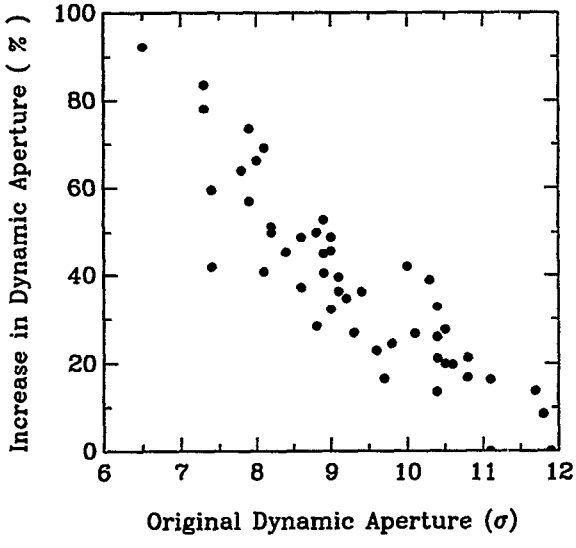

Figure 4: The increase of the DA after the sorting vs. the DA without the sorting for beam 1 of the fifty samples of the unmixed configuration.

unmixed configuration, respectively. It shows that, in general, the smaller the unsorted DA, the larger the increase of the DA after the sorting. For example, before the sorting, two worst cases of the mixed configuration, case 9 for beam 1 and case 37 for beam 2, have a DA of about 6σ. After the sorting, the DA becomes larger than 9.5σ for both cases, which is more than 60% gain in the DA. As the DA without the sorting increases, the gain of the DA after the sorting diminishes. It is understandable that if the original system is already quite linear, the sorting will not result in a substantial improvement. In Table 1 and 2, we list the DA with or without sorting for five samples of the mixed and unmixed configuration. These are the five worst cases in the 100 random samples of the LHC collision lattice with the mixed or unmixed configuration. The DA after the global correction is also listed for a comparison [10]. It shows that the DA of the LHC collision lattice can be increased to 9σ with the sorting of MQX.

4 SUMMARY

The sorting scheme for the insertion quadrupoles of the LHC IRs based on the self compensation of random field errors in each triplet has been shown to be a very effective means to increase the dynamic aperture of the LHC during collisions even though only a limited number of quadrupoles are available for the sorting. Since the sorting scheme is based entirely on the local compensation of multipole field errors in each triplet, it is very robust, i.e. the sorted lattice should be superior to unsorted one even when other factors are included. The effectiveness of the sorting has also been demonstrated with different working points of the LHC [8]. It should be noted that the sorting of magnets requires a reliable cold measurement of multipole components of all the magnets. It is assumed that the cold measurements will be conducted for all MQX. In this study, we assumed that all 32 MQX of the LHC are available for the sorting, i.e. the cold measurement of all MQX can be completed before installing any of them. Practically, however, there will be constraints from the construction and installation schedules which could prevent the pool of the quadrupoles available for sorting from being large. If that was the case, sorting would be less effective. The merit of sorting, however, lies in the fact that it can coexist with any other correcting measures without introducing any harmful side effects. It therefore provides an additional measure for controlling the effects of magnetic field errors.

5 REFERENCES

[1] L. Michelotti and S. Ohnuma, IEEE Trans. Nucl. Sci., N **30**, 2472 (1983).

[2] R.L. Gluckstern and S. Ohnuma, IEEE Trans. Nucl. Sci., NS-32, 2314 (1985).

[3] S. Ohnuma, IEEE Trans. Nucl. Sci., NS-34, 1176 (1987).

[4] M. Li and S. Ohnuma, in *Proceedings of the 1989 Particle Accelerator Conference*, (1989), p. 897; in *Proceedings of the 2nd European Particle Accelerator Conference*, (1990), p. 1175.

[5] M. Giovannozzi, R. Grassi, W. Scandale, and E. Todesco, Phys. Rev. E **52**, 3093 (1996).

[6] L. Schachinger, SSC report SSC-N-123, (1986).

[7] J. Shi and S. Ohnuma, Particle Accelerators **56**, 227 (1997).

[8] J. Shi, Nucl. Instr. & Meth., A**430**, 22 (1999).

[9] Reference harmonic for MQX are also available on the US-LHC project web page: http://www/agsrhichome.bnl.gov/LHC.

[10] J. Shi, "Global Correction of Magnetic Field Errors in LHC Interaction Regions", in this prodeddings.

REAL-WORLD SORTING OF RHIC SUPERCONDUCTING MAGNETS*

J. Wei†, R. Gupta, M. Harrison, A. Jain, S. Peggs, P. Thompson, D. Trbojevic, P. Wanderer
Brookhaven National Laboratory, Upton, NY 11973, USA

Abstract

During the seven-year construction of the Relativistic Heavy Ion Collider (RHIC), more than 1700 superconducting dipoles, quadrupoles, sextupoles, and multi-layer correctors have been constructed and installed. These magnets have been sorted at several production stages to optimize their performance and reliability. For arc magnets, priorities have been put first on quench performance and operational risk minimization, second on field transfer function and other first-order quantities, and finally on nonlinear field errors which were painstakingly optimized at design. For Interaction-Region (IR) magnets, sorting is applied to select the best possible combination of magnets for the low-β^* interaction points (IP). This paper summarizes the history of this real-world sorting process.

1 INTRODUCTION

The RHIC magnet system consists primarily of superconducting dipole, quadrupole, sextupole and corrector magnets for guiding, focusing, and correcting the counter-circulating ion beams into the design orbits in the regular arcs of the machine lattice. A large complement of special superconducting magnets is also required for steering the beams into collisions at the six interaction regions (IR) where the ion beams interact. During the seven-year construction cycle, more than 1700 superconducting magnets have been constructed, measured, installed and tested. In order to optimize the performance of these magnets, sorting has been applied whenever possible.

For a majority of the arc magnets, priorities have been put first on quench performance and operational risk minimization and second on field transfer function and other first-order quantities. Since nonlinear field errors were painstakingly optimized at design, and their sorting priority was low. For IR magnets, sorting was applied to select the best possible combination of magnets for 2 out of 6 IRs where β^* will be lowered to 1 meter for high luminosity experiments. In order to minimize the relative misalignment between magnets in a common cryostat, sorting was also applied both before and after cryostat assembly. In contrast to an idealized magnet sorting, sorting in a real world is often constrained by the assembly and installation schedule, available storage space, etc. This paper summarizes the history of this real-world sorting process. In Section 2, we review the overall procedure of magnet analysis, acceptance, and sorting. In Sections 3 and 4, we summarize the actual sorting experience for arc and IR magnets.

* Work performed under the auspices of the US Department of Energy.
† Email: weil@bnl.gov

2 MEASUREMENT DATA ANALYSIS

Besides reaching fields with substantial margins above the required range, all of the RHIC magnets must meet stringent requirements for field quality, reproducibility, and long-term reliability. In order to fulfill this goal, a committee of magnet division and RHIC accelerator physics personnel jointly reviewed the field quality, quench test performance, survey and other engineering aspects of the magnets. After individual magnet elements (coldmasses) are measured and tested, the magnetic field quality data, including transfer function, field angle, multipole harmonics, magnetic center offsets, etc. at all the test currents, [1] are recorded along with the warm mechanical survey measurements of the fiducial positions, sagitta, mechanical length and field angle. The data are transferred from the magnet division into the RHIC SYBASE database, and then analyzed by studying trends, comparing with the expected values, and evaluating the deviation from the mean using the computer program MAGSTAT [2]. As shown in Fig. 1, after their review and acceptance, magnets contained in their own cryostats (e.g. arc dipoles) are sorted for their candidate installation locations. Magnets belonging to a common cryostat assembly go through a second stage of

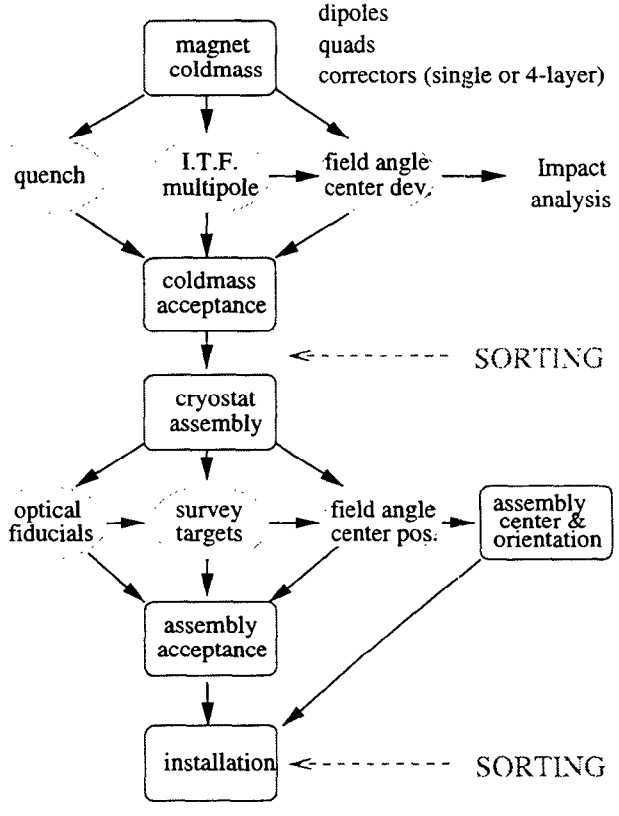

Figure 1: Magnet acceptance and sorting procedure.

review, acceptance and sorting. At this stage, the assembly is surveyed with either colloidal-cell optical or stationary-coil pick-up (antenna) techniques to locate the magnetic centers of the components relative to the cold mass fiducials and the externally accessible cryostat fiducials. This survey data is transferred into the database and analyzed using the computer program SURVSTAT [3]. Based on a second-round review and balance of both coldmass and assembly data, the assemblies are sorted for final installation.

3 ARC REGION MAGNET SORTING

RHIC arc dipoles, quadrupoles and sextupoles are industry-built magnets. Despite close communication and detailed quality assurance procedures, unexpected changes in the manufacturing process still occurred. Magnet acceptance review and the subsequent sorting played an essential role in optimizing the final performance.

3.1 Arc Dipoles

During the acceptance, a drop in the integral transfer function (ITF) of about 0.1% was noticed and traced to the narrower width of the phenolic insulator used between the coil and the iron. Although the problem was corrected, about 20 magnets were affected. These magnets were sorted along with all subsequent dipole magnets. The sorting procedure was based on the strength minimization of dipole correctors required to compensate for the variation in the integral transfer function. With sorting, the maximum current required for such compensation was decreased from 12 A to about 3 A.

The dominant multipoles of the dipole magnets are b_2 (normal sextupole) and b_4 (normal decapole) resulting from the dipole symmetry of the magnets, and a_1 (skew quadrupole) resulting from the asymmetric vertical placement of the magnet cold mass in the cryostat. Due to the relatively high injection energy and the small diameter of the coil filaments, the persistent current effects are small. Magnet design has minimized b_2 and b_4 for both injection and storage currents by optimizing the cross-sections of the coil and the yoke taking into account the persistent current and saturation effects. The minimization of a_1 is achieved by sorting the yoke weight during the assembly process so that the lower half yoke is heavier than the upper half.

Among the eight dipoles allocated as spare magnets, five of them have off-normal skew quadrupole component (a_1 up to -5.9 units [4]), some caused by a known coil size mismatch; one has an excessive twist (2.5 mr standard deviation in body field angle) along the magnet body, and one has low transfer function at high fields.

3.2 Arc Quadrupoles

At the early stage of industrial manufacture, midplane shims were incorrectly changed on 5 quadrupoles, resulting in a b_3 of about -6 units. These magnets were sorted and distributed among the two rings to minimize their effects.

The dominant multipoles of the quadrupoles are b_5 and a_5 resulting from the quadrupole symmetry of the coil and the end configuration, and b_3 resulting from the asymmetry between the horizontal and vertical planes. b_3 was compensated in the design by making the coil to midplane gap appropriately asymmetric, while b_5 was reduced by compensating the body with the ends of the magnet.

Among the eight quadrupoles allocated as spare magnets, four of them are of concern with off-normal coil size or low collaring pressure, some resulting in large a_2; two have excessive b_2 (-5 units); one has an engineering repair.

3.3 Arc Sextupoles

In general, the performance of the sextupole magnets exceeded the design goal. However, the epoxy contained in about 42 magnet coils is significantly weaker than normal. Consequently, the average quench currents (about 170 A) of these magnets, although exceeding the design operating current (100 A), are lower than the average of the regular magnets (above 200 A). To minimize possible long-term effects, these magnets have been sorted and allocated to the focusing locations around the two rings where the required strength of the sextupoles for chromaticity correction is about 50% of that at the defocusing locations.

3.4 Arc Trim Quadrupoles

Trim quadrupoles all have minimum quench currents above 200 A, well exceeding the design operating current of 100 A. One trim quadrupole coldmass was designated as a spare due to rust on the yoke caused by rain damage.

3.5 Arc Correctors

All of the correctors, either single-layer or four-layer, were built in-house and cold tested. After initial training, all the magnets quench above the design operating current of 50 A. Since the dipole corrector layers are all powered individually, the variation in the integral transfer function (typically 1% rms) is of little concern. Correctors with layers of excessive field angle deviation (up to ~20 mr) or erratic quench training were selected as spare magnets.

3.6 Arc CQS Assembly

Arc corrector, quadrupole, and sextupole magnets were welded into a single "CQS" assembly. The CQS assembly also includes a beam position monitor and (for some) a recooler. The CQS components need to be aligned with each other so that their magnetic centers are on a straight line. It was found in the early stage of installation that "Springs" (made of G-10 plastic) needed to be installed or refitted in the support posts, confining the coldmass transversely while allowing free longitudinal motion. Special welding stripes were applied to the CQS shell to align the magnetic centers of the individual coldmasses for assemblies that exceeded a tolerance of 0.25 mm. Subsequently, the welding sequence is carefully choreographed to balance "curling" distortions against each other.

Correctors with large misalignments can generate serious feed-down harmonics. Two early CQSs with corrector offsets larger than 2 mm have been removed from the tunnel, and were later corrected.

4 IR MAGNET SORTING

The IR triplet cryostat contains two dipoles, six quadrupoles, and six four-layer corrector packages of the two rings. Field imperfection of the IR magnets limits the machine performance at collision when β^* is squeezed. Among the 6 interaction points, 2 of them are planned to run at a low β^* of 1 m. Most sorting efforts have been to select the best IR magnets for these 2 "golden" IPs.

4.1 IR Dipoles

In general, two IR dipoles, one on each side of the IP, are powered by the same shunt power supply. Sorting has been performed to pair dipoles of similar transfer function to the same IP. Two dipoles with off-normal transfer function are assigned to special locations where individual shunt supplies exist. Early magnets with imperfect field quality (large b_2) were assigned to non-golden region. Since the outstanding random error is a_1, magnets of similar a_1 are sorted to the opposite side of the same IP to minimize their action kicks [5]. One dipole is designated as a spare due to erratic quench performance.

4.2 IR Quadrupoles

The manufacturing sequence of IR quadrupoles follows the level of required performance, starting with the less-critical Q1. Several iterations were made on the magnet cross section to optimize the field quality. Application of tuning shims is also practiced at this stage.

In one Q2 quadrupole, an excessive amount of axial variation in multipole errors was found (change of 15 units of a_2) and suspected to be due to cracked insulators. The quench performance, though adequate, was lower than average. Efforts were made at the last stage of installation to replace this "golden candidate" with a "spare candidate".

Due to lack of time for cryogenic testing, 11 out of 72 IR quadrupoles were measured only at room temperature. Because of imperfect correlation between the warm and cold measurements, the field quality of these magnets is less well known than the field quality of magnets which have been cold tested. Since this information is the critical base for IR correction, these magnets were sorted to "non-golden" IRs. Spare magnets were mostly selected based on off-normal multipole errors. One quadrupole with a partially inserted shim was first allocated as a spare but later installed to meet schedule requirements for the first sextant test.

4.3 IR Correctors

Sorting on IR correctors was performed along with the quadrupoles before their attachment to minimize the relative magnetic center offset and field angle. After sorting, for CQ combinations with excessive relative offset and roll, shimming adjustment were made before welding of the assembly.

4.4 IR CQ Assembly

IR correctors were welded to IR quadrupoles to form CQ assemblies. At a later stage of IR CQ assembly, electric shorts were found at the octupole leads of IR correctors precipitated by a routing misdesign. Rework was done on all the correctors which were still in coldmass state. For correctors designated as "golden" and yet with their end plates already welded on, their end plates were removed to allow a complete rework. About 8% of the CQ assemblies fully installed in the machine were not reworked, and their chance of octupole layer malfunction is less than 10%.

Table 1: Summary of RHIC magnet sorting ($n = 1$ is quadrupole).

Magnet	Number (used+spare)	Sorted quantity
Arc dipole	288+8	ITF, yoke weight (a_1) twist, b_2
Arc quad.	372+8	coil size, midplane shim size collaring pressure coil saddle crack repair, b_2
Arc sext.	288+12	epoxy level (quench)
Arc corr.	420+10	quench, field angle
D5I	12+1	vacuum vessel straightness
D5O	12+1	vacuum vessel straightness
D96	48+1	
Trim quad.	72+6	rust on yoke
CQS	282+8	corrector offset
CQT	72+6	
CQ	60+2	
Interaction region magnets:		
IR dipole	24+2	quench, ITF, b_2, a_1
IR quad.	72+6	data availability (schedule) axial variation of a_2 partial shim, multipoles
IR corr.	72+6	center offset, roll
DX dipole	12+1	
IR CQ	72+6	potential corrector shorts
Total	1692+65	

4.5 Separating Dipoles DX

After a design iteration based on the prototype magnet, the field errors (b_2, b_4) of these large-bore (18 cm coil diameter) dipoles were greatly reduced and are well within the capability of IR correction [6].

We thank members of the Magnet Acceptance Committee for their contribution.

5 REFERENCES

[1] P. Wanderer, CERN 98-05 (1998) p. 273.

[2] J. Wei, G. Ganetis, R. Gupta, M. Harrison, M. Hemmer, A. Jain, F. Karl, S. Peggs, S. Tepikian, P.A. Thompson, D. Trbojevic, and P. Wanderer, EPAC96 (1996) p. 2222.

[3] J. Wei, R. C. Gupta, A. Jain, S. G. Peggs, C. G. Trahern, D. Trbojevic, and P. Wanderer, PAC95 (1995) p. 461.

[4] Multipole errors are normalized to 10^{-4} of their integral strength at a reference radius of about 2/3 coil radius. $n = 1$ is quadrupole.

[5] J. Wei, W. Fischer, V.Ptitsin, R. Ostojic, J.Strait, PAC99 (1999).

[6] A. Jain, PAC99 (1999).

Workshop on LHC Interaction Region Correction Systems, BNL, Upton, New York, 1999

INTERACTION REGION CORRECTION EXPERIENCE AT LEP

John M. Jowett,
CERN, Geneva, Switzerland

Abstract

I briefly review the corrections applied to the interaction region of LEP with a view to what might be relevant to the LHC.

1. INTRODUCTION

As something of a phoenix rising from the decommissioning of LEP, the LHC necessarily shares some characteristics of its illustrious leptonic progenitor. Yet the two machines differ to the extent that most of the matters discussed so far in this workshop have been irrelevant in the design and operation of LEP! Having been asked to review the experience in correcting the LEP interaction region, I can only ask: are there aspects of interaction region correction at LEP, not discussed so far in this workshop, that might have some bearing on the LHC?

More specifically, the two machines have the same circumference and a similar number of magnetic elements (per ring in the case of the LHC); each is subject to similar movements of the very same tunnel floor and each has superconducting interaction region (IR) quadrupoles. On the other hand, their beams, their energies, their magnetic field strengths and most of their hardware components are radically different.

I cannot do more than mention the main points in this brief, informal summary. I hope it will be taken as a set of pointers to the fuller information that you can find through the references.

2. LINEAR OPTICS

The standard set-up of LEP's physics optics includes a correction of the vertical Twiss function at each IP to its nominal value $\beta_y^* = 0.05\,\mathrm{m}$. This is done very simply by measuring the change in tune for small changes of the IR quadrupole strengths. The same quadrupoles are then trimmed to rematch β_y^*.

On many occasions, adjustments of β_y^* and errors of the IR quadrupoles have been related to β-beating and phase advance errors measured around the ring. Corrections of the interaction region cannot be considered in isolation. For a recent example, see [1].

Compensation of the betatron coupling due to the experimental solenoids is also a routine matter, modulo minor historical glitches. The compensation by means of nearby tilted quadrupoles is computed by the standard technique of zeroing the off-diagonal blocks of an appropriate transfer matrix. The basis of the calculation is a model in which the measured longitudinal field profile of each solenoid is obtained using several slices of solenoid interspersed with slices of IR quadrupole. This procedure works well.

3. NONLINEAR DYNAMICS

Thanks, mainly, to the synchrotron radiation, the physical effects determining the dynamic aperture in LEP are utterly different from those in hadron rings like RHIC or the LHC. At high energy, the dominant non-linear fields causing large amplitude particles to be unstable are those of the chromaticity correction sextupoles, the accelerating fields of the RF cavities and the *designed quadrupole gradient* of the interaction region quadrupoles [2]. (In LEP, quadrupoles must be considered as *nonlinear* elements because the radiation loss in them is $\propto p^2 K_1^2 (x^2 + y^2)$ where p, x and y are a particle's momentum and transverse coordinates and K_1 the quadrupole gradient.)

Although we know the multipole components of the superconducting interaction region quadrupoles from the magnetic measurements [3,4], they are not strong enough to make any significant difference to the dynamic aperture [5]. This was the case, both for the original set of quadrupoles (MQC type) installed for LEP1 operation (up to 65 GeV per beam) and the stronger ones (MQCC type) that replaced them for LEP2 (up to 100 GeV).

A MAD description of the multipole gradients of the MQCCs is available in the standard repository of files describing the LEP optics.

At the highest energies, the gradient of the interaction region quadrupoles is limited by the radiative beta-synchrotron coupling instability. The only ways to overcome this effect are to increase the RF voltage, which is no longer possible, or to reduce the strength of the interaction region quadrupoles. Thus, this instability translates into a lower limit on b_y^*. Since this instability arises because of the radiation damping, there is no corresponding effect in the LHC.

4. ALIGNMENT OF BEAM POSITION MONITORS

Beam-based alignment techniques have been used extensively at LEP to measure the offsets between beam position monitors and quadrupole magnets [6,7,8]. The favored technique is the so-called "K-modulation" in which a quadrupole gradient is modulated at a frequency well below the betatron frequency. Moving the closed orbit in the quadrupole to minimize the response locates the magnetic center and determines the offset of an adjacent beam position monitor.

This method revealed [7] that there were indeed substantial misalignments between the magnetic centers of the quadrupoles and the beam position monitors. The offsets for the first generation of the superconducting quadrupole magnets for LEP (MQC type) show large offsets of up to $-2\,\mathrm{mm}$. Their replacements for LEP II (MQCC type) have offsets only up to $-1\,\mathrm{mm}$.

It goes without saying that, once these offsets were taken account of in the orbit measurements, there were clear benefits for machine operation and performance.

5. MOVEMENTS OF IR QUADRUPOLES

At three of LEP's four IPs, the innermost quadrupole (QS0) is imbedded deep inside the detector and supported from the main tunnel floor by a cantilever structure (see Figure 1). At the fourth (IP2, for the L3 detector) the three innermost quadrupoles (QS0, QS1A and QS1B) are supported together with the inner parts of the detector in a 32 m long support tube. This tube can be moved with motorized jacks.

Because of movements of these support structures, vertical orbit correction is the most frequent task carried out by the operators during physics fills. In 1994 for example [7], over 13000 vertical corrections were done during physics data-taking, or while setting up for it. The orbit corrector magnets near QS12 and QS8 in the experimental straight sections were by far the most popular correctors, not surprisingly since they are at a vertical phase difference of $n\pi$ from the low-β quadrupoles. (At the time, the orbit correction algorithms were programmed to avoid using other correctors nearer the IP).

As by far the strongest quadrupoles in LEP, the interaction region quads are the dominant source of orbit and optical errors. Because there is a vertical phase advance $\Delta\mu_y \approx \pi$ between them, these occur according to well-known patterns depending on the symmetry of the movements around the IP.

Serious attention has to be given to the correction of these linear effects. A few years into LEP operation, hydrostatic leveling systems were added to monitor their movements [7]. Other systems, based on differential pressure in water columns and potentiometers that measure relative movements of luminosity monitors and main detectors, provide further information. Careful analysis of the results, taking out the effects of applied orbit corrections, showed strong correlations between measured movements of the QS0 quadrupoles and computed orbit correction kicks [8].

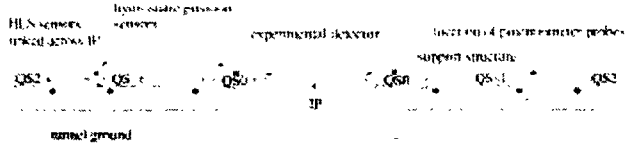

Figure 1: Interaction region around an experimental detector (not to scale), reproduced from [8].

6. BEAM SEPARATIONS

Another important class of corrections associated with the interaction regions in LEP is related to the separations of the beams at the collision point. Generally, these could be corrected by adjusting the electrostatic separation at the IPs. In LEP, there are three different physical origins of separation between beams:

1. **Applied electrostatic fields** designed to separate the beams in some part of the machine (e.g., at different times, the horizontal pretzel scheme used to separate in the arcs or the local vertical bumps near the IPs used in a "bunch-train" scheme).
2. **Synchrotron radiation.** The two beams have different orbits because of the interplay between the strong energy loss by synchrotron radiation in the arcs and its replacement by clustered RF cavities. These so-called "energy-sawtoothing" effects cause the beams to have different momentums at the same place in the ring, and therefore different orbits (for further discussion, see [9]).
3. **Beam-beam effects.** Different bunches in the same beam can experience different sequences of beam-beam forces resulting in different orbits; these are similar to the so-called "PACMAN" effects in hadron colliders. These were particularly pernicious in the "bunch-train" scheme because there was no means to correct them, except in an average sense, to maximize the luminosity over all bunch encounters [10].

7. OPTICAL DIFFERENCES BETWEEN BEAMS

In the LHC, the two beams circulate in different vacuum chambers. Despite being closely related thanks to the twin-bore magnet design, the magnetic fields acting upon them can be somewhat different. Thus, in principle, their optics can be different. In LEP, despite being in the same vacuum chamber, subject to essentially the same magnetic (and some electric) fields, the two beams have different optics because of the energy-sawtoothing (the same physical origins as the orbit separations discussed above). In practice, corrections are difficult to make for this kind of effect. The operators try to keep the distribution of RF voltage as symmetric as possible. At top energy, however, there is little reserve voltage left to provide much latitude for this. Fortunately, however, there is usually enough symmetry in the distribution of accelerating voltage that differences in b_y^* between the beams are generally small, of the order of 5 %.

Some detailed measurements and calculations, with illustration of the effects of synchrotron radiation on the optical functions around the ring, can be found in [11].

8. CONCLUSIONS

Although there is no need to correct higher-order multipoles in the superconducting low-β quadrupoles,

several other, more basic, corrections of LEP's interaction region are important. The quadrupoles move with their support structures, generating closed-orbit displacements. To equalize luminosity and minimize the dominant source of errors in the linear optics, the optical functions at the interaction points have to be corrected by adjusting the gradients. Beam-based alignment has been very important in determining the misalignment of the magnetic centers of the beam-position monitors relative to those of the quadrupoles themselves. One can hardly overstate the need to pay close attention to alignment of machine components in the interaction region of the LHC and to provide effective means to cope with any misalignments that arise after all.

Another class of corrections are those associated with differences of orbits and optics between the beams. Generally these can be corrected or lived with. The worst class of effects are differences between different bunches of the same beam. We should not forget that these can also arise in the LHC and may be very difficult to deal with.

REFERENCES

[1] G. Morpurgo, "Do we understand the luminosity imbalance?", Proceedings of the 9th Workshop on LEP Performance, Chamonix, 1999, CERN-SL-99-007 DI (1999) and http://www.cern.ch/CERN/Divisions/SL/publications/chamx99/PAPERS/GM8_1.PDF

[2] See, e.g., J.M. Jowett, "Realistic Prediction of Dynamic Aperture and Optics Performance for LEP", Proc. 1999 Particle Accelerator Conference, New York City, 29 March - 2 April 1999, http://ftp.pac99.bnl.gov/Papers/Wpac/TUP86.pdf and references therein.

[3] P.J. Ferry et al, "Analysis of the Performance of the Eight Superconducting Quadrupoles for the LEP Low-Beta Insertions", Proceedings of the 11th International Conference on Magnet Technology, Tsukuba, Japan, Elsevier 1989, pp. 253–8.

[4] A. Ijspeert, T.M. Taylor, M. Begg, "Construction and Test of Superconducting Quadrupoles for the LEP2 Low-Beta Insertions", Proceedings of the Fourth European Particle Accelerator Conference, London 1994, World Scientific, 1994, pp. 2277–9.

[5] There does not seem to be a published reference on this point. I know that it has been checked independently by A. Verdier and Y. Alexahin for different optics. It is also plausible based on a comparison of the magnitudes of kicks due to these multipoles (at amplitudes close to the dynamic aperture) with those due to the lattice sextupoles.

[6] I. Barnett et al, "Dynamic Beam Based Calibration Of Orbit Monitors At LEP",

[7] Frank Tecker, "Methods of Improving the Orbit Determination and Stability at LEP", Ph.D. Thesis, RWTH Aachen, March 1998, PITHA 98/7.

[8] F. Tecker, "Low-Beta Quadrupole Movements As Source Of Vertical Orbit Drifts At LEP", CERN-SL/96-40 (BI), 1996.

[9] J.M. Jowett, "Beam Dynamics at LEP", Proceedings of the Advanced ICFA Beam Dynamics Workshop on "Beam Dynamics Issues for e^+e^- Factories", Frascati, 20–25 October 1997, Frascati Physics Series, 1998.

[10] M. Böge et al, "Measurements of Collision Offsets and Difference in Vertical Dispersion at the LEP Interaction Points", Proceedings of the European Particle Accelerator Conference, Sitges 1996, IOP Publishing, 1996.

[11] J.M. Jowett, "Effect of RF Configuration on β_y^* Measurements in LEP", CERN SL MD Note 240 (1997).

Correction schemes for the LHC lattice at collision

T. Sen, N. Gelfand and W. Wan, FNAL, Batavia, IL 60510

Abstract

Normal form analysis and tracking results show that both normal and skew resonances are driven strongly by the nonlinear fields of the IR quadrupoles. We report here on the possibility of improving the dynamic aperture by compensating these resonances with the use of correctors placed in the IRs. The effectiveness of local correction schemes in the presence of beam-beam interactions is also studied.

1 INTRODUCTION

The target dynamic aperture for the LHC at collision is 12σ at 10^5turns. The dynamic aperture with only random errors from version 2.0 of the Fermilab and KEK error harmonics is about 11σ at 10^5turns [1]. Systematic uncertainties and errors in the ends reduce the dynamic aperture to about 9σ at 10^5turns [2]. Local correction schemes based on minimizing the action kick from each multipole [2] have been investigated as a means of increasing the dynamic aperture to the target value. Here we investigate a global compensation method based on minimizing low order resonances as a complementary method to improve the dynamic aperture. We also examine the efficacy of idealized versions of local correction schemes when beam-beam interactions are included.

2 RESONANCE STRENGTHS FROM TRACKING

The basic lattice was derived from MAD 5.1. In the high luminosity insertions, Fermilab error harmonics V2.0 were used for the quadrupoles in IR5 and KEK error harmonics V2.0 were used for the quadrupoles in IR1. This is the so-called "unmixed case". Using this lattice, the program COSY INFINITY [3] was used to generate a Taylor map. The arcs are represented by 5th order maps and the IRs are represented by 9th order maps. These are concatenated to generate a single map for the lattice. The Taylor map is tracked to calculate either the dynamic aperture or amplitude growth.

Tune scans were done to identify the resonances that drive amplitude growth. Particles were placed at initial amplitudes of 3, 5 and 7 σ and their amplitude growth was recorded over 1000 turns at each tune. The tune scan was done in two ways: 1) the vertical tune Q_y was held fixed and the horizontal tune Q_x was varied, 2)Q_x was held fixed and Q_y was varied. This was done for 30 seeds.

Figure 1 shows the amplitude growth in both planes, with seed 1 for multipole errors, for a particle initially at 5σ as a result of tune scans in the horizontal and vertical planes. In this case, the $Q_x + 2Q_y$ and $2Q_x + Q_y$ resonances are of sufficiently large widths to produce a broad resonance. The other resonance causing a large amplitude growth is the fourth order resonance $2Q_x + 2Q_y$. Figure 2 shows the results of similar scans with seed 9. Again, the third order sum resonances and the $2Q_x + 2Q_y$ resonance cause large amplitude growth.

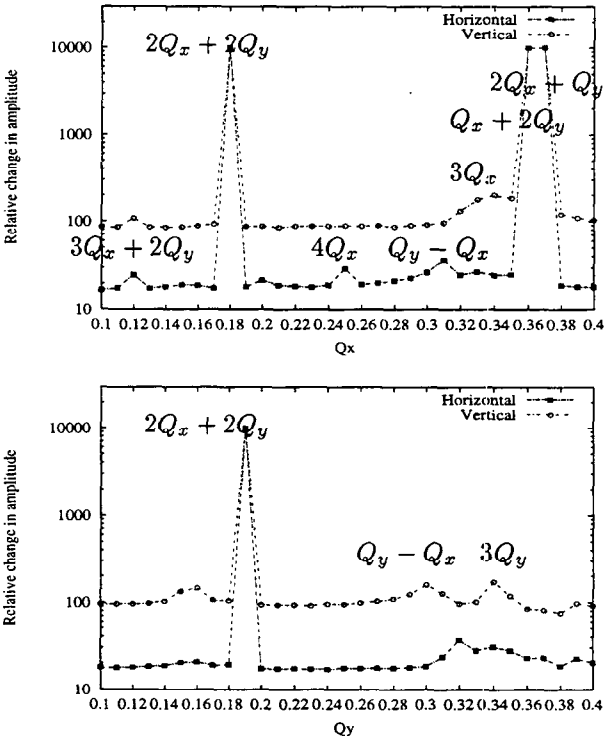

Figure 1: Amplitude growth with horizontal (top) and vertical (bottom) tune scans for seed1. For the horizontal tune scan, the vertical tune is kept constant at 0.32 while for the vertical scan the horizontal tune is kept constant at 0.31. We have identified some of the resonances that are associated with large amplitude growth. Note that the normal Q_x+2Q_y and skew $2Q_x+Q_y$ resonances have overlapped producing a broad resonance. This seed had the smallest dynamic aperture of all the seeds tracked.

In the majority of cases, the skew resonance $2Q_x + Q_y$ and the fourth order normal resonance $2Q_x + 2Q_y$ were found to cause large amplitude growth. Figure 3 shows normalized histograms over 30 seeds of the relative amplitude growth due to these resonances. For example, in about 70% of the cases the skew $2Q_x + Q_y$ resonance caused a relative amplitude growth of more than 10^4. These tracking results show that even with the random nature of the multi-

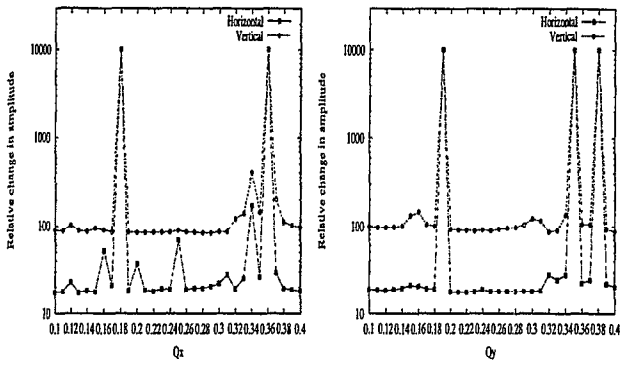

Figure 2: Amplitude growth with horizontal (left) and vertical (right) tune scans for seed9. In this case, the sum third order resonances Q_x+2Q_y and $2Q_x+Q_y$ are distinct. The dynamic aperture for this seed was near the average over all the seeds.

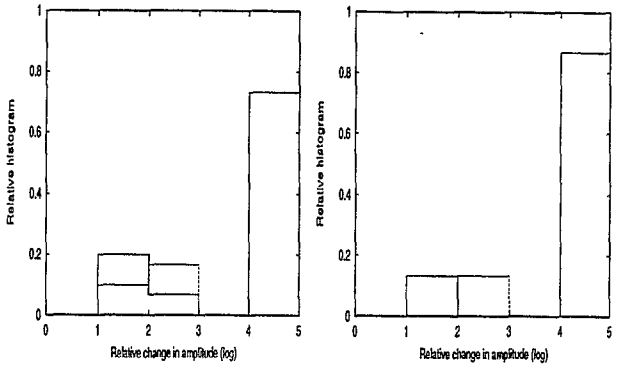

Figure 3: Normalized histograms of the relative amplitude growth (shown on a log scale) due to the resonances $2Q_x + Q_y = 186$ (left) and $2Q_x + 2Q_y = 245$ (right). The histograms represent data from tracking with 30 seeds. For example, in more than 70% of the cases, the $2Q_x+Q_y = 186$ resonance leads to a 10^4fold or larger amplitude growth.

pole errors, the same, relatively few, low order resonances are responsible for amplitude growth. This encourages the hope that compensating these resonances may increase the dynamic aperture. At the nominal tunes ($Q_x = 63.31$, $Q_y = 59.32$), the 4th order resonance $2Q_x + 2Q_y = 245$ should not be excited. In this paper we choose to minimize only third order resonances.

3 RESONANCE STRENGTHS FROM NORMAL FORMS

The normal form $\mathcal{N}$ of a map $\mathcal{M}$ is obtained via

$$\mathcal{N} = \mathcal{A}^{-1}\mathcal{M}\mathcal{A} \tag{1}$$

where

$$\mathcal{A} = e^{:F:} \tag{2}$$

The notation :: signifies a Poisson bracket operation. The generating function F of the similarity transformation is

$$F = \sum_{j,k,l,m} f_{jklm} J_x^{(j+k)/2} J_y^{(l+m)/2} e^{-i\psi_{j,k,l,m}} \tag{3}$$

where $\psi_{j,k,l,m} = (j-k)(\psi_x+\psi_{x,0})+(l-m)(\psi_y+\psi_{y,0})$. and J_x, J_y are the linear actions. The resonances of order $n = |j-k|+|l-m|$ are $n_xQ_x \pm n_yQ_y \equiv (j-k)Q_x \pm (l-m)Q_y = p$. These resonances also appear in higher orders $n+2, n+4, \ldots$ in the generating function. The strength of an nth order resonance is taken to be the absolute value of the complex generating function.

$$\mathcal{F}(n_x, n_y) = |\sum_{\substack{j,k,l,m \\ j-k=n_x, l-m=n_y}} f_{jklm} J_x^{(j+k)/2} J_y^{(l+m)/2} e^{-i\psi_{j,k,l,m}}| \tag{4}$$

COSY INFINITY is used to generate the normal form of the map and also evaluate the resonance strengths.

Third order resonance strengths, both normal and skew, were calculated at an amplitude of 8σ, close to the dynamic aperture. These resonance strengths included the contributions from higher order multipoles (the "sub-resonance" contributions). For example, the resonance $Q_x + 2Q_y$ has primary contributions from b_3 and subsidiary contributions from b_5, b_7, b_9. Similarly the skew resonance $2Q_x+Q_y$ has primary contributions from a_3 and subsidiary contributions from a_5, a_7, a_9.

4 CORRECTION WITH SEXTUPOLES

Correcting all four third order sum resonances $3Q_x, Q_x + 2Q_y, 2Q_x + Q_y, 3Q_y$ requires two sextupoles for each resonance or eight in all. In order to minimize the sextupole strengths, the phase advance between the sextupoles correcting a resonance have to be chosen appropriately. For example, the optimal phase advances between the sextupoles correcting the $Q_x + 2Q_y$ resonance satisfy $\Delta\psi_x + 2\Delta\psi_y = \pi/2$. In this case the corrector strengths are minimal and both the real and imaginary parts of the driving term can be corrected. However in the study reported here, we restricted ourselves to placing sextupole correctors in the MCBX and MCQS packages in the IRs. The phase advances between them are odd multiples of π and therefore far from optimal. The β functions in these correctors however are larger than they would be for sextupole correctors placed in the arcs.

In IR1 and IR5, normal sextupoles, labelled NS1,...NS4 in Figure 4, are placed in MCBX packages between Q2a, Q2b and after Q3 on both sides of the IP for a total of eight normal sextupoles. Within a single IR, the normal sextupoles in a family e.g. NS1, -NS1, are placed at locations of nearly equal beta functions in both planes and have the same strength but with opposite signs. Their contribution to the linear chromaticity is therefore zero while the phase advance between them is nearly π. A total of four sextupole strengths are available to correct the real and imaginary parts of the two normal resonances. Skew

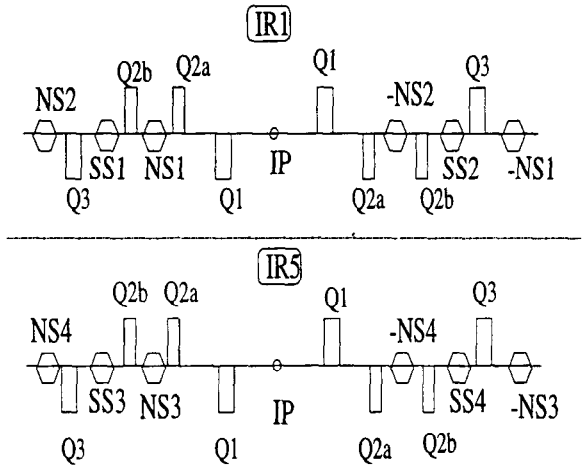

Figure 4: Placing of the 4 families of sextupoles for reducing the third order resonance strengths.

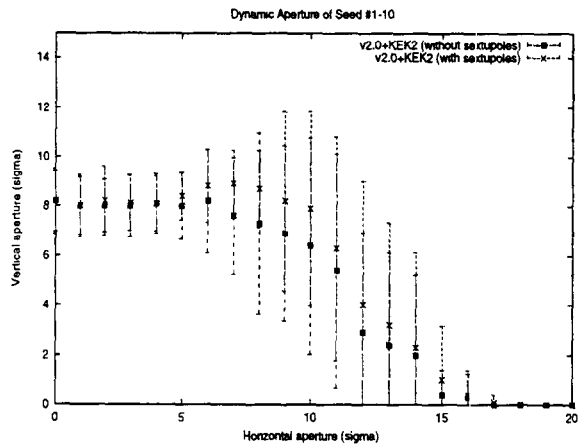

Figure 5: Dynamic aperture at different regions in amplitude space with the use of sextupoles. At each value of the initial horizontal amplitude, the dynamic aperture is averaged over 10 random seeds. There is little change in the dynamic aperture along either the x or y axis. The largest gain in dynamic aperture, about 2σ, occurs close to the diagonal.

sextupoles, labelled SS1,... SS4 in Figure 4, are placed in MCQS packages after Q2b, also on both sides of the IP in IR1 and IR5, for a total of four skew sextupoles to correct the two skew resonances. Equal weighting was given to these four resonances and COSY INFINITY was used to minimize these resonances using up to the maximum sextupole field of 0.067T at the reference radius of 17mm.

Table 1 shows the resonance strengths after correction as a fraction of their original values before correction for ten seeds. The resonance strength here is the absolute value of the complex driving term. In most of these cases, one or more of the resonance strengths are lowered. Reducing all the sum third order resonances does not seem possible in general with the available sextupole strengths.

The dynamic aperture was calculated after the correction of these sum resonances. Figure 5 shows the dynamic aperture in amplitude space. At each horizontal amplitude, the dynamic aperture is averaged over ten random seeds for the multipole errors. There was no improvement in the dynamic aperture along the y axis. This could be because the vertical tune is sufficiently close to the $3Q_y$ resonance that reducing this resonance strength by factors of two or less is not sufficient to improve the dynamic aperture. The largest improvement is seen close to the diagonal. The improvement in dynamic aperture along the x axis is also small.

In those cases, where resonances are dramatically reduced, there is a significant improvement in the dynamic aperture. For example, with seed 3, both the $3Q_x$ and $2Q_x + Q_y$ resonances are down to about 5% and the dynamic aperture increases by 2.6σ. With seed 10, the $3Q_y$ resonance is down to 5% of its original strength while the others have increased, yet the dynamic aperture increases by 0.8σ. It is clear that overall, the gain in dynamic aperture by attempting to minimize all the sum third order resonances with the present locations of the sextupoles is only modest. It is more likely that the resonances can be better compensated if the sextupoles are placed in the arcs so that the phase advances can be chosen appropriately. Other strategies that are possible include weighting one or two of the resonances more strongly than the others in doing the resonance correction. This is being explored.

Table 1: Fractional change in third order resonance strengths using sextupoles, seed by seed. $f(n_x, n_y)$ is the relative strength of the $n_x q_x + n_y q_y = n$ resonance after and before correction. The last column shows the change in dynamic aperture $\Delta\langle DA\rangle$ due to these sextupoles.

Seed	f(3,0)	f(0,3)	f(2,1)	f(1,2)	$\Delta\langle DA\rangle$
1	0.99	0.61	0.45	0.19	0.65
2	1.07	0.75	0.57	1.42	0.19
3	0.06	1.64	0.05	0.23	2.58
4	0.97	0.81	1.01	0.98	0.31
5	0.36	1.03	0.78	30.04	0.52
6	0.35	1.91	0.94	0.17	0.59
7	0.15	0.37	1.85	0.60	-0.29
8	0.81	0.27	0.53	1.27	-0.88
9	0.41	0.50	0.61	1.34	0.20
10	1.04	0.05	1.43	2.92	0.84

5 CORRECTION WITH OCTUPOLES

Another way to avoid excitation of dangerous resonances is to reduce the tune footprint of the beam. The tune shift with amplitude depends quadratically on the sextupole strengths but linearly on the octupole strengths. Octupoles are therefore better suited for this purpose. There are three detuning terms to be minimized: $\partial Q_x/\partial J_x, \partial Q_x/\partial J_y, \partial Q_y/\partial J_y$. Three pairs of octupoles are used with members in a pair set

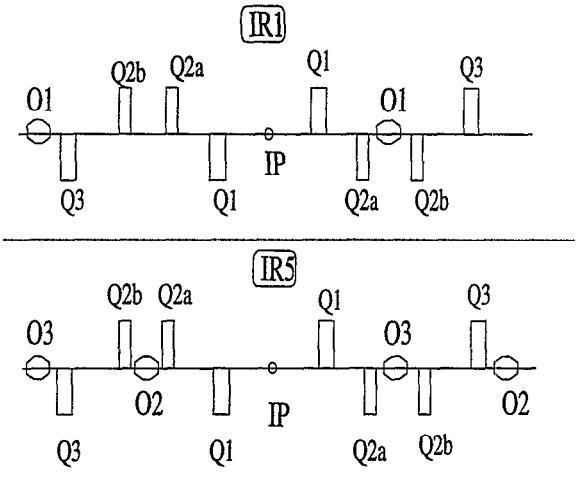

Figure 6: Placing of the 3 families of octupoles for reducing the tune shift with amplitude.

to the same strength and placed at nearly the same values of the beta functions. Members of the 3 families labelled $O1, O2, O3$ are shown in Figure 6.

The main purpose of the octupoles is to reduce the tune shift with amplitude. Figure 7 shows that the tune footprint for seed 1 is significantly smaller when the octupoles are used. However the orbit is not centered in the octupoles due to the crossing angle. Consequently they also affect the third order resonance strengths due to the feed-down into sextupole components. Table 2 shows the fractional resonance strengths after using the octupoles. The changes that occur with the octupoles are not controlled. For example, with seed 1 all the sum resonances were reduced while with seed 9, three of the four sum resonances increased in strength. In order to check that the feed-down

Table 2: Fractional third order resonance strengths after reducing the tune spread with octupoles.

Seed	f(3,0)	f(0,3)	f(2,1)	f(1,2)	$\Delta(DA)$
1	0.83	0.27	0.08	0.18	1.89
2	0.42	2.26	0.85	1.24	-1.46
3	0.34	1.87	0.49	0.22	0.55
4	3.29	0.52	4.90	0.84	0.57
5	0.86	0.83	1.30	25.70	0.04
6	0.32	1.42	0.62	0.22	0.17
7	0.09	0.55	1.93	0.62	2.61
8	2.46	0.77	0.14	1.89	1.57
9	0.57	1.19	1.52	1.23	1.65
10	1.05	0.53	0.31	1.07	-1.47

from the octupoles is responsible for the changes in resonance strengths, the octupoles were displaced transversely so that they were centered on the closed orbit. In this case, there was no change in the third order resonance strengths.

Figure 8 shows the average dynamic aperture over 10 seeds with and without the use of octupoles. The average increase in dynamic aperture with the use of the octupoles is somewhat greater than that obtained with the sextupoles. In particular, the dynamic aperture also increases along the y axis. Reducing the tune shift at large amplitudes therefore appears more beneficial in avoiding the effects of the $3Q_y$ resonance.

6 SEXTUPOLES AND OCTUPOLES TOGETHER.

When both sextupoles and octupoles are used, a two step procedure is necessary. Due to the fact that octupoles

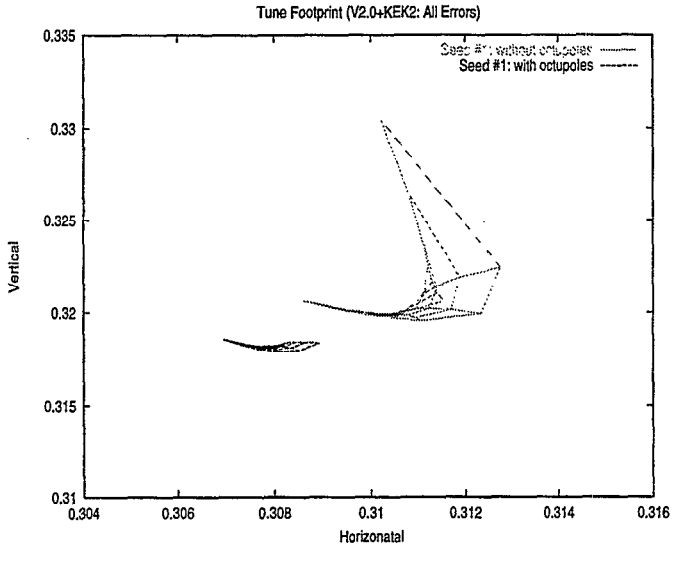

Figure 7: Tune footprint with and without octupoles for seed1.

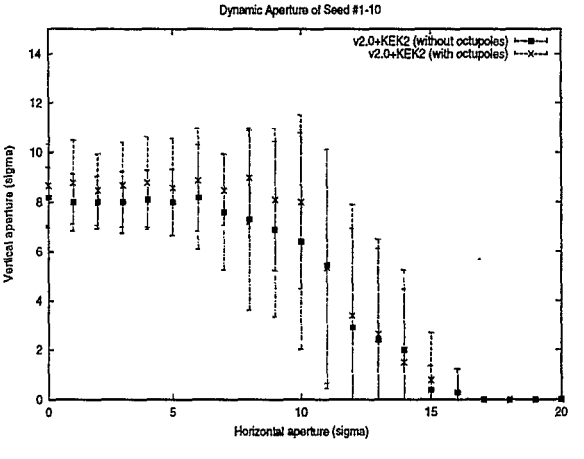

Figure 8: Dynamic aperture at different regions in amplitude space with the use of octupoles. At each value of the initial horizontal amplitude, the dynamic aperture is averaged over 10 random seeds. The octupoles help to increase the dynamic aperture along the y axis as well as close to the diagonal.

Table 3: Fractional third order resonance strengths after correction with octupoles and sextupoles.

Seed	f(3,0)	f(0,3)	f(2,1)	f(1,2)	$\Delta\langle DA\rangle$
1	0.49	0.18	0.07	0.10	2.69
2	0.47	1.74	0.72	1.40	-1.03
3	0.24	3.35	0.40	0.16	0.22
4	2.67	0.59	2.02	1.09	0.75
5	0.33	0.93	0.94	49.87	0.41
6	0.33	1.32	0.55	0.22	-0.10
7	0.12	0.14	0.29	0.48	2.49
8	1.31	0.98	1.48	1.58	1.69
9	0.48	0.97	1.29	0.98	2.22
10	0.74	0.07	1.07	1.42	0.49

change the third order resonance strengths via feed-down, it is difficult to do a simultaneous compensation of resonance strengths and tune shifts with amplitude. In the two step procedure, first octupoles are used to reduce the tune footprint and a new map of the lattice is obtained with these octupole correctors. The third order resonances of this new map are then compensated with sextupoles.

Table 3 shows the fractional resonance strengths after correction with the octupoles and sextupoles. Compared to the fractional strengths shown in Table 2, most of the resonance strengths have decreased. For example, with seed 1 the $3Q_x$ resonance is reduced to nearly half its value with octupoles alone and the increase in dynamic aperture changes from 1.89σ to 2.69σ.

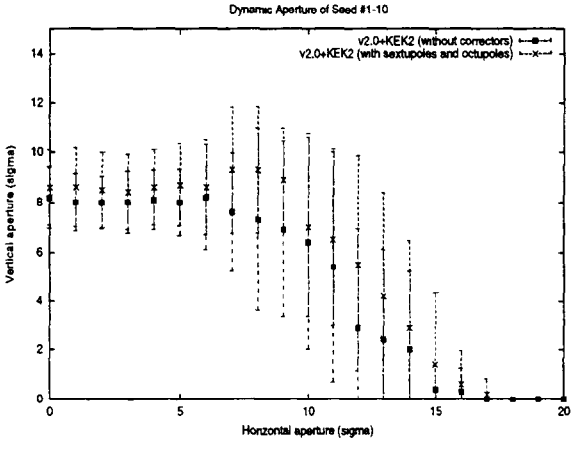

Figure 9: Dynamic aperture at different regions in amplitude space with the use of sextupoles and octupoles. At each value of the initial horizontal amplitude, the dynamic aperture is averaged over 10 random seeds. As with octupoles alone, sextupole and octupole correctors help to improve the dynamic aperture at almost all angles in physical space.

Figure 9 shows the average dynamic aperture over 10 seeds with and without the use of sextupoles and octupoles. Again, as was the case with only octupoles, there is some improvement in the dynamic aperture along the y-axis. Overall, the gain in dynamic aperture is larger than with either sextupoles or octupoles alone.

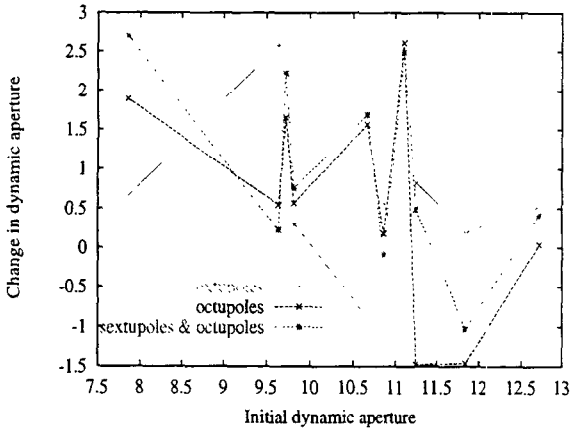

Figure 10: The change in dynamic aperture as a function of the initial dynamic aperture for each of the correction schemes.

Figure 10 shows the change in dynamic aperture as a function of the initial aperture for the different schemes. It is clear that the variation in dynamic aperture from seed to seed due to the action of the sextupoles is quite different from the variation due to the octupoles. For example, the maximum increase with sextupoles occured with seed 1 while the maximum with octupoles occured with seed 7. Octupoles were most effective in increasing the smallest dynamic aperture (seed 1). In almost all cases, the addition of sextupoles to octupoles helped improve the quality of the correction.

Table 4: The dynamic aperture (DA) with the use of low-order correctors. $\langle DA\rangle$ is calculated after 10^3 turns and averaged over 10 random seeds for the multipole errors. The last column shows the maximum increase in DA over these seeds with the use of the correctors.

Correction	$\langle DA\rangle \pm \sigma_{\langle DA\rangle}$	Max $\Delta\langle DA\rangle$
No correction	10.5 ± 1.4	
Sextupoles	11.0 ± 1.4	2.58
Octupoles	11.2 ± 1.4	2.61
Sextupoles & octupoles	11.5 ± 1.2	2.69

Table 4 summarizes the change in the dynamic aperture, averaged over emittance space and 10 seeds, obtained with use of the low order correctors. On average, the sextupoles increase the dynamic aperture by 0.5σ, octupoles by 0.7σ and the two together by 1σ. These schemes can be improved. One possibility is to identify the important resonances, seed by seed, and compensate only those resonances. For the preliminary study reported here, we compensated all the third order sum resonances for every seed. Lower order resonances such as the second order

Table 5: Idealized versions of the local correction schemes 2 and 4 where the systematic and random values of the specified multipoles are set to zero. Tracking calculations in this paper did not include the systematic uncertainties (db_n, da_n).

Scheme	Zeroed random multipoles
2	(b_3, b_4, b_5, b_6) & (a_3, a_4, a_5, a_6)
4	$(b_3, b_4, b_5, b_6, b_{10})$ & (a_3, a_4, a_5, a_6)

$Q_y - Q_x$ resonance also appear to be associated with amplitude growth (seen in Figures 1 and 2). This is one of several resonances that can be compensated by octupoles.

7 LOCAL CORRECTION SCHEMES WITH BEAM-BEAM

Beam-beam interactions have a significant impact on the dynamic aperture [1]. We have examined the impact of idealized versions of local correction schemes when beam-beam interactions are included. In the idealized versions we set to zero the systematic and random value of the specified multipoles. Table 5 shows the local correction schemes 2 and 4 as proposed in [2]. In practice, the local correction schemes will not be quite as effective as the idealized versions used here.

The tracking results reported in this section, both with and without beam-beam interactions, were done with the program TEVLAT [4]. The lattice was also derived from MAD5.1 but the IR quadrupoles were mixed, i.e. Fermilab error harmonics V2.0 were used in Q2a, Q2b and KEK V2.0 were used in Q1 and Q3.

In order to be consistent in evaluating the correction schemes, we will compare the dynamic aperture with and without the beam-beam interactions at the same number of turns. We have found that when the beam-beam interactions are included, particles must be tracked for a minimum of 10^5 turns in order to get meaningful results [1]. It is important to note that the dynamic aperture with beam-beam interactions drops faster with the number of turns than without.

Figure 11 shows the dynamic aperture for five seeds with and without the beam-beam interactions when no correction is applied.

Figure 12 shows the dynamic aperture in both cases with the idealized scheme 2. The dynamic aperture with the beam-beam improves by about 1σ compared to the case when no corrections are applied. As expected, the improvement is smaller compared to the case when the beam-beam interactions are not included.

Figure 13 shows the dynamic aperture in both cases with the idealized scheme 4. In this case, the dynamic aperture without beam-beam improves dramatically by about 4.7σ compared to the case without correction. When the beam-beam interactions are included, the dynamic aperture increases by 3.2σ to 12.4σ. This scheme is clearly

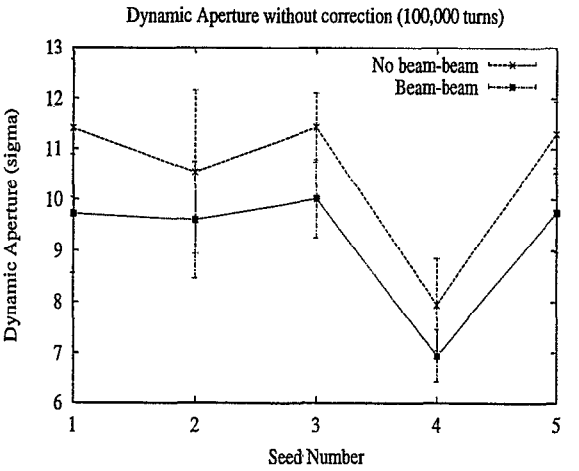

Figure 11: Dynamic aperture with and without the beam-beam interactions without any correction. Particles are tracked for 10^5 turns over 10 angles in emittance space. The average reduction in dynamic aperture due to the beam-beam is 1.3σ.

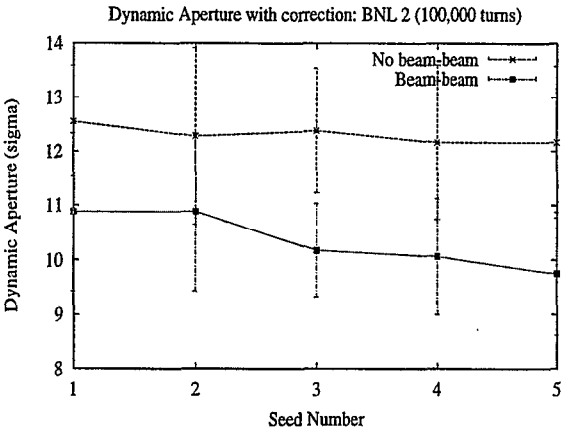

Figure 12: Dynamic aperture with and without the beam-beam interactions with the idealized local correction scheme 2. Particles are tracked for 10^5 turns over 10 angles in emittance space.

quite effective in improving the dynamic aperture, albeit by a smaller amount, even when the beam-beam interactions are included. Most of the increase is due to eliminating the large $\langle b_{10} \rangle = -0.25$ contribution to the dynamic aperture.

Table 6 summarizes the average change in dynamic aperture with and without the beam-beam interactions for the different correction schemes.

8 SUMMARY

Using only sextupoles and octupoles in IR1 and IR5 we attempted to increase the dynamic aperture. These multipoles were used to compensate sum third order resonances and reduce the tune shift with amplitude. Ten random seeds were used for the multipole errors. Averaged over the

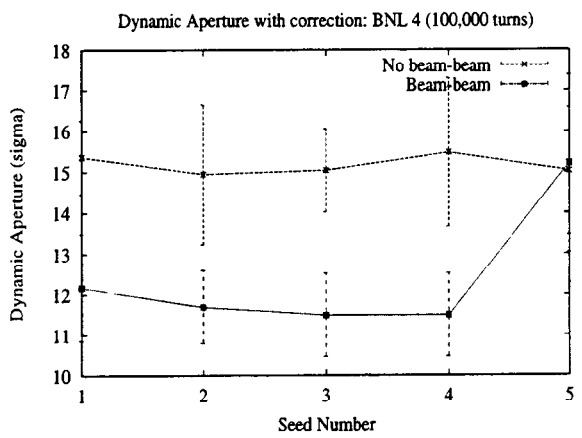

Figure 13: Dynamic aperture with and without the beam-beam interactions with the idealized local correction scheme 4. Particles are tracked for 10^5 turns over 10 angles in emittance space.

seeds, these multipoles increased the dynamic aperture by about 1σ. The maximum increase in dynamic aperture over these seeds is 2.7σ. This increase is encouraging because it demonstrates that resonance compensation works in principle. Our use of the sextupoles was constrained by placing them in the IRs. The relevant phase advances between these sextupoles correcting a resonance is an odd multiple of π while at optimal locations these phase advances would be odd multiples of $\pi/2$. This can be achieved by placing the sextupole correctors in the arcs. Resonance compensation may be further improved by first doing a more detailed search for the important resonances at the working point, using the method of frequency analysis for example. Low order coupling resonances such as $Q_y - Q_x$ may require a dedicated compensation. Important resonances of higher order than third will require higher order multipoles. We believe that resonance compensation can be a useful complement to the local correction scheme.

We have also investigated the efficacy of idealized versions of the local correction schemes when beam-beam interactions are included. As expected, the increase in dynamic aperture is not as large compared to the case when beam-beam interactions are not included. However the increase with scheme 4 (where $b_{10} = 0$) is still significant, about 3σ. This demonstrates that the local correction can still be very useful, even in the presence of the beam-beam interactions. We believe that in order to improve upon the local correction, compensation of the beam-beam driven resonances should be investigated.

Table 6: Average dynamic aperture without and with beam-beam and different idealized local correction schemes. The dynamic aperture is calculated after 10^5 turns and averaged over 5 random seeds. No systematic uncertainties db_n, da_n are included.

Correction Scheme	No Beam-Beam $\langle DA \rangle \pm \sigma_{\langle DA \rangle}$	With Beam-beam $\langle DA \rangle \pm \sigma_{\langle DA \rangle}$
No correction	10.52± 1.04	9.21 ± 0.88
Scheme 2	12.31± 1.33	10.35 ± 1.19
Scheme 4	15.17± 1.40	12.41 ± 1.29

9 REFERENCES

[1] T. Sen, N. Gelfand, C. Johnstone, W. Wan, *Effect of the beam-beam interactions on the dynamic aperture and amplitude growth in the LHC*, Proc. CERN Beam-beam Workshop, April 1999

[2] J. Wei et.al., *Interaction region local correctionfor the LHC*, PAC 1999

[3] M. Berz, COSY INFINITY Version 7, Technical report MSUCL-977 revised. National Superconducting Cyclotron Laboratory, Michigan State University, 1996

[4] A. Russell, private communication

Global Correction of Magnetic Field Errors in LHC Interaction Regions

J. Shi*
Department of Physics & Astronomy, University of Kansas, Lawrence, KS 66045, USA

Abstract

Global compensation of the field errors based on the minimization of nonlinearities in a one-turn map was found to be very effective in reducing the detrimental effects of magnetic field errors in the LHC during collision. With a few groups of low-order correctors, nonlinear terms in the one-turn map can be minimized order-by-order and, consequently, the dynamic aperture is substantially increased and the phase-space region occupied by beams becomes much more linear. One advantage of the global correction is the possibility of further optimization of the correction based on a direct measurement of a one-turn map with beam-dynamics experiments.

1 INTRODUCTION

During collisions, the dynamic aperture of the LHC is limited by the multipole field errors of superconducting high-gradient quadrupoles (MQX) of the inner triplets of the interaction regions (IRs). Control of these field errors is one of the primary tasks in the design of the LHC IRs. With the current reference harmonics of Fermilab and KEK MQXs [1], correctors are necessary for the IRs in order to meet the dynamic aperture requirement of the LHC. Because of the beam separation in the triplets due to an angle crossing of colliding beams, high-order multipoles of the field errors feed down to low-order nonlinearities of the system and they are important to the aperture limitation. It is, however, difficult to correct those high-order multipoles errors by using the traditional methods of local correction since it is difficult and costly to build high-order multipole correctors. The global correction of magnetic field errors based on the minimization of the nonlinearities in a Poincaré map of a circular accelerator is an alternative way to reduce the detrimental effects of both the systematic and random field errors [2]. In a circular accelerator, the nonlinear beam dynamics can be described by a Poincaré map known as one-turn map. The one-turn map contains all global information of nonlinearities in the system. By minimizing the nonlinear terms of a one-turn map order-by-order with a few groups of multipole correctors, one can reduce the nonlinearity of the system globally [2]. In this paper, the effectiveness and feasibility of the global correction of the magnetic field errors in the triplets of IRs is investigated for the LHC collision lattice. It was found that the global correction strategy is effective and efficient in increase of the dynamic aperture and improvement of the linearity of the phase-space region occupied by beams for the LHC during collisions. One advantage of the global correction of nonlinear fields is that the correction may be further optimized during the commission of an accelerator based on measurements of a one-turn map in beam-dynamics experiments. Methods for a direct measurement of a one-turn map with beam-dynamics experiment has recently been proposed and technique problems associated with such a measurement has been studied in detail [3, 4, 5, 6].

This paper is organized as follows. In Section 2, we discuss the principle of global correction of nonlinear fields. In Section 3, the test lattice for the LHC during collisions is presented. In Sections 4, the effectiveness of the global correction on the improvement of the dynamic aperture and the improvement of the linearity of the phase space are studied. In Section 5, we discuss the robustness of the global correction. Section 6 contains a conclusion.

2 GLOBAL COMPENSATION OF THE NONLINEAR FIELDS

Neglecting the coupling between the transverse and longitude motion, at any "check-point" of an accelerator, the transverse motion of beam particles can be described mathematically by a 4-dimensional one-turn map in the form of Taylor expansion

$$\vec{Z}\,' = \mathcal{M}\vec{Z} = \sum_{n=1}\left(\sum_{i+j+k+l=n} \vec{u}_{ijkl}\ \xi_x^i\ \eta_x^j\ \xi_y^k\ \eta_y^l\right) \quad (1)$$

where $\vec{Z} = (\xi_x, \eta_x, \xi_y, \eta_y)$ is the normalized phase-space vector and $\eta_{x,y}$ are the conjugate momenta of $\xi_{x,y}$. $\vec{Z} = 0$ is the closed orbit and $\vec{u}_{ijkl}$ are constant coefficients containing all global information of nonlinearities of the system. If the close orbit is at the center of magnets, the nth-order terms of a one-turn map are the contributions from the multipole components of the error fields with order up to n. On the other hand, if the close orbit is not at the center of magnets due to magnet misalignments or beam crossing at interaction points, high-order multipole errors feed down to low-order terms of the one-turn map and, consequently, $\vec{u}_{ijkl}$ of order n are functions of all multipole components. For an accelerator, since the phase-space region near the origin is of most interest, low-order terms of a one-turn map are usually more important than high-order terms of the map. The low-order multipole components of error fields are therefore important to the beam dynamics. Because of the feed-down effect, however, the high-order multipole errors contribute also to low-order terms of the map and become important to the beam dynamics as well. The global correction of the nonlinearities is based on an

* This work is supported by the National Science Foundation under Grant No. PHY-9722513 and the University of Kansas General Research Fund.

assumption that with a few groups of multipole correctors, $\vec{u}_{ijkl}$ with $i+j+k+l \geq 2$ can be minimized order-by-order and, consequently, the nonlinearities of the system can be substantially reduced. In order to minimize undesirable $\vec{u}_{ijkl}$ with a few parameters of the correctors, we postulate that the nth-order undesirable nonlinearity in a one-turn map can be characterized by the magnitude of its nth-order undesirable coefficients which are defined by

$$\lambda_2 = \left(\sum_{i+j+k+l=2} \left| \vec{u}_{ijkl} - \vec{u}^0_{ijkl} \right|^2 \right)^{1/2} \qquad (2)$$

and

$$\lambda_n = \left(\sum_{i+j+k+l=n} \left| \vec{u}_{ijkl} \right|^2 \right)^{1/2} \qquad \text{for } n > 2, \qquad (3)$$

where $\vec{u}^0_{ijkl}$ of $i+j+k+l=2$ denote the quadratic terms contributed by sextupole chromaticity correctors. To minimize the undesirable nonlinearities, the quadratic nonlinearity for the chromaticity correction needs to be subtracted from the $\vec{u}_{ijkl}$. For convenience, we define the nth-order global correction when all λ_i with $i = 2, ..., n$ are minimized order-by-order using the multipole correctors up to the nth order. For example, for the 2nd-order global correction λ_2 of quadratic terms of a one-turn map will be minimized by using sextupole correctors and for the 3rd-order global correction both λ_2 and λ_3 will be minimized by using sextupole and octopole correctors. To implement the global correction of the nonlinear fields during design and construction of an accelerator, the one-turn map is obtained by using the method of Lie algebra [7] or automatic differentiation (differential algebra) [8] with measured magnetic field errors. During the commission of an accelerator, the global correction of the nonlinear fields may be further optimized if a one-turn map can be extracted with desired accuracy directly from beam dynamics measurements. Such a beam-based global correction needs only a measurement of low-order map since the study showed [2] that the low-order global correction is usually sufficient even in the case that the high-order multipole errors are important.

To illustrate this minimization procedure, let us consider four global correctors of the nth-order multipole for minimizing the nth-order nonlinear terms of the map. Consider the situation that these correctors are installed at locations where the closed orbit is at the center of the correctors. Suppose that a one-turn map is measured at a "check-point" between the 1st and 4th corrector. Let $\exp\left\{ : C^{(i)}_{n+1}\left(\vec{Z}\right) : \right\}$ be the Lie transformation for the ith corrector, where $i = 1, ..., 4$ and $C^{(i)}_{n+1}$ is a homogeneous polynomial of $\vec{Z}$ in degree $n+1$; $\mathcal{M}_i$ be the transfer map between two adjacent correctors when $i = 1, 2, 3$ and between the "check-point" and the adjacent correctors when $i = 0, 4$; and

$$\mathcal{M}_{i4} = \prod_{k=i}^{4} \mathcal{M}_k, \qquad (4)$$

where $\mathcal{M}_{04}$ is the one-turn map of the ring without the nth-order correctors. The one-turn map of the ring with the nth-order correctors can be written as

$$\mathcal{M} = \mathcal{M}_{04} \prod_{i=1}^{4} \exp\left\{ : C^{(i)}_{n+1}\left(\mathcal{M}^{-1}_{i4}\vec{Z}\right) : \right\}. \qquad (5)$$

Let $\mathcal{R}_{i4}$ be the linear transfer matrix associated with $\mathcal{M}_{i4}$. Then

$$\mathcal{M}^{-1}_{i4}\vec{Z} = \mathcal{R}^{-1}_{i4}\vec{Z} + \sigma_2(\vec{Z}), \qquad (6)$$

where $\sigma_{k+1}(\vec{Z})$ represents a remainder series consisting of terms higher than the kth-order, and

$$C^{(i)}_{n+1}\left(\mathcal{M}^{-1}_{i4}\vec{Z}\right) = C^{(i)}_{n+1}\left(\mathcal{R}^{-1}_{i4}\vec{Z}\right) + \sigma_{n+2}(\vec{Z}). \qquad (7)$$

It should be noted that Eq. (7) is valid only when the closed orbit is at the center of the correctors, otherwise, terms lower than the $(n+1)$th-order are also involved. Since the lowest-order terms in the remainder series $\sigma_{n+2}(\vec{Z})$ are the $(n+2)$th-order, for the minimization of the nth-order terms, $\sigma_{n+2}(\vec{Z})$ can be neglected and

$$\mathcal{M} \simeq \mathcal{M}_{04} \prod_{i=1}^{4} \exp\left\{ : C^{(i)}_{n+1}\left(\mathcal{R}^{-1}_{i4}\vec{Z}\right) : \right\} \qquad (8)$$

where $\mathcal{M}_{04}$, the one-turn map without the nth-order correctors, and $\mathcal{R}_{i4}$, the linear transfer matrices, can be either calculated based on the design lattice and the measured field errors or directly measured from beam-dynamics experiments. By using Eq. (8), the nth-order nonlinearity of $\mathcal{M}$ can then be minimized by adjusting the nth-order correctors $C^{(i)}_{n+1}$. It should be noted that for the beam-based global correction, only one measurement of $\mathcal{M}_{04}$ is required for the minimization of λ_n.

3 THE TEST LATTICE

The test lattice used in this study is the LHC version 5.0. The LHC has four interaction regions (IRs): IR1 and IR5 are high luminosity interaction points ($\beta^* = 0.5$ m) and IR2 and IR8 low luminosity points. The layout of the inner triplets of four IRs is almost identical. Each inner triplet comprises four superconducting high gradient quadrupoles (MQX), Q1, Q2A, Q2B, and Q3. Due to the beam separation and the large β_{max}, the beam dynamics during collisions is dominated by the field errors of MQX. In this study we therefore consider only the field errors of MQX. The random multipole components of MQX are chosen with Gaussian distributions centered at zero and truncated at $\pm 3\sigma_{b_{n+1}}$ or $\pm 3\sigma_{a_{n+1}}$ where $\sigma_{b_{n+1}}$ and $\sigma_{a_{n+1}}$ are the rms value of the nth-order normal and skew multipole coefficient, respectively. Reference harmonics of version 2.0 is used in this study for both Fermilab and KEK MQX [1]. The uncertainty of a systematic error is simply added to the systematic error in such a way that it maximizes the systematic error. Due to the consideration of a larger systematic b_{10} in KEK quadrupoles, two different arrangement

of MQX, mixed and unmixed configuration, are studied. In the unmixed configuration, the Fermilab MQX are installed in the triplets of IP1 and IP2, and the KEK MQX in the triplets of IP5 and IP8. In the mixed configuration, four MQX in each triplet are mixed with two quadrupoles from Fermilab and another two from KEK. In this case, the Fermilab MQX are installed at Q2A and Q2B and KEK MQX at Q1 and Q3. Since the β_{max} ($\sim$ 4700 m) in the triplets of IP1 and IP5 is more than 10 time larger that that of IP2 and IP8, the field quality in the triplets of IP1 and IP5 is far more important than that of IP2 and IP8. To compensate the error fields in the triplets of IP1 and IP5, each triplet contains three corrector packages. In this study, we use four groups of correctors, one in each triplet of IP1 and IP5, to minimize λ_n order-by-order. To test the global nature of the correction, we also include four corrector packages outside the triplets to corrector the nonlinear fields in the triplets. Each package of the corrector contains normal and skew components of a desired multipole corrector. It was found that in the sense of improvement of the dynamic aperture, the correctors outside the triplets is as effective as the correctors in the triplets for the global correction of the field errors in the triplets [2]. In this study, the crossing angle of two counter-rotating beams is taken to be 300 μrad. The fractional parts of horizontal and vertical tunes are $\nu_x = 0.31$ and $\nu_y = 0.32$, respectively.

4 EFFECT OF THE GLOBAL CORRECTION OF NONLINEAR FIELDS

To study the effect of the global correction of nonlinear fields, dynamic aperture (DA) of the system are calculated before and after the correction. In order to reduce the sensitivity of the DA to the choice of initial launch point for tracking in phase space, we define an aperture as the shortest distance from the origin in the four-dimensional normalized phase space during the tracking. To find the DA, the launch point is moved away from the origin until the particle is lost. No physical aperture limit is imposed in the ring and a particle is defined to be lost if $x^2 + y^2 \geq (10\ \mathrm{cm})^2$ where x and y are its horizontal and vertical coordinates, respectively. The DA defined in this manner is found to be relatively insensitive to the choice of launch point in phase space. Tracking of particle motions has been done without synchrotron oscillations and momentum deviations. The DA has been calculated with 10^5-turn tracking. To improve the statistical significance of the simulations, we have used 50 different samples of random multiple components generated with different seed numbers in a random number generator routine.

Figures 1 and 2 are the DA of 50 random samples with or without the global correction of the nonlinear fields for the unmixed and mixed configuration, respectively. Without any correction (Figs. 1a and 2a), the smallest and the average DA of 50 samples is found to be 5.5σ and 7.9σ for the unmixed configuration and 6.5σ and 8.0σ for the mixed

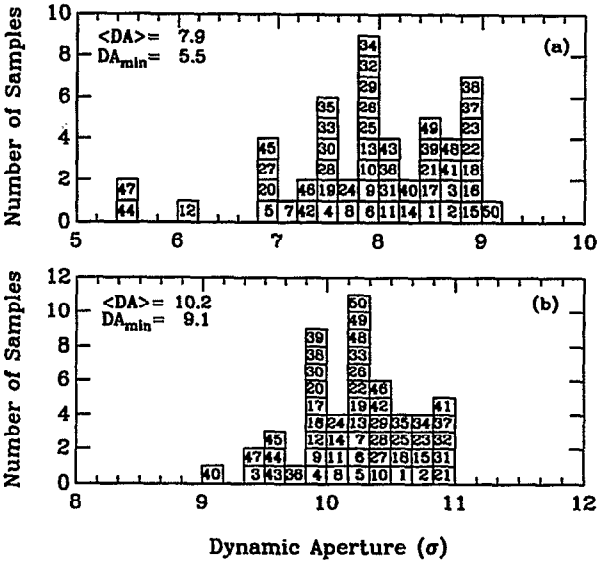

Figure 1: Dynamic aperture of fifty samples of the LHC collision lattice with the unmixed configuration. (a) without any correction for the nonlinear fields; (b) with the 3rd-order global correction for the nonlinear fields using four sextupole and octopole correctors. The number in each block identifies each sample.

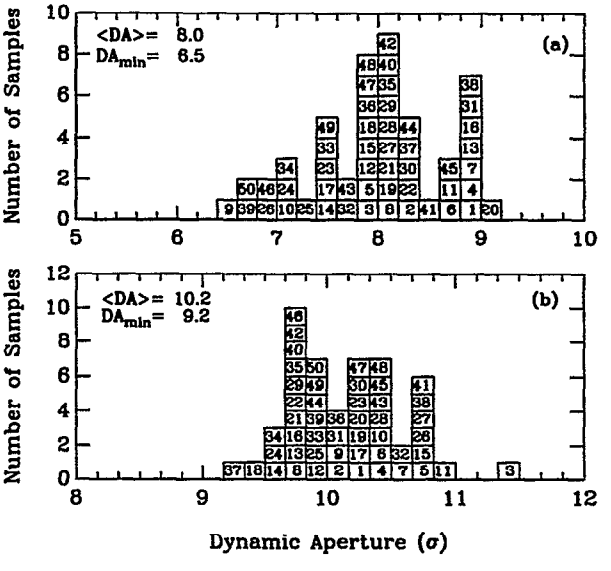

Figure 2: The same as in Fig. 1 but with the mixed configuration.

configuration, respectively, where σ is the transverse beam size. At the high luminosity IPs, $\sigma = 15.9\mu$m. A smaller DA for the unmixed configuration is due to a larger b_{10} in KEK quadrupoles. After the 3rd-order global compensation with sextupole and octopole correctors outside the triplets (Figs. 1b and 2b), the smallest and the average DA increases to 9σ and 10σ for both configurations. It should be noted that with the conventional (local) correction of the field errors, high-order correctors have to be used in order to achieve a significant improvement in the DA [9].

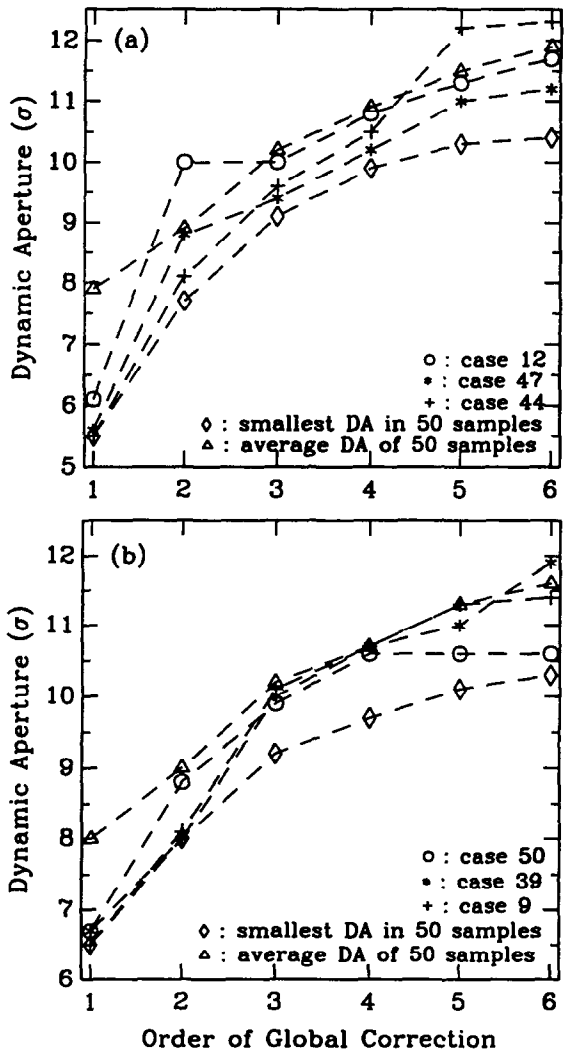

Figure 3: The DA after the global correction vs. the order of the correction. $n = 1$ indicates the cases without the correction. (a) The unmixed configuration. Case 12, 47, and 44 are three worst cases without the correction. (b) The mixed configuration. Case 9, 39, and 50 are three worst cases without the correction.

Because of the beam separation in the triplets, high-order multipoles of the field errors feed down to low-order terms of the one-turn map so that they are important to the DA. In the conventional correction, the field errors are compensated locally based on the errors of each magnets and, therefore, the high-order correctors have to be used in order to reduce the effects of high-order multipoles. For the global correction of the field errors, on the other hand, a few sextupole correctors can minimize the dominant nonlinear terms, quadratic and cubic terms, of the map and achieve a significant reduction of the nonlinearity of the system.

Fig. 3 plots the DA after the global correction as a function of the order of the correction. It shows that as the order increases the further improvement of the DA becomes less pronounced, which indicates that the lower-order (quadratic and cubic) nonlinear terms of the one-turn

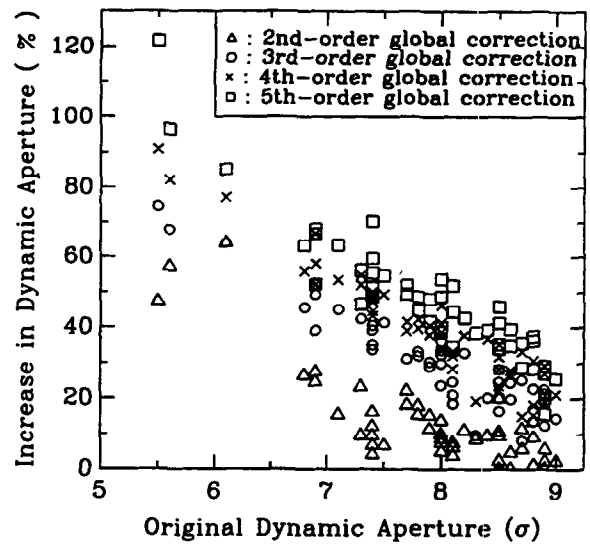

Figure 4: The increase of the DA after the global correction vs. the DA without the correction for the fifty samples of the unmixed configuration.

map dominates the nonlinear dynamics of the system. In Fig. 4, the percentage increase of the DA after the global correction is plotted *vs.* the original DA without any correction. In general, the smaller the original DA, the larger the increase of the DA after the correction. For example, without any correction, two worst cases of the unmixed configuration, case 44 and 47, have a DA smaller than 6σ (see Fig. 1a). After the 2nd-order correction, the DA gains about 50% for both cases. After the 3rd-order correction, the DA becomes larger than 9σ for both cases, which is a more than 60% gain in DA. As the original DA increases, the gain of the DA after the global correction diminishes. It is understandable that if the original system is already quite linear, the correction of the nonlinear fields will not result in a substantial improvement.

A strong nonlinearity in the lattice can lead to a substantial degree of amplitude dependence of betatron tunes even in a phase-space region near the origin, and this may result in crossings of dangerous resonances and a reduction in the dynamic aperture. Minimizing the amplitude dependence of tunes is thus desirable for a stable operation of an accelerator. Previous studies [10, 11, 12] showed that both the local correction for the systematic field errors and the sorting of magnets for the random field errors are effective in reducing the amplitude dependence of tunes. The effect of the global correction of the nonlinear fields on the amplitude dependence of tunes are also studied by using the method of normal form. In Figs. 5 and 6, the detuning functions, $\delta\nu_x$ and $\delta\nu_y$, for case 44 of the unmixed configuration are plotted as functions of the action variables I_x and I_y, respectively, where $\delta\nu_x$ and $\delta\nu_y$ are calculated at IP1. Without any correction, both horizontal and vertical tune strongly depend on I_x and I_y as shown in Figs. 5a and 6a. Figs. 5b and 6b show the nonlinear tune shifts after the 3rd-order global correction. A comparison between

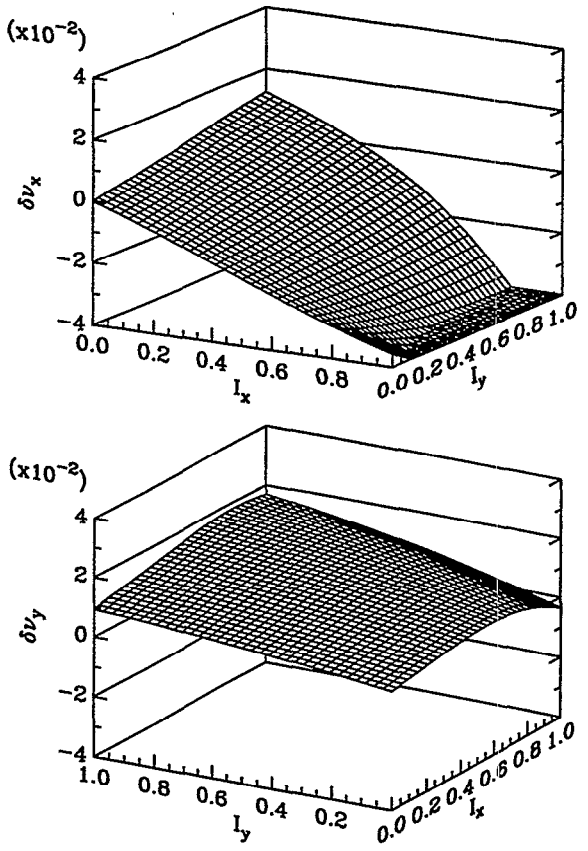

Figure 5: Amplitude dependence of tunes of case 44 of the unmixed configuration without any correction. $\delta\nu_x$ and $\delta\nu_y$ are calculated at IP1. The unit of I_x and I_y is 10^{-8} m. At IP1, $I_x + I_y = 10^{-8}$ m corresponds to $\sim 6\sigma$.

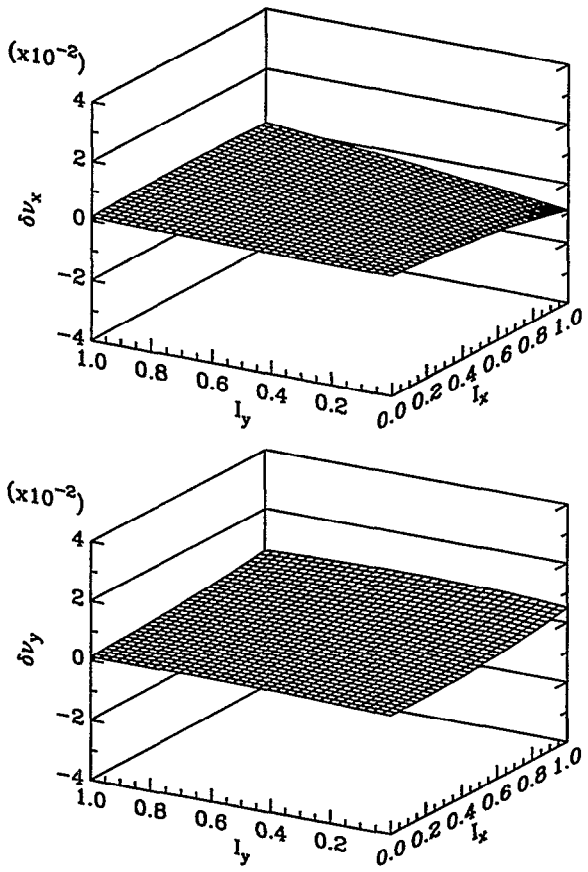

Figure 6: The same as Fig. 5 but with the 3rd-order global correction.

the uncorrected and corrected lattice shows that the global correction effectively suppresses the nonlinear tune shift. Other cases have a similar situation.

The improvement of linearity of the phase-space region near the origin can also be directly examined with phase-space plots. Figs. 7 and 8 are the phase-space plots of case 44 of the unmixed configuration before and after the global correction, which shows that the phase-space region occupied by the beams becomes much linear after the global compensation of the field errors even in the case that only four sextupole correctors are used. It should be noted that the dynamic aperture calculated from the tracking of 10^5 turns does not really tell the performance when the storage time of at least several hours is in question. However, by examining the linearity of phase space together with the amplitude dependence of tunes, one may get a better idea of the long-term storage performance.

It should be noted that even though the results reported in this section are all for the working point of $\nu_x = 0.31$ and $\nu_x = 0.32$, the effectiveness of the global compensation has also been demonstrated on the LHC lattice with other working points.

5 ROBUSTNESS OF THE GLOBAL CORRECTION OF NONLINEAR FIELDS

The use of the global correction requires the knowledge of a one-turn map. A one-turn map, either calculated based on the design lattice and the measured field errors or measured directly from beam-dynamics experiments, always contains errors or uncertainty. The sensitivity of the global correction to the uncertainty in the map is important to the feasibility of the global correction scheme. The uncertainty in the map can be divided into two parts, the uncertainty in linear transfer matrices and the uncertainty in nonlinear terms of the map. The former is mainly due to the lack of knowledge on the linear lattice and the latter due to both the uncertainty of linear lattice and the errors in the multipole measurement or the measurement errors in beam-dynamics experiments. Previously, the global correction was found to be not very sensitive to the uncertainty in the nonlinear terms of the map [2]. Since the global correctors may not be close to the sources of nonlinear fields, the uncertainty in the linear transfer matrices, on the other hand, could make the global correction ineffective. To investigate the effect of the uncertainty in the linear transfer matrices $\mathcal{R}_{i4}$, we

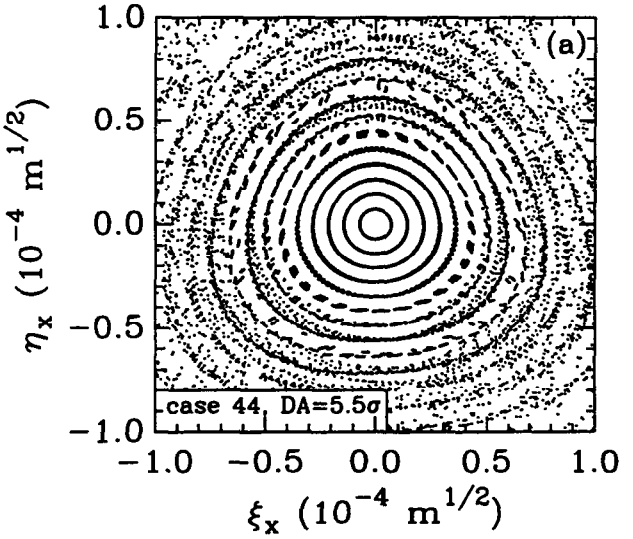

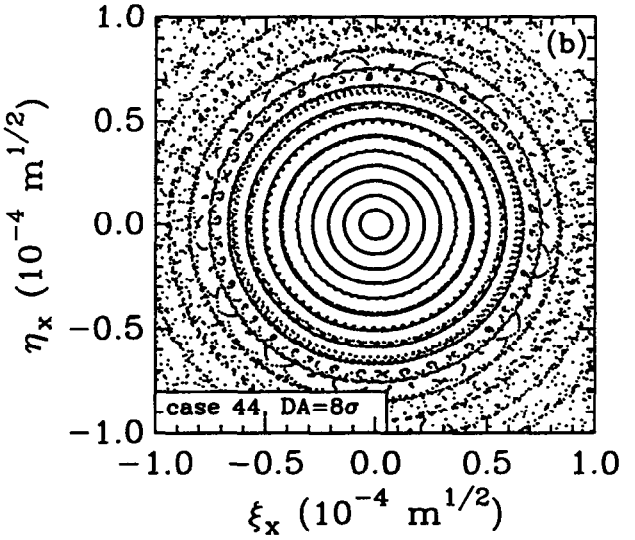

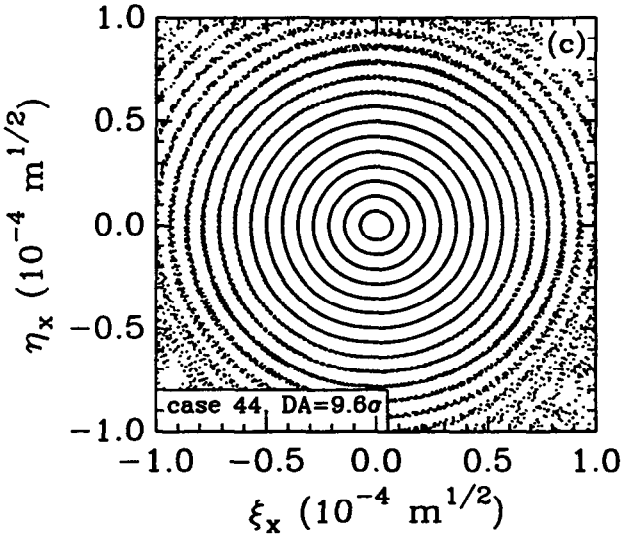

Figure 7: Normalized phase-space plot on the horizontal plane at IP1 for case 44 of the unmixed configuration. (a) without any correction; (b) with the 2nd-order global correction; and (c) with the 3rd-order global correction.

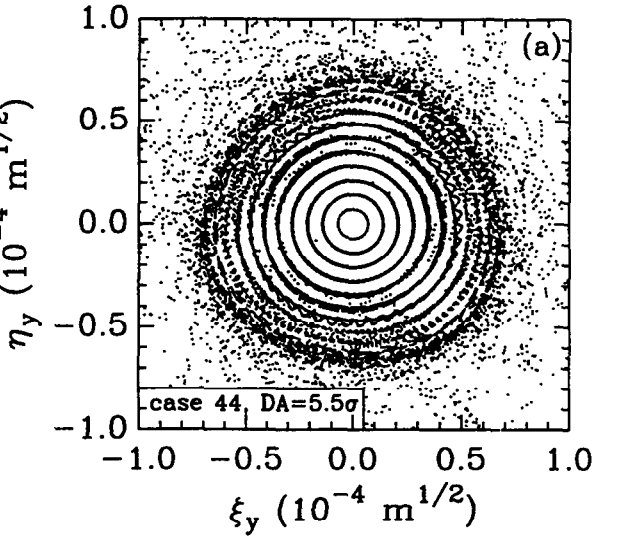

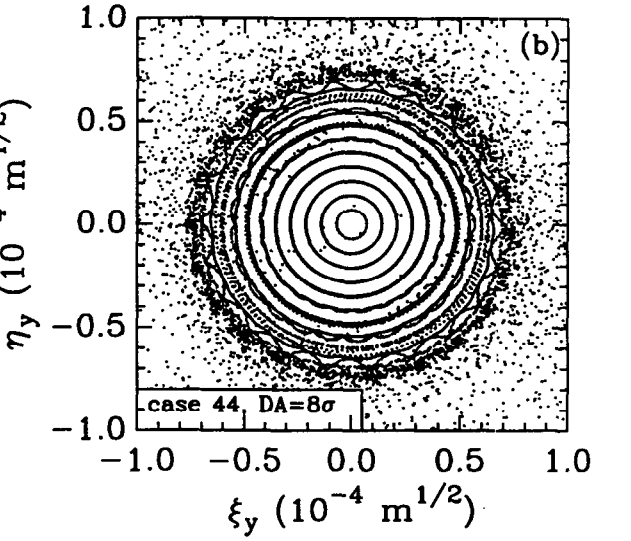

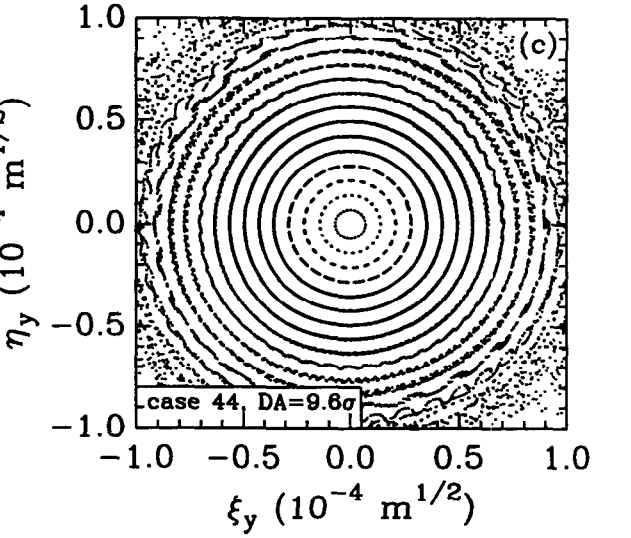

Figure 8: The same as Fig. 7 but for normalized phase-space plot on the vertical plane.

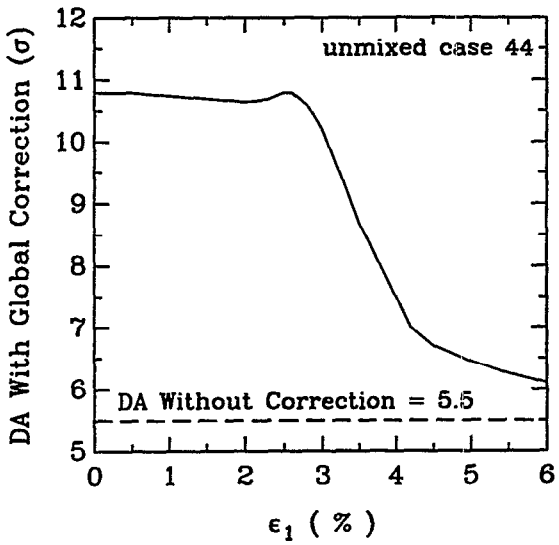

Figure 9: The DA after the 4th-order global correction vs. the uncertainty in linear transfer matrices ϵ_1 for case 44 of the unmixed configuration.

assume that the error of matrix element r_{lk} of $\mathcal{R}_{i4}$ is

$$\delta r_{lk} = \epsilon_1 f r_{lk} \qquad (9)$$

where ϵ_1 is the maximal percentage of errors in matrix elements of $\mathcal{R}_{i4}$ and f is a random number in [-1, 1]. Fig. 9 plots the DA after the 4th-order global correction as a function of ϵ for case 44 of the unmixed configuration, which shows that uncertainty of 3% or less in linear transfer matrices have little impact on the global correction, but uncertainty of 5% or more can make the global correction ineffective. It should be noted that a measurement of the linear transfer matrices with better then 3% uncertainty is achievable when the measurement system is well debugged. Moreover, since the global correctors can be adjusted during operation of an accelerator, the global correction can be fine tuned when the knowledge of the linear lattice is improved.

6 CONCLUSIONS

The global correction of magnetic field errors based on the minimization of nonlinearities in a one-turn map is an effective means to suppress the detrimental effects of systematic as well as random field errors in the LHC during collisions. With a few groups of multipoles correctors, nonlinear terms in a one-turn map can be minimized order-by-order and, consequently, the nonlinearity of the system is significantly reduced which results in an increase of the dynamic aperture and improvement of the linearity of the phase-space region occupied by beams. Compared with the local corrections of the field errors, the global correction has several advantages. (a) The random field errors of large number of magnets can be compensated with a few groups of independent powered correctors. (b) Since the low-order nonlinear (quadratic and cubic) terms of the map usually dominate the beam dynamics, only low-order (sextupole and octopole) correctors are needed for the global correction even though high-order multipoles are important to the beam dynamics due to the feed-down effect. (c) The global correction of the nonlinear fields may be further optimized with a direct measurements of a one-turn map in beam-dynamics experiments. This beam-based correction is especially important when there is a significant uncertainty in the field measurement of magnets or a significant change of the field errors during the operation of a superconducting ring. While the global correction of the field errors partially suppresses the low-order nonlinear effects of the random and systematic errors, the local corrections of the field errors, on the other hand, can effectively compensate low-order systematic errors to a large extent. It is, therefore, important to stress that the global correction of the field errors should never be considered as "cure-all" in dealing with the nonlinearity in superconducting magnets and it should be regarded as a complement to the local correction of the field errors.

7 REFERENCES

[1] Reference harmonics for Fermilab and KEK MQX are available on the US-LHC Project web page: http://www/agsrhichome.bnl.gov/LHC.

[2] J. Shi, "Global Compensation of Magnetic Field Errors with Minimization of Nonlinearities in Poincaré Map of a Circular Accelerator", preprint, (1998).

[3] V. Zieman, Part. Accel. **55**, 419 (1996).

[4] C. Wang and J. Irwin, SLAC report SLAC-PUB-7547, (1997).

[5] S. Peggs and C.Tang, BNL report RHIC/AP/159, (1998).

[6] R. Bartolini and F. Schmidt, Part. Accel. **59**, 93 (1998).

[7] A. Dragt, in *Physics of High-Energy Particle Accelerators*, AIP Conf. Proc. No. 87, edited by R. A. Carrigan *et al.*, (AIP, new York, 1982).

[8] M. Berz, Part. Accel. **24**, 109 (1989).

[9] J. Wei, V. Ptitsin, F. Pilat, S. Tepikian, in *Proceedings of the 1998 European Accelerator Conference*, (1998).

[10] M. Giovannozzi, W. Scandale and F. Schmidt, CERN SL/93-29 (AP), LHC Note 230, (1993).

[11] J. Shi and S. Ohnuma, Part. Accel. **56**, 227 (1997).

[12] J. Shi, Nucl. Instr. & Meth., A**430**, 22 (1999).

Corrector Engineering Challenges and Issues

A. Ijspeert, M. Karppinen

CERN, Division LHC, Geneva, Switzerland

1. Introduction

The inner triplets of the LHC will each house two combined horizontal and vertical correction dipoles, MCBX, and a skew quadrupole corrector, MQSX. Both magnet types will have enlarged apertures of 90 mm to create place for additional nested corrector windings. From the construction and performance point of view the MCBX will not have more than two corrector layers, whereas the lower background field of about 1.5 T in the MQSX allows the mounting of up to three multipole layers in it. This paper describes the MCBX orbit correctors and the experience obtained with the two prototypes, some aspects of the correction windings and their limitations, and the parameters of the future MQSX skew quadrupole.

2. Low-β Dipole Corrector MCBX

2.1. Design

The MCBX-magnet, whose main parameters are listed in Table I, features a horizontal dipole nested inside a vertical one. The coils of the 0.6 m long single-bore magnet are wound with 7 or 9 rectangular superconducting wires pre-assembled as flat cables. To create the required ampere-turns the individual wires are then connected in series on the end plate.

Table I: Main parameter of low-b dipole MCBX

	Horizontal dipole	Vertical dipole	
MAGNETICS			
Nominal strength	3.3	3.3	T
Integrated field	1.2	1.1	Tm
Magnetic length	0.37	0.34	m
Peak field in coil	4.4	4.8	T
GEOMETRY			
Overall length	0.55		m
Coil length	0.5	0.5	m
Coil inner diameter	90	123.7	mm
Coil outer diameter	119.7	146.8	mm
Yoke inner diameter	200/180[1]		mm
Yoke outer diameter	470/330[1]		
Overall outer diameter	500/350[1]		mm
ELECTRICS			
Nominal Current	0-511	0-599	A
Number of turns/coil	414	406	
Stored energy/magnet	17.9	25.2	kJ
Self inductance/magnet	0.137	0.140	H
CONDUCTOR			
Cross section	1.6	1.6	mm^2
Cross section(metal)	1.3	1.3	mm^2
Copper/NbTi ratio	1.6	1.6	
Filament diameter	10	10	μm
Twist pitch	18	18	mm
Current density (NbTi)	1022	1198	A/mm^2
Margin to quench	51.7	46.2	%

[1] First/second prototype magnet

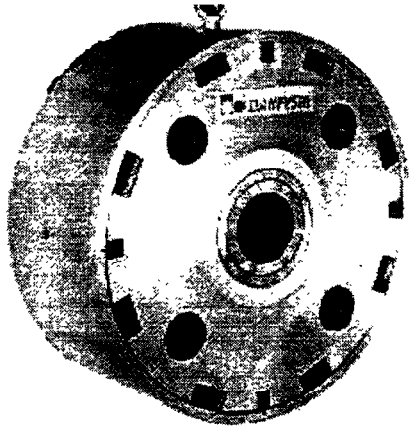

Figure 1: Mechanical model of the first MCBX prototype magnet

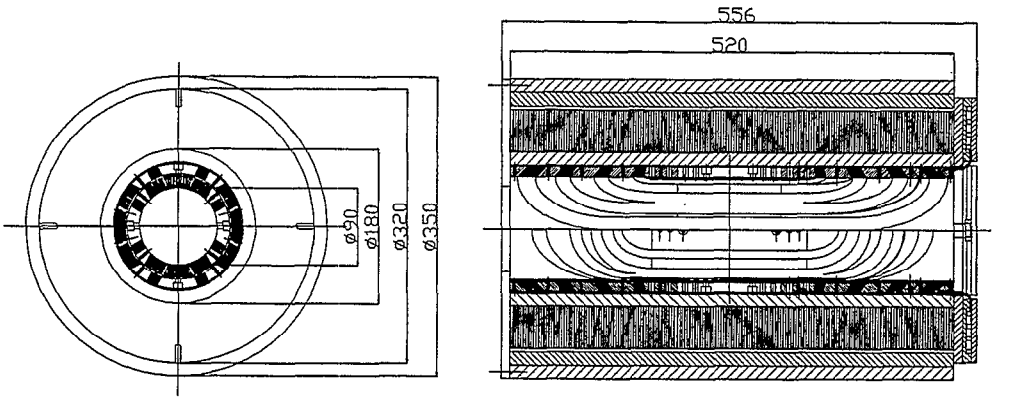

Figure 2: Second MCBX prototype magnet

Figure 1 illustrates the cross-section of the first prototype magnet with an outer diameter of 500 mm. After that a second prototype, whose cross-section is shown in Figure 2, was made using identical coils but with a yoke that was slimmed down by suppressing the holes for the heat exchangers and the busbars. The vacuum impregnated coils containing CNC-machined end spacers are pre-compressed with an aluminium shrinking cylinder. The yoke consists of scissors-laminations to back up the coil rigidity and to centre the coil assembly. Each lamination is designed to support the coils radially in one azimuthal direction only. This is made by off-centring the hole in the lamination by 1 mm with respect to the outer boundary. By sequentially stacking four laminations at angular orientations of 0, 90, 180, 270 degrees respectively the coils can be effectively supported and centred. The laminations move inwards during the cooldown and the blocking keys stop the movement at a pre-defined temperature building-up a circumferential stress in the stainless steel outer shell.

2.2. Magnetics

The nested dipole coils are individually powered and can produce both a horizontal and a vertical field. The nominal field integral is 1 Tm in any direction as shown in Figure 3, which gives a maximum kick angle of 42.8 μrad at 7 TeV. The working point on the load-line for the LHC corrector magnets with vacuum impregnated coils is typically below 60 %. The tolerances for the maximum allowed field errors are very tight in the low-β triplet, where β-functions rise to over 4000 m to achieve the maximum luminosity at full energy.

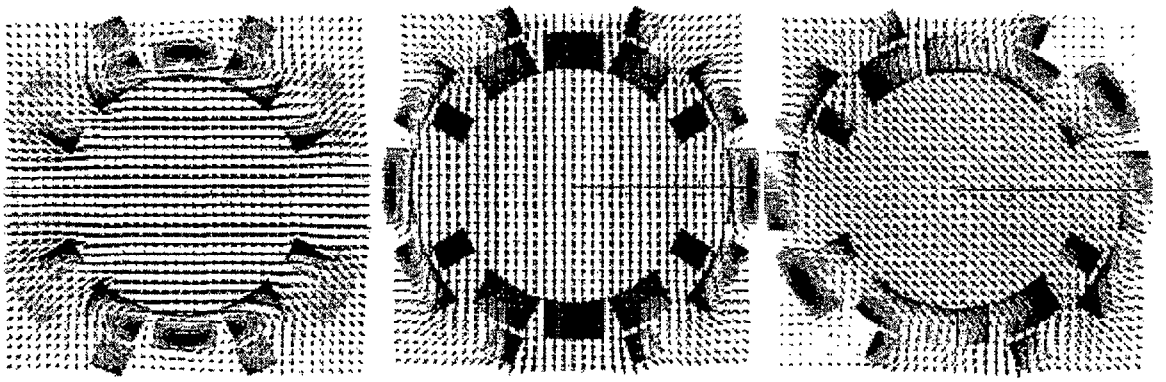

Figure 3: MCBX, different field combinations

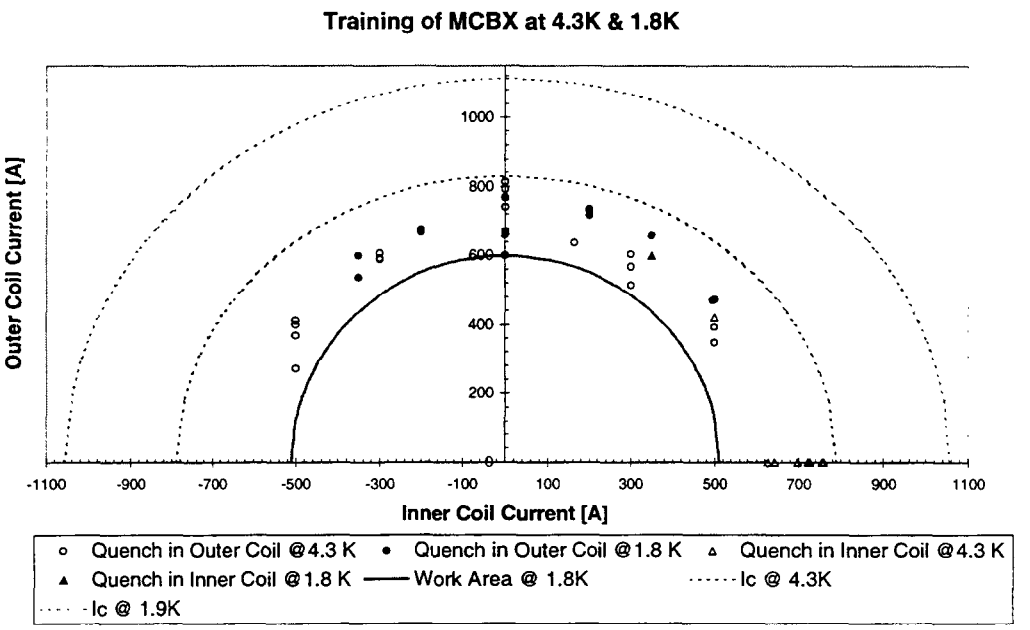

Figure 4: Training of the first MCBX prototype magnet

2.3. Test Results

The first MCBX prototype has undergone the first test campaign including training quenches, static magnetic measurements at warm and at cold, and ramped measurements to study the persistent current effects in the nested coils. After 5 and 6 quenches the vertical and horizontal dipoles were respectively trained to their estimated short-sample current in liquid helium (4.3 K).

Figure 4 presents the training history for different field combinations during the first thermal cycle. The horizontal and vertical axes give the current in the inner and outer coils, respectively. The innermost ellipse shows the working area of the magnet i.e. the 1 Tm field in any direction. The magnet showed always some training with different field combinations as the position of the peak field changes and also the electro-magnetic forces act in different directions. It should be noted that to limit the stress in the coils the maximum current was kept below 800 A. We hope in a next test to go beyond this level and explore the ultimate limits of this magnet. There was also only a minor improvement in the performance when the magnet was cooled to1.9 K.

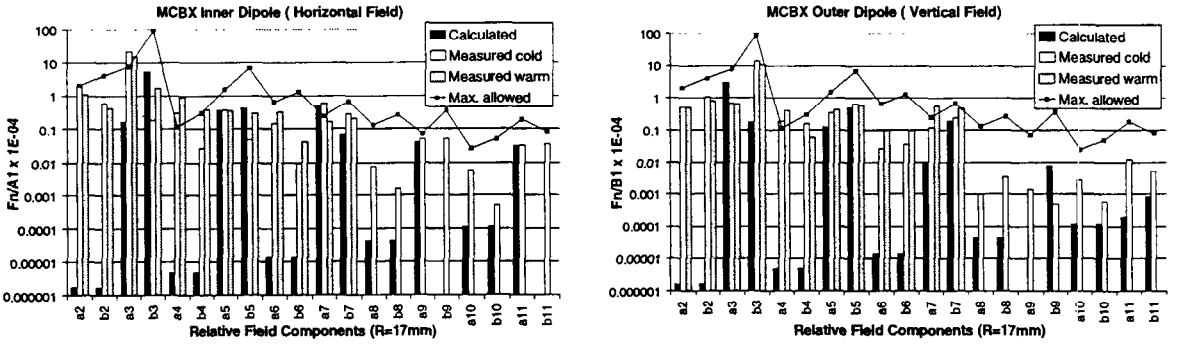

Figure 5: Measured and calculated multipole content of the inner and outer coils in comparison with the maximum allowed field errors

Both static and ramped magnetic measurements were carried out. Figure 5 compares the measured relative multipoles from the inner and outer coils at warm and at cold to the calculated values. There was also a good agreement between the measured and calculated field errors arising from the persistent currents.

3. Skew Quadrupole MQSX

The MQSX skew quadrupole has not yet been made as a prototype. The mechanical design will be similar to the MCBX comprising vacuum impregnated coils, scissors-laminations, and a shrinking cylinder. The preliminary parameter list for two different design alternatives is given in Table II. The coils of the 500 A design are counter-wound in the same way as the LHC spoolpiece correctors and the low-current version is wound with a flat cable of 10 wires. The disadvantage of the latter case is that in total 39 electrical connections have to be made on the end plate.

Table II: Preliminary design parameters of low-b Skew Quadrupole MCQSX

	Low-current version	High-current version	
MAGNETICS			
Nominal strength	22	22	T/m
Magnetic length	0.4	0.4	m
Peak field in coil	1.5	1.5	T
GEOMETRY			
Overall length	0.6	0.6	m
Coil length	0.5	0.5	m
Coil inner diameter	90	90	mm
Coil outer diameter	104.6	95	mm
Yoke inner diameter	128.6	119	mm
Yoke outer diameter	330	330	
Overall outer diameter	350	350	mm
ELECTRICS			
Nominal Current	0-55	0-500	A
Number of turns/coil	536	53	
Stored energy/magnet	0.9	0.6	kJ
Self inductance/magnet	596	5	mH
CONDUCTOR			
Cross section	0.28	0.913	mm^2
Cross section(metal)	0.21	0.689	mm^2
Copper/NbTi ratio	3.58	1.7	
Filament diameter	7	7	μm
Twist pitch	14	14	mm
Current density (NbTi)	1175	1926	A/mm^2
Margin to quench	76	62.5	%

4. Correction windings

4.1. Magnetics

Each inner triplet contains three corrector packages. The MCBX-magnets will accommodate two nested windings combining layers for either b_6-b_3 or b_5-b_4 corrections and the ones for the a_3-a_4-a_6 corrections will be located in the MQSX. The windings in the MCBX are subjected to a background field of 3 T, which sets a high demand for alignment tolerances due to the associated unbalanced forces. The background field in the MQSX is 1.5 T, however for coil construction and cooling reasons it is considered that it should not have more than three nested layers. The length of the layers will be adapted to the magnet in which they are housed.

Figure 6 illustrates how the magnetic forces on the correction windings will be pointing in different directions. To withstand these forces two options are possible. One is to incorporate the windings in the dipole or quadrupole coil assembly and then vacuum impregnate them all together. The other option is to assemble each set of correction windings as an independent insert rigid enough to withstand the magnetic forces. The second modular option has been taken as it allows more flexibility when it comes to the choice of correction windings.

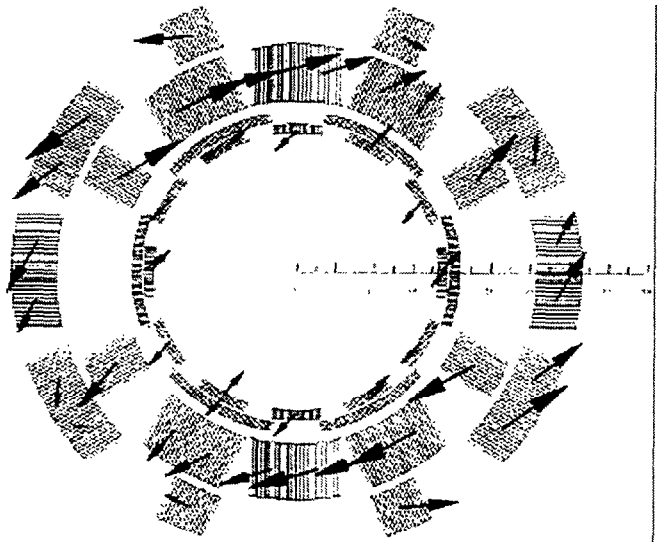

Figure 6: Magnetic forces in the coil blocks of MCBX and b_3-b_6 correction windings

4.2. Design

The cross-section of an insert combining b_3 and b_6 coils is shown in Figure 7. The coils are counter-wound around fiberglass central posts with a 600 A superconducting wire. To reduce the number of connections on the end plate each coil has two radial winding layers. The six dodecapole coils are mounted and aligned with dowel pins on a 1.5 mm thick fiberglass tube. Fiberglass filler pieces are located between the coils prior to wrapping the coil assembly with a pre-preg bandage. Once cured the outer diameter is turned to a precise dimension and the three sextupole coils are assembled in the same way followed by another layer of pre-preg bandage. Finally, an aluminium cylinder is shrunk around the magnet assembly and owing to its higher thermal contraction factor than that of the coils, the radial pressure and therefore the azimuthal pre-compression in the coils increases during the cool down.

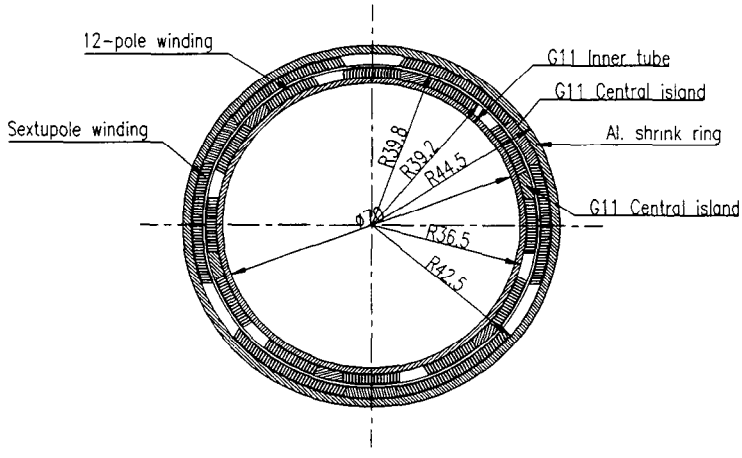

Figure 7: Cross-section of the b_3-b_6 insert

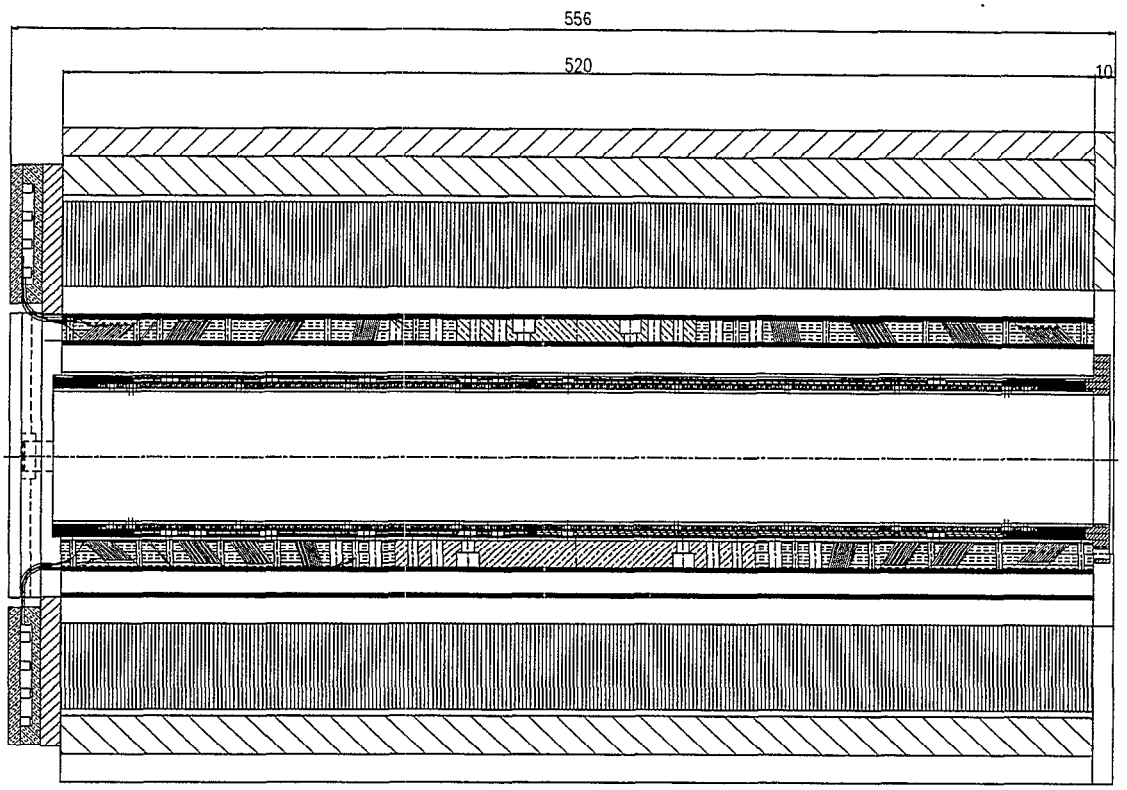

Figure 8: MCBX-b_3-b_6 assembly

The inter-coil connections are done on an end plate, which also includes the dowel pin holes to align the corrector insert with respect to the magnet in which it is housed (see Figure 8). The centering in the non-connection end of the insert is done by means of a precisely machined disk dowelled to the connection end of the MCBX.

4.3. Limitations

Besides the space limitations the choice of the operating current sets certain limits for the design. It is in principle desirable to make the correction windings using a wire that is as thin as possible in order to run at low currents. However, it is important that the inductance does not increase to point where the voltage developed during a quench becomes unacceptably high. It appeared that 50 A is a very minimum. For the first b_3-b_6 prototype the counter-winding technique used for spool-piece correctors of the LHC was adapted. If these coils are wound with a flat cable for easy fabrication, in the same way as several of the LHC correction magnets, the serial connections have to be made on the end flange. Therefore, there is an optimum to be found for the operation at the lowest possible current while keeping the number of connections to be made at the end to a practical level. This might turn out to be something like 100 A.

Another limitation is the field that can be generated by a correction winding. The overlapping dipole field limits the current density in the correction windings. Furthermore, when the correction winding is made of several layers, the additional layers are less effective in creating field as they are further away from the center of the magnet. The result of a number of calculations has been summarized in Figure 9. The field that can be generated on the inner rim of the correction coil is given as a function of the strength of the overlapping dipole field and as a function of the correction coil thickness. It is valid for multipoles from order 3 to 10 and allows estimation of the correction strength that can be obtained.

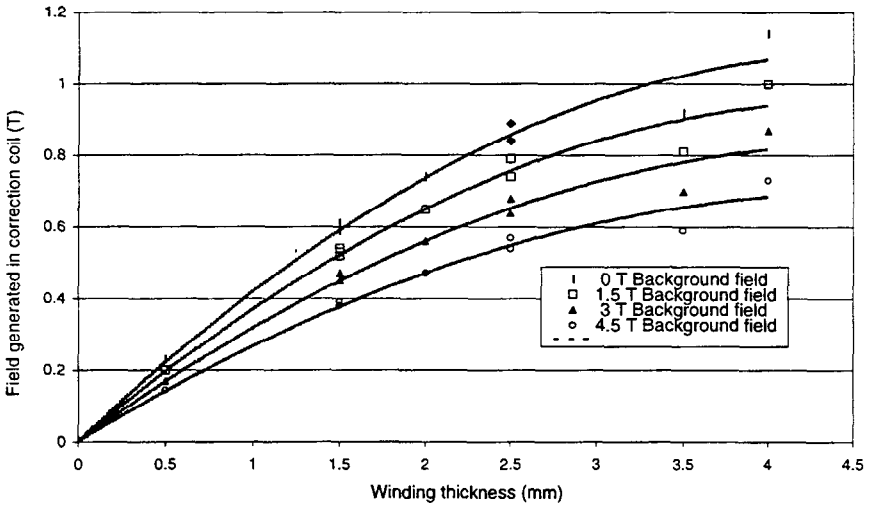

Figure 9: Correction field as function of thickness of correction winding (in overlapping fields of 0 to 4.5 T respectively). Any multipole order from 3 to 10

5. Proposed Correction Packages

In view of the recommendations of this Workshop [6] to consider three correction layers in the C1 and C2 packages (MCBXA and MQSXA in the CERN naming convention) and two correctors in the C3 package (MCBXB), a preliminary design was made to estimate the possible wire sizes and current ratings. He results of this study, Table III and IV, indicate that the required corrector strengths can be reached in all cases with nominal currents close to 120 A, which is one of the LHC corrector powering standards. The only exception are the b6 and a4 correctors which are limited by the criteria of margin-to-quench of at least 40%, and have strengths lower than given in [6]. Further studies are required to define the optimal design for these two correctors which would satisfy all criteria.

Table III: Preliminary parameters of the correction windings in the MCBX

	MCBXB		MCBXA			
	MCTX b_6-corrector	MCSX b_3-corrector	MCDX b_5-corrector	MCDSX a_5-corrector	MCOX b_4-corrector	
MAGNETICS						
Field at 17 mm radius	0.017	0.029	0.012	0.012	0.027	T
Magnetic length	0.5	0.5	0.5	0.5	0.5	m
Background field	3.3	3.3	3.3	3.3	3.3	T
GEOMETRY						
Overall length	0.6	0.6	0.6	0.6	0.6	m
Coil length	0.55	0.55	0.55	0.55	0.55	m
Coil inner diameter	73	81	73	78	83	mm
Coil outer diameter	366	82.46	75.92	80.92	85.92	mm
ELECTRICS						
Nominal Current	140	100	85	110	125	A
Number of turns/coil	63	34	37	39	52	
CONDUCTOR						
Cross section	0.28	0.28	0.28	0.28	0.28	mm^2
Cross section(metal)	0.21	0.21	0.21	0.21	0.21	mm^2
Copper/NbTi ratio	3.58	3.58	3.58	3.58	3.58	
Margin to quench	41	62	66	56	50	%

Table IV: Preliminary parameters of the correction windings in the MQSX

	MCTX a_6-corrector	MQSX MCOSX a_4-corrector	MCSSX a_3-corrector	
MAGNETICS				
Field at 17 mm radius	0.010	0.046	0.068	T
Magnetic length	0.5	0.5	0.5	m
Background field	1.5	1.5	1.5	T
GEOMETRY				
Overall length	0.6	0.6	0.6	m
Coil length	0.55	0.55	0.55	m
Coil inner diameter	73	79	84	mm
Coil outer diameter	75.92	81.92	87.92	mm
ELECTRICS				
Nominal Current	155	180	120	A
Number of turns/coil	31	50	71	
CONDUCTOR				
Cross section	0.28	0.28	0.28	mm^2
Cross section(metal)	0.21	0.21	0.1	mm^2
Copper/NbTi ratio	3.58	3.58	3.58	
Margin to quench	70	40	60	%

6. Planning

The planning of the design and fabrication of the LHC corrector magnets gives priority to the magnets that must be installed in the arcs. Their installation comes earliest and determines the date of commissioning of the machine. The corrector magnets for the insertion regions and inner triplets therefore come slightly later. As Table V shows the deliveries are planned as from September 2001.

Table V: LHC Corrector program

Planspe7.xls	A. Ij. 1-6-99	Work distribution corrector magnets
		X = required delivery
C = conception	D = design	d = design drawing firm A = approval S = spec. approval O = order D = delivery I = installation

	YEAR/	1999												2000										2001										2002									
		J	F	M	A	M	J	J	A	S	O	N	D	J	F	M	A	M	J	J	A	S	O	N	D	J	F	M	A	M	J	J	A	S	O	N	D	J	F	M	A	M	J	J	A	S	O	N	D
Supercond.	Wire					S					O							D																												
		Some wire is needed earlier for sextupoles -> intermediate order																																											
MAIN DIPOLE																																													
Spool sextupole	MCS	A	S				O				D							X	D																											
Spool decapole	MCD	D	d	d	d	A	S					O							X				D																						
Spool octupole	MCO	D	d	d	d	A	S					O							X				D																						
		Conclusion 1) Produce Type 2 dipoles first 2) make intermediate sextupoles for first up to 30 MB's in house																																										
MAIN QUADRUPOLE																																													
Sextupole/Dip.	MSCB			C	C	C	D	D	A	S					O						X			D																					
								d	d	d																																		
Tuning quad.	MQT/S						C	C	D	D	A	S			O						X			D																					
										d	d																																	
Lattice Octupole	MO							C	C	D	D	A	S			O					X			D																					
												d	d																																
		Problem for fabrication. Installation can start in time but manufacturing capacity not able																																											
		to cope with installation rate (some "holes" could be left)																																											
DISP. SUPPR.																																													
Long Trim Quad.	MQTL						C	C	D	D	A	S			O						X			D																					
Orbit Corrector	MCB									C	C	D	D	D	A	S			O		X							D																
		Must be installed first. Critical for installation																																											
INSERT. QUADS																																												
Long Orbit Corr.	MCBL									C	C	D	D	A	S			O						D																					
RF Orbit Corr.	MCBR									C	C	D	D	A	S			O						D																					
Wide Orbit Corr	MCBY										C	C	D	D	D	A	S			O				D																					
Low-b Orbit Corr.	MCBX										C	C	D	D	D	A	S			O				D																					
	(+spools)										C	C	D	D	D	A	S			O				D																					
Low-b Skew Quad.	MCQS										C	C	D	D	D	A	S			O				D																					

References

[1] M. Karppinen, A. Ijspeert, N. Hauge, B.R. Nielsen. "The Development of the Inner Triplet Dipole Corrector (MCBX) for LHC", MT-15, Beijing, China, September 1997.

[2] M. Karppinen, S. Russenschuck, A. Ijspeert, "Automated Design of a Correction Dipole Magnet for LHC", EPAC, Sitges, Spain, June 1996.

[3] Z. Ang, L. Bottura, A. Ijspeert, M. Karppinen, L. Walckiers, N. Hauge, B. Nielsen. "Magnetic Performance of First Low-beta Corrector Prototype MCBX", EPAC, Stockholm, Sweden, 1998.

[4] Ijspeert, J. Salminen, "Superconducting Coil Compression by Scissor Laminations", EPAC, Sitges, Spain, June 1996.

[5] A. Verdier, "Tolerance on the Multipole Components in the Closed Orbit Correctors", LHC Project Note 51, CERN, Geneva, Switzerland, August 1996.

[6] J. Wei, Proc. of this Workshop.

PRINCIPLE OF INTERACTION REGION LOCAL CORRECTION*

Jie Wei,† Brookhaven National Laboratory, USA

Abstract

For hadron storage rings like the Relativistic Heavy Ion Collider (RHIC) and the Large Hadron Collider (LHC), the machine performance at collision is usually limited by the field quality of the interaction region (IR) magnets. A robust local correction for the IR region is valuable in improving the dynamic aperture with practically achievable magnet field quality. We present in this paper the action-angle kick minimization principle on which the local IR correction for both RHIC and the LHC are based.

1 INTRODUCTION

For hadron storage rings like the Relativistic Heavy Ion Collider (RHIC) [1] and the Large Hadron Collider (LHC) [2], the beam size is the largest near the interaction region (IR) triplets during low-β^* operation. Furthermore, beam-beam effects often require a finite crossing angle, resulting in significant closed orbit deviation from the magnet centers. Machine performance at collision energy, measured in terms of the dynamic aperture, thus depends on achieving the highest possible magnetic field quality and alignment accuracy in the IR magnets.

Magnetic multipole correctors located in the IR region provide active means to compensate the impact of the IR magnetic errors. For hadron machines like RHIC and the LHC, the betatron phase advance across each IR triplet is negligible, and the betatron phase advance between the two IR triplet around each Interaction Point (IP) is near 180°. With these well-defined phase relations, IR-by-IR local correction can be effective and robust.

In this paper, we discuss the principle of action-angle kick minimization for IR local correction. Based on this principle, we have designed and implemented multi-layer multipole corrector packages in the RHIC IR region [3] correcting multipole errors up to the 12th-pole order. Similar correction schemes have been proposed for the LHC IR regions [4, 5, 6]. In Section 2, we review the Hamiltonian describing the particle motion under the magnetic multipole environment. In Section 3, we discuss the figures of merit for global and local error compensation. Discussions and summaries are given in Section 4.

* Work performed under the auspices of the US Department of Energy.
† Email: weil@bnl.gov

2 HAMILTONIAN

Under the assumption that the effect of the longitudinal magnetic field is insignificant [7], and that the transverse amplitude of particle motion is small compared with the average bending radius, the magnetic field in a magnet can be expressed in terms of a 2-dimensional multipole expansion

$$B_y + iB_x = B_0 \sum_{n=1}^{\infty} (b_n + ia_n)(x+iy)^{n-1} \qquad (1)$$

where x and y indicate the horizontal and vertical directions, respectively, B_0 is the nominal bending field, and $n = 1$ is dipole term, $n = 2$ is quadrupole term, etc. The Hamiltonian of the charged particle with s as the independent variable is approximately [8]

$$H(x, p_x, y, p_y; s) = -\frac{eA_s}{cp} - \frac{x}{\rho} + \frac{1}{2}\left(p_x^2 + p_y^2\right) \qquad (2)$$

where ρ is the local radius of curvature, $\mathbf{A}$ is given by

$$\mathbf{B} = \nabla \times \mathbf{A}, \qquad (3)$$

with

$$\begin{aligned} A_s &= (\mathbf{A}\cdot\hat{\mathbf{s}})\left(1+\frac{x}{\rho}\right) \\ &= -\left(1+\frac{x}{\rho}\right) B_0 \sum_{m,n=0;m+n>0}^{\infty} (c_{mn} + e_{mn}) x^m y^n \end{aligned} \qquad (4)$$

where the coefficients c_{mn} are given by

$$c_{mn} = \frac{1}{m+n}\begin{pmatrix} m+n \\ n \end{pmatrix} \begin{cases} (-)^{n/2} b_{m+n}, & n \text{ even} \\ (-)^{(n+1)/2} a_{m+n} & n \text{ odd} \end{cases} \qquad (5)$$

In Eq. 5, the coefficients c_{mn} are deduced from the recursive equation [8]

$$\begin{aligned} &(m+2)(m+1)\rho^2 e_{m+2,n} + (n+2)(n+1)\rho^2 e_{m,n+2} \\ &+(m+1)(2m+1)\rho e_{m+1,n} + 2(n+2)(n+1)\rho e_{m-1,n+2} \\ &+(m+1)(m-1)e_{mn} + (n+2)(n+1)e_{m-2,n+2} \\ &= -(m+1)\rho c_{m+1,n} - (m-1)c_{mn} \end{aligned} \qquad (6)$$

with initial conditions

$$e_{1n} = e_{0n} = 0. \tag{7}$$

We introduce a canonical transformation using the generating function

$$F_2(x, p_{x_\beta}, y, p_{y_\beta}) = (x - D_x\delta - x_c) + (y - D_y\delta - y_c), \tag{8}$$

where $\delta = \Delta p/p_0$, $p_0 c = B_0\rho_0$ is the rigidity of the beam, and ρ_0 is the nominal bending radius. The dispersion functions D_x and D_y, and the closed-orbit displacements x_c and y_c are determined by eliminating the terms in the Hamiltonian that are linear in x_β and y_β. The new Hamiltonian is expressed in terms of the betatron displacements x_β and y_β as

$$\begin{aligned} &H(x_\beta, p_{x_\beta}, y_\beta, p_{y_\beta}; s) \\ &= \frac{1}{2}\left(p_{x\beta}^2 + p_{y\beta}^2\right) + \frac{1}{2\rho_0}\left[\left(\bar{b}_2 + \frac{\bar{b}_1}{\rho}\right)x_\beta^2 - \bar{b}_2 y_\beta^2\right] \\ &+ \frac{1}{\rho_0}\left(B_{20}x_\beta^2 + B_{11}x_\beta y_\beta + B_{02}y_\beta^2 + \right. \\ &\left. + B_{30}x_\beta^3 + B_{21}x_\beta^2 y_\beta + B_{12}x_\beta y_\beta^2 + B_{03}y_\beta^3 + \cdots\right). \end{aligned} \tag{9}$$

Retaining terms that are linear in the closed orbit displacements $\Delta_x = D_x\delta + x_c$ and $\Delta_y = D_y\delta + y_c$, the coefficients B_{ij} are given by [9]

$$\begin{aligned} B_{02} &= -\frac{1}{2}(\Delta b_2 - b_2\delta) - b_3\Delta_x + a_3\Delta_y \\ B_{11} &= -a_2 - 2(a_3\Delta_x + b_3\Delta_y) \\ B_{20} &= -B_{02} + \frac{1}{2\rho}(\Delta b_1 - b_1\delta) \end{aligned} \tag{10}$$

$$\begin{aligned} B_{30} &= \frac{b_3}{3} + b_4\Delta_x - a_4\Delta_y \\ B_{21} &= -3a_3 - 3a_4\Delta_x - 3b_4\Delta_y \\ B_{12} &= -3B_{30} \\ B_{03} &= -B_{21}/3 \end{aligned} \tag{11}$$

$$\begin{aligned} B_{40} &= \frac{b_4}{4} + b_5\Delta_x - a_5\Delta_y \\ B_{31} &= -a_4 - 4(a_5\Delta_x + b_5\Delta_y) \\ B_{22} &= -6B_{40} \\ B_{13} &= -B_{31} \\ B_{04} &= B_{40} \end{aligned} \tag{12}$$

$$\begin{aligned} B_{50} &= \frac{b_5}{5} + b_6\Delta_x - a_6\Delta_y \\ B_{41} &= -a_5 - 5a_6\Delta_x - 5b_6\Delta_y \\ B_{32} &= -10B_{50} \\ B_{23} &= -2B_{41} \\ B_{14} &= -5B_{50} \\ B_{05} &= B_{41}/5 \end{aligned} \tag{13}$$

$$\begin{aligned} B_{60} &= \frac{b_6}{6} + b_7\Delta_x - a_7\Delta_y \\ B_{51} &= -a_6 - 6(a_7\Delta_x + b_7\Delta_y) \\ B_{42} &= -15B_{60} \\ B_{33} &= -20B_{51} \\ B_{24} &= 15B_{60} \\ B_{15} &= B_{51} \\ B_{06} &= -B_{60} \end{aligned} \tag{14}$$

$$\begin{aligned} B_{70} &= \frac{b_7}{7} + b_8\Delta_x - a_8\Delta_y \\ B_{61} &= -a_7 - 7a_8\Delta_x - 7b_8\Delta_y \\ B_{52} &= -21B_{70} \\ B_{43} &= -5B_{61} \\ B_{34} &= 35B_{70} \\ B_{25} &= 3B_{61} \\ B_{16} &= -7B_{70} \\ B_{07} &= -B_{61}/7 \end{aligned} \tag{15}$$

$$\begin{aligned} B_{80} &= \frac{b_8}{8} + b_9\Delta_x - a_9\Delta_y \\ B_{71} &= -a_8 - 8a_9\Delta_x - 8b_9\Delta_y \\ B_{62} &= -28B_{80} \\ B_{53} &= -7B_{71} \\ B_{44} &= 70B_{80} \\ B_{35} &= 7B_{71} \\ B_{26} &= -28B_{80} \\ B_{17} &= -B_{71} \\ B_{08} &= B_{80} \end{aligned} \tag{16}$$

$$\begin{aligned} B_{90} &= \frac{b_9}{9} + b_{10}\Delta_x - a_{10}\Delta_y \\ B_{81} &= -a_9 - 9a_{10}\Delta_x - 9b_{10}\Delta_y \\ B_{72} &= -36B_{90} \\ B_{63} &= -28B_{81}/3 \\ B_{54} &= 126B_{90} \\ B_{45} &= 14B_{81} \\ B_{36} &= -84B_{90} \\ B_{27} &= -4B_{81} \\ B_{18} &= 9B_{90} \\ B_{09} &= B_{81}/9 \end{aligned} \tag{17}$$

$$
\begin{aligned}
B_{10,0} &= \frac{b_{10}}{10} + b_{11}\Delta_x - a_{11}\Delta_y \\
B_{91} &= -a_{10} - 10a_{11}\Delta_x - 10b_{11}\Delta_y \\
B_{82} &= -45B_{10,0} \\
B_{73} &= -12B_{91} \\
B_{64} &= 210B_{10,0} \\
B_{55} &= 126B_{91}/5 \\
B_{46} &= -210B_{10,0} \\
B_{37} &= -12B_{91} \\
B_{28} &= 45B_{10,0} \\
B_{19} &= B_{91} \\
B_{0,10} &= -B_{10,0}
\end{aligned}
\tag{18}
$$

where Δb_1 and Δb_2 are the deviation from the design dipole $\bar{b}_1$ and quadrupole $\bar{b}_2$ fields. Regarding the multipole errors as a perturbation, the Hamiltonian given by Eq. 9 can be further rewritten in terms of the action-angle variables $(\phi_x, J_x, \phi_y, J_y)$ as

$$
H(\phi_x, J_x, \phi_y, J_y) = \sum_{i=x,y} \frac{\nu_{i0} J_i}{R_0} + \sum_{l,m=-\infty}^{\infty} A_{lm} e^{il\phi_x} e^{im\phi_y}
\tag{19}
$$

using the relations

$$
z = \sqrt{2J_z\beta_z}\cos\chi, \quad p_z = -\sqrt{\frac{2J_z}{\beta_z}}(\sin\chi_z + \alpha_z\cos\chi_z)
\tag{20}
$$

where $z = x, y$, and

$$
\chi_z = \phi - \frac{\nu_{z0}s}{R} + \int_0^s \frac{ds'}{\beta_z} \approx \int_0^s \frac{ds'}{\beta_z}.
\tag{21}
$$

The action J_z can be written as

$$
J_z = \frac{1}{2\beta_z}\left[z^2 + (\alpha_z z + \beta_z p_z)^2\right].
\tag{22}
$$

Here, ν_{x0} and ν_{y0} are the unperturbed tunes, $2\pi R_0$ is the ring circumference, $\alpha_{x,y}$ and $\beta_{x,y}$ are the Courant-Snyder lattice functions, and A_{lm} represents the error terms which can be deduced from Eq. 9.

3 FIGURES OF MERIT

Conventionally, spread of betatron tunes has been used to guide the design of storage rings. Minimization of the tune spread is often used for global error compensation. Since skew multipoles and odd, normal multipoles do not contribute to the linear tune shift, an extension of such global method is the minimization of nonlinear components of the one-turn map.

The global compensation approaches are valuable for resonance correction as well as dynamic aperture improvement. However, in the case that dominant errors are localized in specific places like the interaction region, global multipole compensation is less robust and often practically difficult to implement during machine operation. Local IR-by-IR compensation employing multi-layer multipole correctors located in the corresponding IR quadrupole triplet region can provide effective correction.

3.1 *Tune spread*

The tune spread is usually defined as the spread of the tune shift of particles with various betatron amplitudes and momentum deviation. To the first order of the multipole errors, the tune shifts can be obtained by [9] averaging the time derivatives of ϕ_x and ϕ_y while keeping only the A_{00} term from the expansion,

$$
\nu_z = \langle \oint \frac{ds}{2\pi}\frac{\partial H}{\partial J_z} \rangle = \nu_{z0} + \oint \frac{ds}{2\pi}\frac{\partial A_{00}}{\partial J_z}
\tag{23}
$$

where $z = x, y$, the sign $\langle\ \rangle$ denotes average over the phase variable, and the integral is performed over the circumference of the closed orbit. Retaining multipole terms up to 11th order ($n = 11$) and closed orbit terms (Δ_x, Δ_y) to the first order, the linear horizontal tune shift is

$$
\begin{aligned}
\nu_x &= \oint \frac{\beta_x ds}{2\pi\rho_0}\Big\{ -\frac{\Delta b_1}{2\rho} + \frac{b_1\delta}{2\rho} - C_0 \\
&\quad + 3C_1\beta_x J_x - 6C_1\beta_y J_y \\
&\quad + \frac{15}{2}C_2\beta_x^2 J_x^2 - 45C_2\beta_x\beta_y J_x J_y + \frac{45}{2}C_2\beta_y^2 J_y^2 \\
&\quad + \frac{35}{2}C_3\beta_x^3 J_x^3 - 210C_3\beta_x^2\beta_y J_x^2 J_y \\
&\quad + 315C_3\beta_x\beta_y^2 J_x J_y^2 - 70C_3\beta_y^3 J_y^3 \\
&\quad + \frac{315}{8}C_4\beta_x^4 J_x^4 - \frac{1575}{2}C_4\beta_x^3\beta_y J_x^3 J_y \\
&\quad + \frac{4725}{2}C_4\beta_x^2\beta_y^2 J_x^2 J_y^2 - 1575C_4\beta_x\beta_y^3 J_x J_y^3 \\
&\quad + \frac{1575}{8}C_4\beta_y^4 J_y^4 \Big\}.
\end{aligned}
\tag{24}
$$

The linear vertical tune shift is

$$\begin{aligned}\nu_y &= \oint \frac{\beta_x ds}{2\pi\rho_0}\{C_0 + 3C_1\beta_y J_y - 6C_1\beta_x J_x \\ &-\frac{15}{2}C_2\beta_y^2 J_y^2 + 45C_2\beta_x\beta_y J_x J_y - \frac{45}{2}C_2\beta_x^2 J_x^2 \\ &+\frac{35}{2}C_3\beta_y^3 J_y^3 - 210C_3\beta_y^2\beta_x J_y^2 J_x \\ &+315C_3\beta_y\beta_x^2 J_y J_x^2 - 70C_3\beta_x^3 J_x^3 \\ &-\frac{315}{8}C_4\beta_y^4 J_y^4 + \frac{1575}{2}C_4\beta_y^3\beta_x J_y^3 J_x \\ &-\frac{4725}{2}C_4\beta_y^2\beta_x^2 J_y^2 J_x^2 + 1575C_4\beta_y\beta_x^3 J_y J_x^3 \\ &-\frac{1575}{8}C_4\beta_x^4 J_x^4\Big\}\end{aligned} \tag{25}$$

where the coefficients are

$$\begin{aligned}C_0 &= \frac{\Delta b_2 - b_2\delta}{2} + b_3\Delta_x - a_3\Delta_y \\ C_1 &= \frac{b_4}{4} + b_5\Delta_x - a_5\Delta_y \\ C_2 &= \frac{b_6}{6} + b_7\Delta_x - a_7\Delta_y \\ C_3 &= \frac{b_8}{8} + b_9\Delta_x - a_9\Delta_y \\ C_4 &= \frac{b_{10}}{10} + b_{11}\Delta_x - a_{11}\Delta_y.\end{aligned} \tag{26}$$

3.2 *Action-angle kick*

The figures of merit for local minimization are the action-angle kicks produced by the IR magnets at each specified multipole order. The action kicks can be expressed as

$$\begin{aligned}\Delta J_x &= -\int ds\frac{\partial H}{\partial\phi_x} = -\sum_{l,m=-\infty}^{\infty} il\Delta J_{lm} \\ \Delta J_y &= -\int ds\frac{\partial H}{\partial\phi_y} = -\sum_{l,m=-\infty}^{\infty} im\Delta J_{lm}\end{aligned} \tag{27}$$

where

$$\Delta J_{lm} \approx \int ds\, A_{lm} \exp\left(il\int_0^s \frac{ds'}{\beta_x}\right)\exp\left(im\int_0^s \frac{ds'}{\beta_y}\right). \tag{28}$$

The correction scheme is simplified by the fact that the action is approximately a constant of motion at the time scale of the revolution period, and that the relative betatron phase is well defined within the high-β IR region. Minimization is performed on every significant multipole error b_n (or a_n). Since the available physical space is usually limited in the high-β region, corrector packages containing multi-layer corrector elements of various multipole content are used. For each multipole order c_n (either a_n or b_n), (a minimum of) two correction elements are implemented for every IR, each located at symmetric locations around the IP. Due to the anti-symmetry of the IR optics, one of the two elements is near the maximum β_x location, and the other is near the maximum β_y location, resulting in an effective compensation. The strengths of these correction elements are determined by minimizing the two quantities

$$\int_L ds\, C_z\, c_n + (-)^n \int_R ds\, C_z\, c_n, \quad z = x, y \tag{29}$$

taking advantage of the negligible betatron phase advance within each triplet, and approximate 180° phase advance between the triplets. The integral is over the entire left-hand-side (L) or right-hand-side (R) triplet. In general, the weights C_z in Eq. 29 are chosen according to the multipoles as:

$$C_x = \begin{cases}\beta_x^{n/2} & \text{for } b_n \\ \beta_x^{(n-1)/2}\beta_y^{1/2} & \text{for } a_n\end{cases} \tag{30}$$

and

$$C_y = \begin{cases}\beta_y^{n/2} & \text{for even } b_n \text{ or odd } a_n \\ \beta_x^{1/2}\beta_y^{(n-1)/2} & \text{for odd } b_n \text{ or even } a_n\end{cases} \tag{31}$$

4 DISCUSSIONS AND SUMMARY

Compared with the tune shift, the action (and angle) kick has similar dependence on the lattice optics β_z for each multipole. Consequently, minimization of action-angle kicks results in a reduction of tune spread and an improvement of the dynamic aperture. The compensation scheme is usually not sensitive to the change of β^*, as long as β^* is low at the IP (usually the only relevant case) so that β at a distance s from the IP satisfies the relation $\beta\beta^* \cong s^2$. In the case of two beams sharing the same IR magnets, the compensation is equally effective for both intersecting beams, since the optics of the interaction region is anti-symmetric. Although closed-orbit deviation (e.g. due to finite crossing angle) is not taken into account, the correction is usually effective since the effect of the magnet feed-down is partially compensated by the feed-down from the correctors.

The most straightforward approach for local correction on multipoles of $n = 3$ and higher order is the dead-reckoning method, setting the corrector strength according to Eq. 29 using bench-measured magnetic multipole errors. Up to 10% of measurement errors and quench/thermal cycle dependent multipole variations can usually be tolerated [3, 5, 6]. The method is also immune to moderate closed-orbit errors and corrector misalignments [6].

Multipole errors of order $n = 1, 2$ produce closed orbit deviation, tune perturbation, and coupling. The effects are

usually compensated using beam-based tuning. In the case that skew quadrupole components and quadrupole misalignment of the IR triplets is significant, local decoupling utilizing the a_2 corrector in the IR can be effective [10]. The corrector strength obtained from the local decoupling scheme is similar to those given by Eq. 29. Beam-based corrections for higher order multipoles have also been pursued by several authors recently [11, 12].

5 REFERENCES

[1] *Relativistic Heavy Ion Collider Design Manual*, Brookhaven National Laboratory (1998).

[2] *The LHC Conceptual Design Report*, CERN/AC/95-05(LHC), CERN (1995).

[3] J. Wei, *Error Compensation in Insertion-Region Magnets*, Particle Accelerators, **55** 439–448 (1996).

[4] J. Wei, V. Ptitsin, F. Pilat, S. Tepikian, N. Gelfand, W. Wan, J. Holt, *US-LHC IR Magnet Error Analysis and Compensation*, European Particle Accelerator Conference, Stockholm, (June 1998) p. 380.

[5] J. Wei, W. Fischer, V. Ptitsin, R. Ostojic, J. Strait, *Interaction Region Local Correction for the Large Hadron Collider*, Proceedings of Particle Accelerator Conference, New York (1999) p. 2921.

[6] W. Fischer, V. Ptitsin, J. Wei, R. Ostojic, J. Strait, *LHC Interaction Region Correction Scheme Studies*, these proceedings.

[7] J. Wei, R.Talman, *Theorem on Magnet Fringe Field*, Particle Accelerators, **55** 339–344 (1996).

[8] L. Micheloti, *Introduction to the Nonlinear Dynamics Arising from Magnetic Multipoles*, AIP Conference Proceedings **153** (1985) p. 236.

[9] J. Wei, M. Harrison, *Tune Spread due to Magnetic Multipoles in RHIC*, Proc. XVth International Conference on High Energy Accelerators, Hamburg, Germany, 1031-1033 (1992).

[10] F. Pilat, S. Tepikian, D. Trbojevic, J. Wei, *The Effect and Correction of Coupling Generated by the RHIC Triplet Quadrupoles* Proc. 1995 Particle Accelerator Conference and International Conference on High-Energy Accelerators, Dallas, Texas (May 1995) 2832 - 2834.

[11] C. Wang, J. Irwin and Y.T. Yan, *Computation of nonlinear one turn maps from measurement with model independent analysis*, Talk given at IEEE Particle Accelerator Conference (PAC 99), New York, NY, 29 Mar - 2 Apr 1999.

[12] J. Shi, *Global Correction of Magnetic Field Errors in LHC Interaction Regions*, these proceedings.

LHC INTERACTION REGION CORRECTION SCHEME STUDIES*

W. Fischer, V. Ptitsin and J. Wei, BNL, USA; R. Ostojic, CERN, Switzerland; J. Strait, FNAL, USA

Abstract

In a companion paper we showed that the performance of the Large Hadron Collider (LHC) at collision energy is limited by the field quality of the interaction region quadrupoles and dipoles. In this situation, the dynamic aperture can be increased through local multipole correctors. Since the betatron phase advance is well defined for magnets that are located in regions of large beta functions, local corrections can be very effective and robust. We compare possible compensation schemes and propose a corrector layout to meet the required dynamic aperture performance.

1 INTRODUCTION

In the LHC the field errors of the FNAL and KEK triplet quadrupoles are a leading source of the dynamic aperture reduction at collision [1]. Local interaction region correctors are thus proposed to reach the LHC target dynamic aperture of 12 times the transverse rms beam size ($12\sigma_{xy}$).

During the past two years of magnet proto-type manufacturing, testing, and field quality analysis of the US-LHC magnets, there has been several iterations of the magnet design that leads to improvement of the field quality. Accordingly, there has been several iterations of the proposed compensation schemes for the IR region [2, 3]. First, body-end compensation of the systematic b_6 is not planned due to the reduced b_6 in the lead end and the uncertainty in b_6 measurement. Then, magnetic tuning shims are no longer planned due to the reduction of the random b_3 and b_4 errors and mechanical complications associated with shimming. Finally, the corrector layout and strength requirements are modified after CERN's decision have the Q1 and Q3 quadrupoles built by KEK, and to have the Q2A and Q2B quadrupoles built by FNAL.

Fig. 1 shows the tentative location of the proposed correctors assumed for this study. We choose the corrector strenght such that the action angle kick accross the interaction region is minimized [4]. For this, two correctors per order and interaction region are needed. An accurate measurement of the multipole errors in the quadrupoles is necessary. A local correction scheme like this does not prevent the implementation of global correction schemes proposed in references [5, 6] in the future. During the workshop, it became clear that as the systematic b_{10} in the body of KEK-built quadrupoles is further reduced, it is neither necessary nor desirable to plan for any b_{10} correctors. On the other hand, due to strength requirements for the b_6 correction, fewer layers of correction elements should be designed in the corrector package that contains the b_6 element. Fig. 2 shows the final proposed layout from the workshop [7].

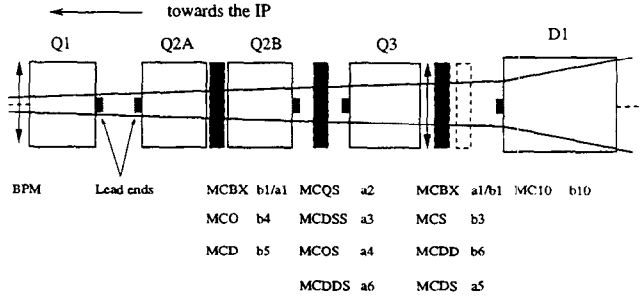

Figure 1: Tentative layout of the LHC inner triplet region assumed for the study of this paper.

In Sec. 2 the correction algorithm is presented in short. In the following section the effectiveness of four correcion schemes is evaluated with element-by-element particle tracking over 1,000 turns. Only IP1 and IP5 are corrected in these studies.

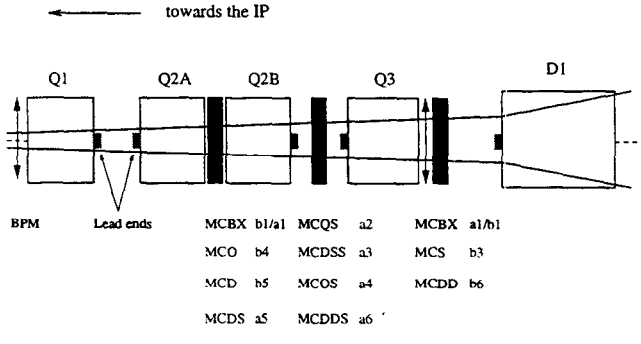

Figure 2: Final proposed layout of the LHC inner triplet region from this Workshop.

2 IR COMPENSATION SCHEMES

The error compensation is based on the minimization of action-angle kicks [4] produced by each multipole error b_n (or a_n) over a pair of inner triplets. Using two correction elements of each multipole order c_n (either a_n or b_n), we

* Work performed under the auspices of the US Department of Energy.

minimize the sum

$$\int_L dl C_z B_0 c_n + (-)^n \int_R dl C_z B_0 c_n, \quad z = x, y \qquad (1)$$

taking advantage of the negligible betatron phase advance within each triplet and D1, and approximate the phase advance between the triplets by 180°. The integral is over the entire left-hand-side (L) or right-hand-side (R) MQX triplet and D1. In dipoles B_0 is simply the main field, in quadrupoles it is the field at the reference radius R_{ref}. In general, the weights C_z in Eq. 1 are chosen according to the multipoles as:

	even b_n	odd b_n	even a_n	odd a_n
C_x	$\beta_x^{n/2}$	$\beta_x^{n/2}$	$\beta_x^{(n-1)/2}\beta_y^{1/2}$	$\beta_x^{(n-1)/2}\beta_y^{1/2}$
C_y	$\beta_y^{n/2}$	$\beta_x^{1/2}\beta_y^{(n-1)/2}$	$\beta_x^{1/2}\beta_y^{(n-1)/2}$	$\beta_y^{n/2}$

The compensation is equally effective for both intersecting beams, since the optics of the interaction region is anti-symmetric. However, it does not take into account the closed-orbit deviation due to the crossing angle, and the fact that the crossing planes are respectively vertical and horizontal in the two high luminosity interaction points. On the other hand, the effect of this closed orbit feeddown is partially compensated by the feeddown from the correctors.

3 CORRECTION SCHEME COMPARISON

There are three corrector packages (MCX1, MCX2, MCX3) in each triplet (see Fig. 1 and Fig. 2). Each MCX1 and MCX3 contains two dipole layers, and each MCX2 contains a skew quadrupole layer. A straightforward approach (scheme 1, see Tab. 1) is to have 3 additional layers of nonlinear skew multipoles (a_3, a_4, a_6) for MCX2, and two additional layers of nonlinear multipoles for MCX1 and MCX3. These layers could be a combination of any of b_3, b_4, b_5 and b_6 layers. For each multipole, two correction elements, located symmetrically at both sides of the IP, can be activated to minimize the kick in both the x and y directions (compare Eq. 1). Due to the lattice symmetry both beams are corrected.

Scheme 1 increases the dynamic aperture by 38% in the unmixed and 28% in the mixed case. With an additional a_5 corrector (scheme 2) the improvement is 42% and 32% respectively. A further improvement can be achieved using a b_{10} corrector, as shown in Tab. 2. However, a b_{10} corrector is difficult to built is not needed with the KEK multipole error table version 3.0 [1].

Fig. 3 depicts the effect of correction scheme 4 on the tune space. The tune spread of particles with transverse amplitudes up to 6 times the rms beam size is reduced from more than 4×10^{-3} to about 7×10^{-4}.

We also investigated the effect of misalignment of the corrector layers. With an rms misalignment of 0.5mm in the horizontal and vertical planes we find no degradation of the dynamic aperture(see Tab. 3).

Table 1: Interaction region correction schemes. Only the non-linear correctors are shown.

	MCX1	MCX2	MCX3	remark
scheme 1	2 layers b_4, b_5	3 layers a_3, a_4, a_6	2 layers b_3, b_6	
scheme 2	3 layers b_3, b_5, b_6	3 layers a_3, a_4, a_6	2 layers b_4, a_5	
scheme 3	2 layers b_4, b_5	3 layers a_3, a_4, a_6	2 layers b_3, b_6	scheme 1 $+ b_{10}$
scheme 4	3 layers b_3, b_5, b_6	3 layers a_3, a_4, a_6	2 layers b_4, a_5	scheme 2 $+ b_{10}$

Table 2: Comparison of local IR corrector effectiveness assuming that the interaction region quadrupole errors are measured to a 5% rms accuracy. The dynamic aperture (DA) is given in units of σ_{xy}. The physical aperture of 60 mm corresponds to about $14\sigma_{xy}$.

Case	DA mean	DA rms	DA min
UNMIXED:			
no correction	8.5	1.4	7
scheme 1	11.8	2.4	8
scheme 2	12.1	2.2	9
scheme 3	15.4	1.8	12
scheme 4	15.9	1.7	13
MIXED:			
no correction	10.0	1.5	8
scheme 1	12.8	1.1	10
scheme 2	13.2	1.3	11
scheme 3	16.1	1.8	13
scheme 4	17.6	1.6	14

Table 3: Effect of corrector displacement. The dynamic aperture (DA) is given in units of σ_{xy}.

Case	DA mean	DA rms	DA min
MIXED scheme 4	17.6	1.6	14
MCX1-3 displaced with 0.5 mm rms	17.8	1.3	15

The required strength of the multipole correctors can be provided by 50cm long spool pieces wound using the LHC sextupole corrector wire and operating at less than 50% margin at 600A [8]. At IP2, the IR correctors are also designed to reduce the effect of the D1 errors during low-β heavy ion operations [9]. We computed the maximum corrector strength order by order out of a distribution of 80 values (systematic multipole error with positive and negative sign $\times$ 10 random error seeds $\times$ 2 interaction regions $\times$ 2

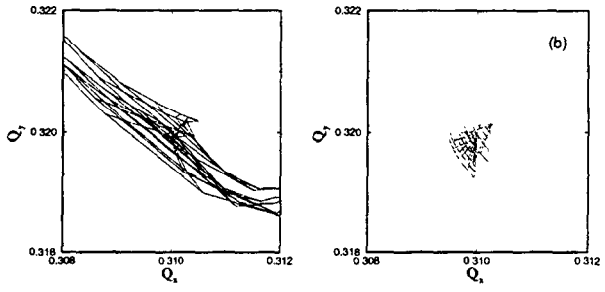

Figure 3: Effect of IR multipole correction on the covered tune space. (a) shows the uncorrected machine and (b) the corrected machine with scheme 4.

correctors per interaction region). The result for correction scheme 2 is shown in Fig. 4 for the KEK multipole error tables version 2.0 and 3.0 (both together with the FNAL multipole error table version 2.0). The available correction strength is sufficient for all orders of multipole errors.

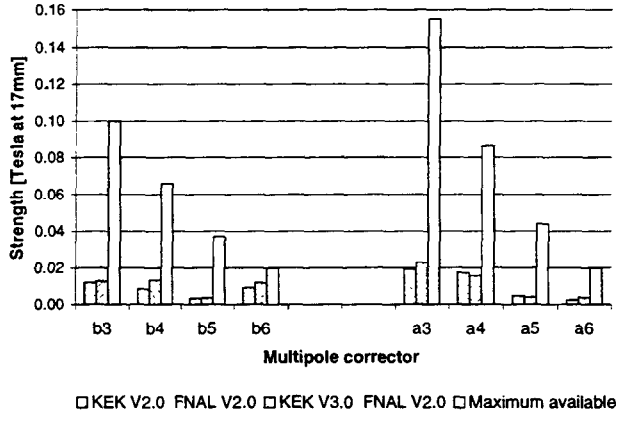

Figure 4: Available and needed corrector strength for scheme 2. The needed corrector strength shows the maximum out of a distribution of 20 machines with two correctors each at IP1 and IP5.

4 SUMMARY

Local nonlinear interaction region correctors, up to multipole order 6, are proposed for compensating the interaction quadrupole errors. These correctors can improve the dynamic aperture by 2-3σ_{xy}. The required correction strength is well within the available strength.

We thank J. Gareyte, J.-P. Koutchouk, O. Brüning and J. Miles for lattice assistance and discussions, and many others, including M. Harrison, A. Ijspeert, J. Kerby, M.J. Lamm, S. Peggs, T. Sen, R. Talman, T. Taylor and A.V. Zlobin.

5 REFERENCES

[1] W. Fischer et al., "LHC interaction region quadrupole error impact studies", these proceedings.

[2] J. Wei et al., "US-LHC IR magnet error analysis and compensation", EPAC 1998 proceedings (1998) p. 380.

[3] J. Wei et al., "Interaction region local correction for the Large Hadron Collider", PAC 1999 proceedings (1999) p. 2921.

[4] J. Wei, "Principle of interaction region local correction", these proceedings.

[5] T. Sen et al., "Correction schemes for the LHC lattice at collision", these proceedings.

[6] J. Shi, "Global correction of magnetic field errors in LHC interaction regions", these proceedings.

[7] J. Wei, J. Strait, J.-P. Koutchouk, T. Taylor, "Summaries", these proceedings.

[8] M. Karppinen, private communications.

[9] V. Ptitsin, W. Fischer and J. Wei, "LHC interaction region correction in heavy ion operation", these proceedings.

LHC INTERACTION REGION CORRECTION IN HEAVY ION OPERATION*

V. Ptitsin, W. Fischer, J. Wei, BNL, Upton, NY

Abstract

In heavy ion operation the LHC interaction region at IP2 will have a low-β optics for collisions. The dynamic aperture is therefore sensitive to magnetic field errors in the interaction region quadrupoles and dipoles. We investigate the effect of the magnetic field errors on the dynamic aperture and evaluate the effectiveness of local interaction region correctors. The dynamic aperture and the tune space are computed for different crossing angles.

1 INTRODUCTION

The LHC heavy ion collision lattice uses a low-β insertion at IP2 in addition to low-β insertions at IP1 and IP5 [1]. This produces large values of the β functions in corresponding interaction region triplet quadrupoles and D1 dipoles. Furthermore, all interaction regions utilize orbit separation and crossing angle schemes. Such schemes lead to large orbit excursion inside the interaction region quadrupoles and dipoles, thus shifting the beam into the field regions with larger nonlinear fields. The basic parameters for the LHC proton and ion operation are listed in Table 1.

Table 1: Basic LHC parameters for proton operation at injection and collision and heavy ion operation at collision. E denotes the particle energy, ν_x/ν_y the horizontal and vertical tunes, ξ_x/ξ_y the horizontal and vertical chromaticities, ϵ_N the normalized transverse emittance, and σ_p the rms momentum spread.

Quantity	p injection	p collision	ion collision
E [GeV]	450	7000	7000/charge
ν_x/ν_y	63.28/59.31	63.31/59.32	63.31/59.32
ξ_x/ξ_y	2/2	2/2	2/2
ϵ_N [rad]	3.75×10^{-6}	3.75×10^{-6}	1.5×10^{-6}
σ_p	4.7×10^{-4}	1.1×10^{-4}	1.14×10^{-4}

We use tune footprints and the dynamic aperture (DA) to evaluate the magnetic multipole error impact and the effectiveness of correction schemes. The dynamic aperture target is set at a 12σ average over a number of random multipole error selections with a minimum of 10σ, determined after 100,000 turns. We aim at tune spreads of less than 10^{-3} for particles with amplitudes of up to 6σ.

2 TRACKING SETUP

The Fortran version of the TEAPOT code was used for the tracking studies. We restricted our investigation to 1,000 turns. Previous studies indicate that tracking up to 10^5 turns further reduces the dynamic aperture by $0.5-1.0\sigma$ [2].

For every case we use 10 sets of randomly generated multipole errors, based on the error tables (version 2.0 for the FNAL built quadrupoles, version 2.0 and 3.0 for the KEK built quadrupoles, version 1.0 for the warm and cold D1 magnets) [2]. We excluded orbit and coupling errors from our simulations. Particles are started with 2.5σ of the momentum distribution and tracked in 6 dimensions.

3 RESULTS FOR LIMITING CROSSING ANGLE

The interaction region configuration of the lattice for heavy ion operation used at the tracking studies is shown in Table 2. In this section we investigate the case with the maximum crossing angle in all interaction points.

Table 2: Interaction region configuration parameters.

	IP1	IP2	IP5	IP8
separ. [mm]	0	0	0	1.5 hor
angle[μrad]	$\pm$150 v	$\pm$150 v	$\pm$150 h	$\pm$100 v
β_x^*/β_y^* [m]	0.5/0.5	0.5/0.5	0.5/0.5	33/33

We investigated two possible schemes of interaction region quadrupole arrangements. In the *unmixed* scheme KEK-built magnets are installed at IP1, IP2 and FNAL-built magnets at IP5, IP8. In the *mixed* scheme each interaction region contains both KEK-built (Q1,Q3) and FNAL-built (Q2A,Q2B) quadrupoles. The majority of our cases is for the mixed scheme. Table 3 presents a summary of the tracking results.

The beam dynamics is mainly determined by the magnetic field errors in the interaction region quadrupoles. However, the cold D1 magnets at IP2 reduce the dynamic aperture further by up to 2σ.

An important observation is the dynamic aperture of 10.2σ average and 6σ minimum when when errors were only installed in the IP2 quadrupoles and dipoles. This is below the target dynamic aperture.

In the cases where errors were only installed at IP2 the dynamic aperture rms values are quite large. In these cases we found a vertical dynamic aperture which is about 4-5 σ smaller than the the horizontal one.

* Work performed under the auspices of the US Department of Energy.

Table 3: Comparison of dynamic aperture (DA) for various triplet arrangements (10^3-turn DA in units of σ_{xy} with $1\sigma_{xy}$ step size).

Case	DA mean	DA rms	DA min
UNMIXED			
all errors	8.3	1.8	5
errors at IP2 only	9.7	2.4	6
quad error at IP2 only	11.8	3.7	6
MIXED			
all errors	8.5	1.5	5
all errors, no X-angle	13.1	2.1	9
quad errors only	8.9	1.6	6
errors at IP2 only	10.2	2.3	6
quad error at IP2 only	11.7	3.5	6
systematic errors only	9.5	0.8	8
random errors only	12.4	2.2	8
without $n = 3, 4$ errors	9.1	1.8	6
without $n = 5, 6$ errors	11.4	1.4	7
without $n = 7, 8$ errors	8.1	2.5	5
without $n = 9, 10$ errors	9.0	1.7	6
D1 dipole errors only	> physical aperture		

4 RESULTS WITH VARYING CROSSING ANGLE

In the last section we reported on tracking results for crossing angles of $\pm 150\mu$rad at IP3. However, one can adopt a smaller value for the crossing angle. In such a situation the effect of the nonlinear field errors is reduced since the orbit is closer to the central axis of the interaction region magnets. We used the *mixed* arrangement for the interaction region quadrupoles and installed errors only at IP2 and IP8. No local interaction region correction has been applied.

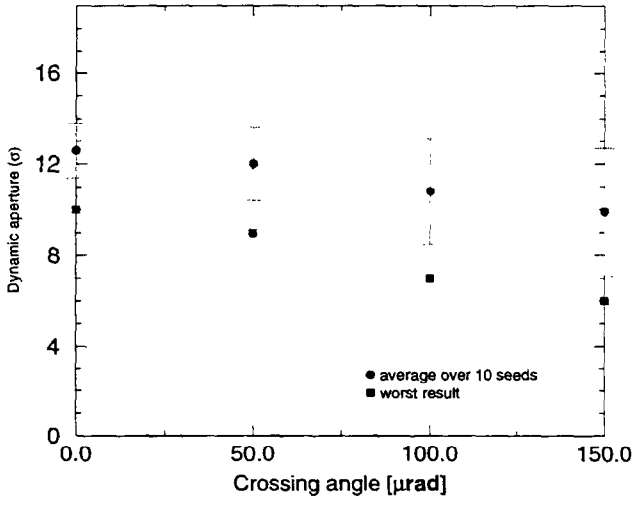

Figure 1: The 1,000 turn dynamic aperture as a function of the crossing angle at IP2.

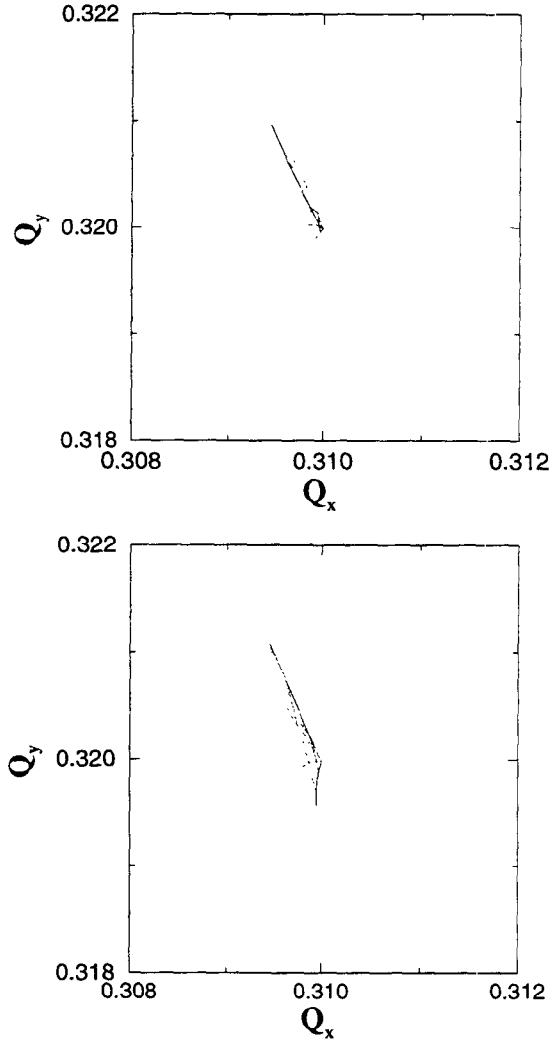

Figure 2: Tune footprints at $\pm 50\mu$rad (top) and $\pm 100\mu$rad (bottom) crossing angle.

Fig. 1 shows the dynamic aperture as a function of the crossing angle. The dynamic aperture increases almost linearly with an decreasing crossing angle. The target dynamic aperture of 12σ is reached at an crossing angle of about $\pm 30\mu$rad.

Fig. 2 and Tab. 4 show the transverse tune space needed for a 6σ beam for different crossing angles. The results in Tab. 4 were obtained from 10 random error distributions. At $\Phi = \pm 50\mu$rad the average tune space reaches the target value of 10^{-3}.

Our results indicate that with a crossing angle larger $30-50\mu$rad interaction region correctors are required at IP2 to reach the target values for tune space and dynamic aperture.

5 INTERACTION REGION CORRECTION

We use the same correction scheme that is applied at IP1 and IP5 (see Ref. [3, 4], scheme 2). The local correction

Table 4: Transverse tune space needed for a 6σ beam as a function of the crossing angle Φ. The average, rms and maximum value of the tune space is computed from 10 random distributions.

Φ [μrad]	average [10^{-3}]	rms [10^{-3}]	max [10^{-3}]
$\pm$150	2.7	1.5	4.9
$\pm$100	1.2	0.7	2.1
$\pm$50	0.8	0.4	1.5

Table 5: Comparison of dynamic aperture (DA) for without and with local correction at IP2.

Case	DA mean	DA rms	DA min
correctors IP1,IP5 only	10.5	3.0	6
correctors IP1, IP2, IP5	17.0	1.7	13

at IP2 improves the dynamic aperture by 7σ at a crossing angle of $\pm 150\mu$rad (see Tab. 5).

The Fig. 3 shows the required and available corrector strengths at IP2. All strength are well within the technical limits.

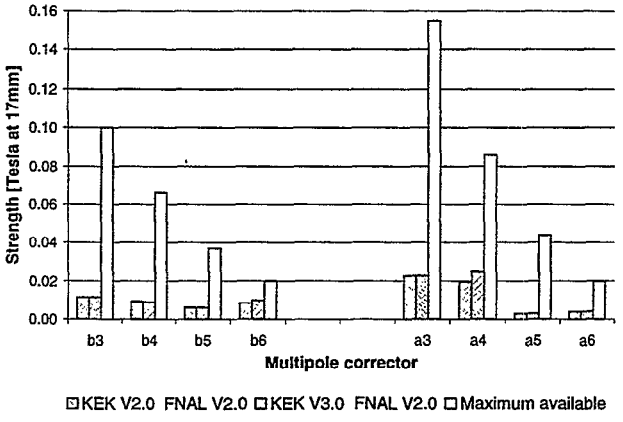

Figure 3: Available and needed corrector strength at IP2. The needed corrector strength shows the maximum out of a distribution of 10 machines.

6 SUMMARY

The magnetic field errors in the cold D1 magnets at IP2 reduce the dynamic aperture by 1.5–2σ. To reach the target values for the maximum tune space and the dynamic aperture the crossing angle must be smaller than $\pm 30\mu$rad if no local nonlinear correction is applied. With local correctors the crossing angle can be safely increased to $\pm 150\mu$rad. The required corrector strength is well within the limits that are technical achievable.

7 ACKNOWLEDGMENTS

We thank J.-P. Koutchouk, O. Brüning and R. Ostojic for lattice assistance and discussions, and many others, including A. Jain, M. Harrison, S. Peggs, S. Plate, J. Strait, R. Talman and E. Willen.

8 REFERENCES

[1] V. Ptitsin, S. Tepikian, J. Wei, "BNL-Built LHC Magnet Error Impact Analysis and Compensation", PAC 1999 proceedings, p. 1575.

[2] W. Fischer et al., "LHC interaction region quadrupole error impact studies", these proceedings.

[3] W. Fischer et al., "LHC interaction region correction scheme studies", these proceedings.

[4] J. Wei, "Principle of interaction region local correction", these proceedings.

LINEAR IR CORRECTIONS

J.-P. Koutchouk,
CERN, Geneva, Switzerland

Abstract

This is a brief report of the status of the CERN studies on linear corrections (orbit and coupling) at the time the US/LHC agreement was passed. I have updated certain of the conclusions whenever possible.

1 ORBIT CORRECTION

1.1 Criterion for the Arc Correction

Given the alignment tolerance which can be either estimated or deduced from LEP measurements, the nominal strength of the arc correctors is set at a level where the probability of exceeding the maximum is 'small', i.e. less than 8%[1]. This will happen at a few places around the machine and will be solved by closing the orbit perturbation at π or further away. These exceptions are allowed as the mechanical aperture at top energy is large in the arcs. This approach allows a better filling factor of the collider. The corresponding criterion for the integrated strength of the dipole corrector per Tesla of integrated gradient strength of the near-by quadrupole is:

$$0.0022 \text{ Tm per Tesla} \qquad (1)$$

1.2 Case of the low-β Triplet

There are two MCBX orbit correctors per triplet, each of them providing 1 Tm (optionally 1.5 Tm). The arc criterion is therefore fulfilled at the 20% (30%) level. This is even optimistic as the closed orbit must be corrected **simultaneously** for the two beams with two correctors. The efficiency of each corrector is thereby reduced.

This was identified and accepted [2] with special provisions:

- we reserve the MCBX's for the correction of the misalignment of the MQX's, i.e. do not use it for beam separation, spectrometer compensation..., except for very small adjustments.
- the alignment tolerances of the MQX are much tighter than elsewhere: 0.3 mm maximum displacement for one quadrupole block, 1 mm maximum for a coherent displacement of a whole triplet [3],
- continuous monitoring of the MQX positions with a stretched wire lodged into a hole in the concrete to straddle the whole insertion,
- quasi 'on-line' realignment with motorized jacks.

1.3 Conclusion

The triplet requires special care. Increasing the strength of the MCBX to the maximum achievable is worth the effort as it will make operation simpler and thereby more efficient at collision time. A rigid triplet arrangement relaxes the alignment tolerances. A precise beam-based measurement of the magnetic axes (K-modulation) would certainly be very helpful.

2 COUPLING CORRECTION

2.1 Relative Importance of the Coupling Sources

We assume a_2 corrected in the arcs. The remaining sources of coupling are mainly the tilt of the quadrupoles: Arc, Matching Sections and Low-β Triplets. Assuming a rms tilt angle of 1 mrad, the respective contributions to the coupling vector c are, for LHC version 2 [4]:

Arc Quadrupoles	$(13.6 + i\ 1.9)\phi_{\text{rms}}$
MS Quadrupoles	$(6.8 + i\ 16.5)\phi_{\text{rms}}$
Triplets	$(93.7 + i\ 165)\phi_{\text{rms}}$

c is given by the quadratic sum of the perturbations, where ϕ is the tilt and the other symbols have their usual meaning:

$$c = \phi_{\text{rms}} \sum^{\oplus} \frac{1}{\pi} \sqrt{\beta\ \beta}\ K l e^{(\ldots)} \qquad (2)$$

The triplets are by far the largest potential source of betatron coupling. This qualitative conclusion surely still applies for the present LHC version.

2.2 Requirement for the Triplet Alignment

In order for the triplet quadrupoles to produce a manageable coupling, it is necessary to align them with respect to each other 10 times better than the arc quadrupoles. This requirement (0.1 mrad rms) seems achievable [5]. The module of the coupling vector (all sources) is then estimated to be 0.03 rms, i.e. a usual value for accelerators.

If the triplet can be made 'rigid', it becomes almost insensitive to tilts: a whole triplet tilted by 1 mrad only contributes to $|c|$ by less than 0.003.

2.3 Requirement for the Quadrupole Twist

A quadrupole twist causes about 20 times less effect than an equivalent tilt. The 2 mrad observed on one of the HGQ should not be a problem.

2.4 Coupling Correctors

The strength of the foreseen MCQS correctors is 30 T/m $\times$ 0.5 m. It can correct tilts of 1.6 mrad in the worst case where the tilts are correlated with the gradient signs. This is largely sufficient and leaves some reserve for the correction of remote sources.

2.5 Other Effects

Orbit and dispersion coupling have not been considered so far.

2.6 Conclusion

The skew corrector foreseen in the triplet corrector package appears largely sufficient. The beam dynamics is however so sensitive to random tilts of triplet quadrupoles that they must be very tightly aligned. The experience of LEP commissioning shows that large coupling causes the loss of beam control by fooling the instrumentation. A 'rigid' triplet is almost immune against tilts.

3 REFERENCES

[1] J. Miles, LHC Project Note 43, 1996.
[2] Minutes of the Parameter and Layout Committee # 11, 1996.
[3] S. Weisz, LHC Project Note 59 (1996).
[4] J.P. Koutchouk, LHC Note 306 (1994).
[5] T. Taylor, private communication, 1994.

Workshop on LHC Interaction Region Correction Systems, BNL, Upton, New York, 1999

LOCAL DECOUPLING IN THE LHC INTERACTION REGIONS

F. Pilat
Brookhaven National Laboratory, Upton, NY 11973, USA

Abstract

Local decoupling is a technique to correct coupling locally and operationally, that is, without a priori knowledge of the underlying skew quadrupole errors. The method is explained and applied to the correction of coupling in the interaction regions of the LHC at collision.

1 INTRODUCTION

The local decoupling method is reviewed in Section 1 with a brief history of its application to different machines and experimental work performed so far. In Section 2 we present preliminary results for the correction of coupling generated by triplet errors in the LHC interaction regions, in the collision configuration.

2 LOCAL DECOUPLING TECHNIQUE

The local decoupling algorithm has been proposed by R. Talman [1] as a technique to correct coupling locally and operationally, since the correction scheme does not require a-priori knowledge of the errors. Conceptually the local correction of coupling is similar to a closed orbit correction where the orbit offsets as measured at the beam position monitors (BPM's) are used in a χ–square minimization that sets the strengths of the dipole correctors. In fact local decoupling was originally proposed by Talman in the framework of a general technique for operational corrections, which includes also closed orbit correction, minimization of vertical dispersion, etc. The idea is to determine corrector strengths by minimizing a *badness function* that i) quantifies the effect to be corrected and ii) is built up by measurable quantities. The next few paragraphs will describe how that can be achieved. A more detailed description can be found in [2].

2.1 Method and formalism

Let's define the one turn 4x4 transfer matrix (in the cartesian space) as:

$$M = \begin{bmatrix} A & B \\ C & D \end{bmatrix}$$

It is possible to find a coordinate transformation $x = G^T X$ to an *eigenbasis* where the 1-turn transfer matrix in the new coordinates is *diagonal*:

$$\underline{M} = G^{T^{-1}} M G^T = \begin{bmatrix} \underline{A} & 0 \\ 0 & \underline{D} \end{bmatrix}$$

$$\text{with} \quad G^T = g \begin{bmatrix} I & R_D \\ R_A & I \end{bmatrix} \quad \text{and}$$

$$R_A = \frac{C + \bar{B}}{\Lambda_A - \mathrm{tr}D} \qquad R_D = \frac{B + \bar{C}}{\Lambda_D - \mathrm{tr}D}$$

$$g = \sqrt{\frac{|\Lambda_D - \mathrm{tr}A|}{|\Lambda_D - \Lambda_A|}}$$

where Λ_A and Λ_D are the eigenvalues of the matrix $M+\bar{M}$.

The A *eigenmotion* describes an *ellipse* in the (x,y) space. The major axis is tilted w.r. to the x axis by an angle θ_A given by:

$$\tan 2\theta_A = \frac{2R_{A11} - \left(\frac{\alpha_A}{\beta_A}\right) R_{A12}}{1 - \left[R_{A11} - \left(\frac{\alpha_A}{\beta_A}\right) R_{A12}\right]^2 - \left(\frac{R_{A12}}{\beta_A}\right)^2}$$

An analogous relation exists between the D eigenmotion and the y axis. The **eigenangles** θ_A and θ_D, not orthogonal in general, are a *measure of coupling* since for the ideal uncoupled case $\theta_A = \theta_D = 0$. Another measure of coupling is the **area of the eigenellipse**, given by $(\pi g^2 |R_{A12}|)/\beta_A$ for the A eigenplane. If the coupling is weak, the areas of the 2 eigenellipses differ only by a multiplicative factor independent of coupling.

2.2 Measurable quantities

By driving the beam in such a way that only 1 mode is excited, the motion at one location in the lattice can be described in pseudo-harmonic form:

$$x = g\cos\psi_A \qquad y = g e_A \cos(\psi_A + \varepsilon_A)$$

$$e_A^2 = \left[R_{A11} - \left(\frac{\alpha_A}{\beta_A}\right) R_{A12}\right]^2 + \left(\frac{R_{A12}}{\beta_A}\right)^2$$

$$\varepsilon_A = -arc\tan \frac{R_{A12}/\beta_A}{R_{A11} - \left(\frac{\alpha_A}{\beta_A}\right) R_{A12}}$$

That is possible if the horizontal and vertical planes are not fully coupled. In practice that means that the uncorrected coupling should be weak, or the machine already has some degree of coupling compensation in place.

The x and y signals are *coherent* (same frequency) and their relationship at a specific position in the lattice is characterized by the *ratio of amplitudes* (e_A) and a *phase difference* (ε_A).

By collecting *turn by turn* x and y positions at a *double plane BPM,* it is possible to measure the quantities e_A and ε_A with a network analyzer. From these one can derive the matrix elements R_{A11} and R_{A12}. The coupling can be locally measured at every double plane BPM in the machine.

2.3 Correction of coupling

A badness function to be used for minimization must quantify coupling and go to zero in the absence of coupling. It must also be build with measurable quantities to be "operational". Measurable quantities are: e_A , the ratio of out of plane vs. in plane oscillations, and the phase difference ε_A.

A natural choice for the ***coupling badness*** B^C function is the following:

$$B^C = \sum_{d=1}^{N^d} e_A^2 \frac{\beta_x(d)}{\beta_y(d)} \qquad N^d \text{ number of detectors (BPMs)}$$

By weighting e^2_A with the ratio of betas one insures that all detector have comparable weight in the minimization process. e_A is a function of the off diagonal matrix elements R_{A11} and R_{A12}. One can calculate the ***influence functions***:

$$R_{A11}(d) = R^o_{A11}(d) + \sum_{a=1}^{N^a} q_a^{skew} T_a^C(d)$$

$$R_{A12}(d) = R^o_{A12}(d) + \sum_{a=1}^{N^a} q_a^{skew} U_a^C(d)$$

where the R^o functions represent the effect of the unknown errors at the position of detector d, T^C and U^C can be calculated from the unperturbed lattice functions for every skew corrector and B^C is a function of the N_a skew quadrupole corrector strengths q_a^{skew}. When $N^d > N^a$ one can determine the **skew quadrupole corrector strengths** by a *fitting procedure* so that the following conditions are met:

$$\frac{\partial}{\partial q_a^{skew}} B^C\left(q_1^{skew} \ldots\ldots q_{N_a}^{skew}\right) = 0$$

The procedure to set the skew quadrupoles for coupling corrections relies only on measurements at double plane BPMs in the ring.

2.4 Brief history of studies and experimental work

Local decoupling is implemented in the code Teapot and the latter has been used to study coupling correction schemes for several accelerators. In particular, local decoupling schemes have been studied for the SSC Collider ring, for the LEP lattice and, more recently, for RHIC. In all cases the schemes worked well is simulation, with residual eigenangles after correction below a fraction of a degree everywhere in the ring. Local decoupling is an integral part of the RHIC decoupling scheme [3]. Two families of skew quadrupoles are used for global decoupling via the minimum tune separation technique. In collision, the additional coupling effect due to the IR triplets is locally corrected by 12 skew quadrupoles, 2 per interaction region. The IR skew quadrupoles can be set either by "dead-reckoning" the measured a_2 errors in the triplet, or by local decoupling. The latter has the advantage of correcting also for the unknown residual alignment errors.

Experimental work on local decoupling has been started at HERA in 1991 and LEP in 1992. Local coupling has been successfully measured in both machines [4]. Setting the skew quadrupoles on the basis of the measurements and verifying the correction of coupling however must still be demonstrated. Local decoupling is part of the correction strategy in RHIC and experiments are planned in the 2000-2001 runs.

3 APPLICATION TO THE LHC INTERACTION REGIONS

A feasibility study of local decoupling for the LHC IR has been started. Even if the a_2 field error in the triplet will be known (and compensated for), the coupling effect due to residual roll errors of the quadrupoles can be quite substantial in the collision configuration. A way to set the skew quadrupoles in the IR correction packages to correct for that can be very useful.

3.1 The correction scheme

The following configuration and correctors has been assumed for the study;

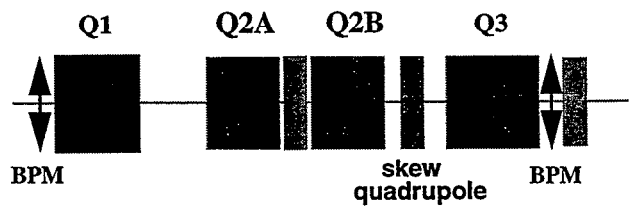

Coupling is measured at the dual plane BPMs in the IRs and the skew quadrupole corrector layer in the IR corrector package is used, with a total of 16 BPMs and 8 skew quadrupoles in the LHC ring. Skew quadrupole correctors are present in IP1, IP2, IP5 and IP8.

3.1 Preliminary results

The effectiveness of the correction has been tested against a distribution of random roll errors in the HGQ quadrupoles. Table 1 summarizes the results.

Table 1: Effectiveness of correction as a function of errors.

RMS roll angle [mrad]	coupling badness (before corr.)	coupling badness (after corr.)	max eigenang (before corr.) [deg]	max eigenang (after corr.) [deg.]
0.2	8.41	0.001	45.0	0.08
0.3	10.47	0.45	45.0	0.34
0.4	11.75	3.16	45.0	6.18
0.5	12.64	6.35	45.0	20.0

Local decoupling is doing a good job in correcting for a random distribution of roll errors up to 0.4mrad. The limit seems to be reached at ~0.5 mrad with the present scheme. A reasonable figure of merit for decoupling quality is to keep the eigenangle less than 10 degrees everywhere in the ring. In simulations that has been verified to correspond to a mininum tune separation of less than 0.001.

Figure 1: Residual coupling around the ring after local decoupling (random alignment errors in the triplet of 0.2 mrad).

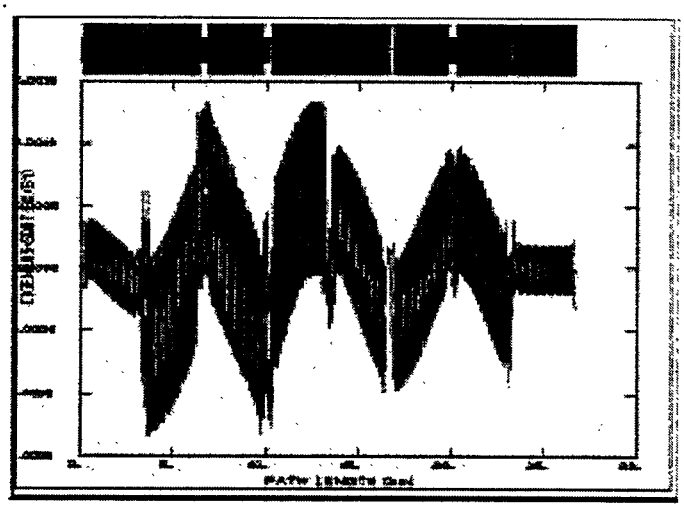

As an example, the integrated skew quadrupole strengths necessary for correcting a random distribution of 0.4 mrad in the triplets are listed in Table 2.

Table 2: Skew quadrupole integrated strengths.

skew quadrupole	interaction region	integrated strength [m^{-1}]
sql1	IP1	$0.573\ 10^{-4}$
sqr1	IP1	$0.259\ 10^{-4}$
sql2	IP2	$0.139\ 10^{-4}$
sqr2	IP2	$-0.138\ 10^{-3}$
sql5	IP5	$0.947\ 10^{-5}$
sqr5	IP5	$0.240\ 10^{-4}$
sql8	IP8	$0.112\ 10^{-4}$
sqr8	IP8	$-0.157\ 10^{-5}$

3.3 Future plans.

A detailed study of decoupling corrections will be done for the LHC Interaction regions, in the framework of a planned study on effect of alignment and linear corrections. Concerning linear decoupling, more specifically, one needs to evaluate different schemes as well as testing a statistically significative number of errors distributions.

4 CONCLUSIONS

Preliminary results on the effectiveness of local decoupling for the LHC at collision are promising. Coupling is reduced to a fraction of a degree everywhere in the ring by operationally setting the skew quadrupoles in the interaction regions on the basis of coupling measurements at the IR beam position monitors. A more detailed study for the LHC is planned as well as experimental work on the decoupling technique at RHIC.

5 REFERENCES

[1] R. Talman, *"A Universal Algorithm for Accelerator Correction"*, Proceedings of the "Advanced Beam Dynamics Workshop on effect of errors in accelerators, their diagnosis and correction", Corpus Christi, October 1991.

[2] L. Schachinger, R. Talman, *"Manual for the program TEAPOT"*, November 1994

[3] F. Pilat, S. Peggs, S. Tepikian, D. Trbojevic, J. Wei,*"The effect and correction of coupling generated by the RHIC triplet quadrupoles"*, PAC95, Dallas.

[4] G. Bourianoff, S. Hunt, D. Mathieson, F. Pilat, R. Talman, G. Morpurgo, *"Determination of coupled-lattice properties using turn-by-turn data"*, Proceedings of the "Stability of Particle Motion in Storage Rings" Workshop, BNL, October 1992.

LIST OF PARTICIPANTS

Bela Erdelyi
Michigan State University, East Lansing, MI 84824
erdelyib@pilot.msu.edu

Wolfram Fischer
BNL, Upton, NY 11973-5000, USA
Wolfram.Fischer@bnl.gov

Mike Harrison
BNL, Upton, NY 11973-5000, USA
harrison@bnl.gov

Albert Ijspeert
CERN, 1211 Geneva 23, Switzerland
Albert.Ijspeert@cern.ch

Animesh Jain
BNL, Upton, NY 11973-5000, USA
jain@bnl.gov

John Jowett
CERN, 1211 Geneva 23, Switzerland
John.Jowett@cern.ch

Jean-Pierre Koutchouk
CERN, 1211 Geneva 23, Switzerland
Jean-Pierre.Koutchouk@cern.ch

Mike Lamm
FNAL, Batavia, IL 60510-0500, USA
lamm@fnal.gov

Norihito Ohuchi
KEK, 1-1 Oho, Tsukuba, Ibaraki 305-0801, Japan
ohuchi@mail.kek.jp

Ranko Ostojic
CERN, 1211 Geneva 23, Switzerland
Ranko.Ostojic@cern.ch

Steve Peggs
BNL, Upton, NY 11973-5000, USA
peggs@bnl.gov

Fulvia Pilat
BNL, Upton, NY 11973-5000, USA
pilat@bnl.gov

Vadim Ptitsin
BNL, Upton, NY 11973-5000, USA
vadimp@bnl.gov

Gianlucca Sabbi
FNAL, Batavia, IL 60510-0500, USA
sabbi@fnal.gov

Phil Schlabach
FNAL, Batavia, IL 60510-0500, USA
schlabach@fnal.gov

Tanaji Sen
FNAL, Batavia, IL 60510-0500, USA
sen@fnal.gov

Jicong Shi
University of Kansas, Lawrence, KS 66045, USA
shi@kubeam.phsx.ukans.edu

Norbert Siegel
CERN, 1211 Geneva 23, Switzerland
Norbert.Siegel@cern.ch

Jim Strait
FNAL, Batavia, IL 60510-0500, USA
strait@fnal.gov

Tom Taylor
CERN, 1211 Geneva 23, Switzerland
Tom.Taylor@cern.ch

Steve Tepikian
BNL, Upton, NY 11973-5000, USA
tepikian@bnl.gov

Dejan Trbojevic
BNL, Upton, NY 11973-5000, USA
dejan@bnl.gov

Peter Wanderer
BNL, Upton, NY 11973-5000, USA
wanderer@bnl.gov

Jie Wei
BNL, Upton, NY 11973-5000, USA
wei1@bnl.gov

Erich Willen
BNL, Upton, NY 11973-5000, USA
willen@bnl.gov